Investigation of the Structure and Function of Type III Secretion Needle and Tip Proteins

by
Lingling Zhang
Peking University, 2003

Submitted to the Department of Molecular Biosciences and the Faculty of the Graduate School of the University of Kansas in partial fulfillment of the requirements for the degree of Doctor of Philosophy

_____

(Dr. William Picking, Mentor, Chair)

_____

(Dr. Roberto De Guzman)

_____

(Dr. Krzysztof Kuczera)

_____

(Dr. Mark Richter)

_____

(Dr. C. Russell Middaugh)

Date defended: April 15, 2009

The Dissertation Committee for Lingling Zhang certifies that this is the approved version of the following dissertation:

Investigation of the Structure and Function of Type III Secretion Needle and Tip Proteins

Committee:

_____

(Dr. William Picking, Mentor, Chair)

_____

(Dr. Roberto De Guzman)

_____

(Dr. Krzysztof Kuczera)

_____

(Dr. Mark Richter)

_____

(Dr. C. Russell Middaugh)

Date approved:_____

Abstract

Many Gram-negative pathogens possess type III secretion systems as part of their required virulence factor repertoire. The type III secretion apparatus (TTSA) spans the bacterial inner and outer membranes and resembles a syringe and a needle. It is used to inject proteins into a host cell's membrane and cytoplasm to subvert normal cellular processes. The external portion of the TTSA is a needle that is composed of a single type of protein that is polymerized in a helical fashion to form an elongated tube with a central channel that is 2–3 nm in diameter. We report the first structure of a TTSA needle protein called BsaL from *Burkholderia pseudomallei* determined by nuclear magnetic resonance (NMR) spectroscopy. The central part of the protein assumes a helix-turn-helix core domain with two well-defined α-helices that are joined by a four-residue linker. Residues that flank this presumably exposed core region are not completely disordered, but adopt a partial helical conformation. The atomic structure of BsaL and its sequence homology with other TTSA needle proteins suggest potentially unique structural dynamics that could be linked with a universal mechanism for control of type III secretion in diverse Gram-negative bacterial pathogens.

The pathogenesis of *Shigella flexneri* requires a functional TTSA to inject host-altering effector proteins directly into the targeted cell. The TTSA exposed needle is an extended polymer of MxiH. Invasion plasmid antigen D (IpaD) resides at the tip of the needle to control *Shigella* type III secretion. IpaD (36.6 kDa) has a dumbbell shape with two globular domains flanking a central coiled-coil that stabilizes the protein. Known structures of IpaD homologs (LcrV from *Yersinia* and BipD from *Burkholderia*) all have a similar overall shape. We have

identified key MxiH residues located in its PSNP loop and the contiguous surface that uniquely contribute to the formation of the IpaD-needle interface as determined by NMR chemical shift mapping. Mutation of some of these MxiH residues severely affects the stable maintenance of IpaD at the *Shigella* surface and thus compromises the invasive phenotype. Other residues could be mutated to give rise to intermediate phenotypes, suggesting they have a role in tip complex stabilization while not being essential for tip complex formation. Initial *in vitro* fluorescence polarization (FP) studies confirmed that specific amino acid changes adversely affect the MxiH-IpaD interaction. Meanwhile, none of the mutations appeared to have a negative effect on the MxiH-MxiH interactions required for efficient needle assembly.

We recently demonstrated that bile salts stimulate recruitment of the translocator protein IpaB to the *Shigella* surface where it stably resides with IpaD at the TTSA needle tip. This process appears to be initiated by a direct interaction between the bile salt and IpaD. FP studies showed that the bile salt deoxycholate (DOC) binds to IpaD. NMR spectroscopy confirms a DOC-IpaD interaction and suggests that the IpaD conformation changes upon DOC binding. We have identified key IpaD residues that appear to contribute to the formation of the IpaD-DOC interface. DOC appears to bind at the middle of the IpaD coiled-coil where the top of the N-terminal globular domain packs against the coiled-coil. Several IpaD residues in the distal globular domain are also perturbed upon the binding of DOC, suggesting an overall conformational change, which may lead to the recruitment of translocator protein IpaB to the needle tip. Mutation of some of these perturbed residues affects the ability of IpaD to recruit IpaB to the bacterial surface and thus impacts the invasive phenotype of *S. flexneri*.

Acknowledgements

I would like to thank my mentors Dr. William Picking and Dr. Wendy Picking. I have been extremely privileged to have two wonderful mentors who have helped me in every aspect of my development as a researcher and as a person. I would like to thank them for the valuable training that I received in the lab. I am thankful for their encouragement for presenting my research at local, regional and national meetings which tremendously helped my professional development. I am extremely grateful to Dr. William Picking and Dr. Wendy Picking for considering their students all the time and providing a fun learning environment for us.

I would like to thank Dr. Roberto De Guzman for teaching me everything NMR and more. I am blessed to have another advisor helping my professional development. I am thankful to him showing me the world of structural biology. I am grateful for his patience as well as being a fun PI to work for. I would like to thank Yu Wang in Dr. De Guzman's lab for his help on my NMR experiments. I am grateful for the financial support received from the Department of Molecular Biosciences and Division of Biological Sciences. I would like to thank my other committee members, Dr. Dr. Krzysztof Kuczera, Dr. Mark Richter and outside member Dr. Russ Middaugh, for serving on my doctoral dissertation committee. I also thank former committee member Dr. Erik Floor who is now retired. I am thankful for all the administrative support provided by John Connolly, *et al*.

I would like to thank our former postdoc fellow Dr. Marianela Espina for showing me the ropes when I started in the lab. I would also like to thank former graduate student Dr. Roma Kenjale for her help in the lab and teaching microbiology laboratory. I would like to thank previous and current undergraduates, Andrew Olive, Nathan Smith and Phil Adam who have contributed to this project in numerous ways. I also thank current lab members postdoc fellow Dr. Nick Dickenson, graduate student Chelsea Epler and undergraduate student Phil Adam. I am extremely grateful for having a group of fun people to work with and everyday I look forward to going to work.

Last but not least, I thank my parents for constantly encouraging me to pursue my dreams. They have been unconditionally supporting my career choices which most of the time are challenging and uncertain instead of being safe. It has been a rollercoaster ride for them sending their only child far away across the ocean. I am grateful for their love, support and encouragement which make me the person I am now. I could not have done this without them.

TABLE OF CONTENTS

LIST OF TABLES AND FIGURES

CHAPTER 1: Introduction

1. *Shigella* and shigellosis

There are approximately 165 million cases of dysentery worldwide each year that result from shigellosis and this leads to more than one million deaths annually (184). Shigellosis causes symptoms ranging from mild diarrhea to severe dysentery accompanied by fever, stomach cramping, severe abdominal pain and frequent stools with blood and mucus (30). The majority of shigellosis cases occur in developing countries involving young children due to poor sanitation, especially the lack of clean water (15). In addition to that, about 580,000 cases of shigellosis are reported in industrialized countries each year, in part due to the emergence of multiple antibiotic resistant strains, and rapid international travel coupled with the need to send humanitarian aid personnel to endemic areas. While it is often underreported in industrialized regions, shigellosis is not unusual in institutional settings like day-cares and nursing homes (125). The Centers for Disease Control estimates 440,000 cases of shigellosis in the United States each year, 85% of which are caused by *S. sonnei* (30).

Shigella is Gram-negative, rod-shaped, nonmotile, facultative anaerobic pathogen that only infects primates. There are three major species of *Shigella* that are responsible for shigellosis: *S. sonnei*, *S. flexneri* and *S. dysenteriae*. *S. sonnei* is the causative agent of most shigellosis cases in industrialized countries, where it accounts for 77% of the cases comparing to 15% in developing countries. *S. flexneri* causes 60% of shigellosis cases in

developing countries. It is the most frequently isolated *Shigella* species around the world. *S. dysenteriae* is the causative agent of epidemic dysentery and is responsible for outbreaks in confined populations like refugee camps. *S. dysenteriae* infection causes more severe symptoms because of the release of Shiga toxin and it is difficult to treat due to its resistance to multiple antibiotics (30).

Shigellosis is transmitted by the fecal-oral route, usually through contaminated food and water. These bacteria can survive the low gastric pH, and thus a very low infectious dose of 10-100 bacteria is sufficient to cause disease (60). The disease is usually self-limiting in healthy adults; however, it can be fatal in young children under the age of five due to dehydration and complications caused by malnutrition in the developing world. Once consumed, the bacteria pass through M cells in the large intestine to access the basal side of the epithelial lining where they encounter macrophages. The pathogens induce apoptosis in the macrophages. They then invade colonic epithelial cells from their basal sides and subsequently spread between epithelial cells using actin-based motility to avoid encountering the outside environment and the host immune response (see Figure 1) (160). *Shigella* invasiveness is due to virulence factors encoded by a 200-kb high molecular weight virulence plasmid, within which a 31-kb conserved region encodes two major loci that are required for the invasive phenotype to encode the type III secretion system (TTSS) (121, 157, 159).

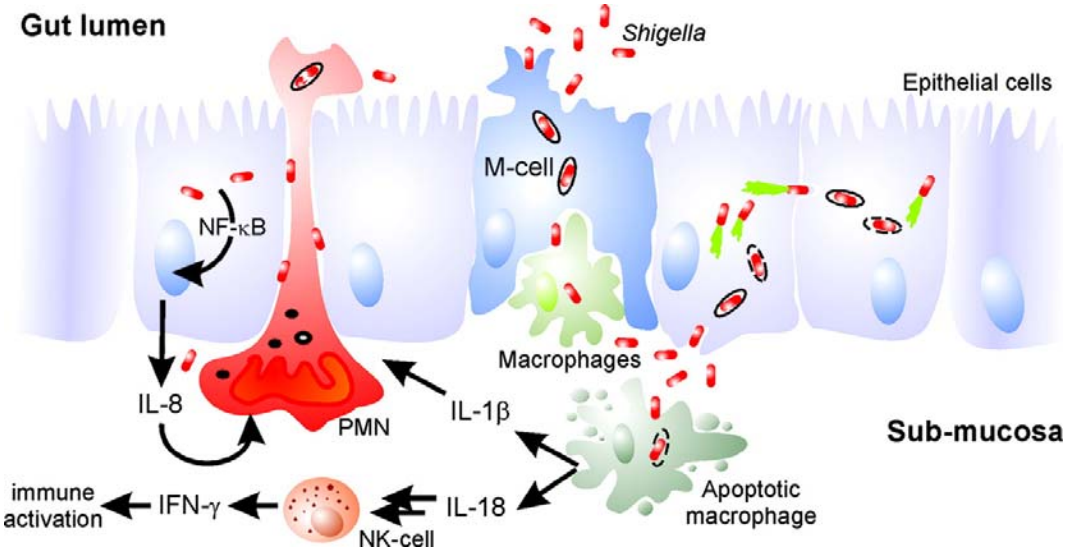

Figure 1. *Shigella* invasion of colonic epithelial cells. *Shigella* crosses the epithelial cell lining through transcytosis by M cells and encounters macrophages, causing apoptosis of the macrophages. The released pathogens invade the epithelial cells from their basal sides and can spread to adjacent cells without encountering outside environment. Proinflammatory signaling activates the innate immune response involving NK cells and PMN (polymorphonuclear leukocyte). The PMNs eventually kill the bacteria (160).

2. Discovery of type III secretion system (TTSS) of *Shigella*

The invasive ability of *Shigella* is due to several virulence factors encoded by a high molecular weight 200-kb virulence plasmid. Two major loci are required for the invasive phenotype and they encode a type III secretion system (TTSS). The *mxi* locus was found to be essential for *Shigella* virulence in 1991, when Maurelli *et al.* identified the *mxiA* and *mxiB* loci as essential virulence components on the *Shigella* virulence plasmid (8). These two genes were part of a large operon with additional *mxi* (major exporter of invasins) genes that are required for transport of the Ipa (invasion plasmid antigen) proteins to the bacterial surface. When either *mxiA* or *mxiB* were inactivated, the resulting strain failed to secrete Ipa proteins into the culture medium. In 1992, Venkatesan *et al.* found that the *spa* locus (surface presentation of antigens) is also required for *Shigella* invasiveness (180). Mutants in this locus also failed to transport Ipa proteins to the bacterial surface. The *mxi* and *spa* gene loci were later found to cooperatively encode a protein secretion apparatus called the type III secretion system (TTSS) (8, 180).

More than 20 protein products encoded by the *mxi* and *spa* loci have been identified and found to be essential for type III secretion (TTS) (171). TTSSs have been shown to mediate communication between many different bacteria and their eukaryotic host cells (96), and they turn out to be a key virulence determinant in the pathogenesis of *Shigella*. More recent findings showed that the TTSS apparatus is a multi-protein assembly that is composed of a basal body spanning the bacterial inner and outer membranes, an external needle-like structure and, most recently, a tip complex at the top of the needle (16, 63,

129). A subset the virulence proteins secreted by the *Shigella* TTSS are called invasion plasmid antigens (Ipa proteins) and at least one of these, IpaD, is secreted to serve as the primary needle tip complex protein. Ipa proteins (IpaB and IpaC) are believed to accumulate in the bacterial cytoplasm before secretion where they are bound to their cognate molecular chaperones (123, 138). These Ipa proteins are subsequently secreted so that they can act together to promote uptake of the bacterium by its eukaryotic host cell. It was just recently shown that IpaD is at the *Shigella* TTSA needle tip prior to secretion induction (63). IpaD was originally thought to be one of the effectors that trigger uptake signals in the host cell, along with IpaB and IpaC. IpaD's role is now known to be much more complicated (details later). The *Shigella* TTSS is activated by intimate host cell contact prior to invasion, however, the mechanism of this induction is not yet well understood. The roles of IpaD and the translocator proteins IpaB and IpaC is this process remain unknown, but will be touched upon in this manuscript (10, 192).

3. Overview of the type III secretion system (TTSS)

There are many different ways for bacteria to transfer effector proteins from their own cytoplasm to the external environment or into host cells. Prime among these is the TTSS which is an essential virulence element used by many Gram-negative plant and animal pathogens to manipulate their hosts (96). The TTSS is conserved among many Gram-negative bacterial species and functions to transport host-altering bacterial effector proteins from the bacterial cytoplasm across the two bacterial membranes, the host cell

membrane, and directly into the host cell cytoplasm in a single step (44, 72). TTSSs have been identified in diverse groups of pathogens. Important human pathogens are among these including enteropathogenic *Escherichia coli* (EPEC), *Salmonella enterica*, *Yersinia* spp., *Shigella* spp., *Burkholderia* spp., and *Pseudomonas aeruginosa*. Illnesses caused by these pathogens range from opportunistic infections by *P. aeruginosa* to gastroenteritis caused by *S. typhimurium, Shigella* and *Yersinia enterocolitica* to overwhelming systemic infections by *Yersinia pestis, Salmonella typhi* and *Burkholderia pseudomallei*. In all cases, the TTSS contributes to infection by allowing the bacteria to communicate with eukaryotic cells. The outcome of this interspecies communication varies with pathogen and host cell type. TTS has also been implicated in plant diseases caused by Gram-negative pathogens, and in flagellar assembly (35, 36, 44, 112).

The most conserved component of TTSSs is the TTS apparatus (TTSA), which is a multi-protein assembly that visually resembles a syringe and needle (16). The TTSA consists of more than 20 different component proteins with a complex basal body spanning the inner and outer membrane and the external needle exposed on the surface of the bacterium (17, 112, 162, 171). While the TTSA is relatively well-conserved among related species, it is also highly adapted to individual bacterial virulence mechanisms (72, 96).

TTSAs (also called secretons or injectisomes) have been purified from *Shigella*, *Salmonella*, and EPEC and visualized by electron microscopy (EM) (17, 112, 162, 171). The extracellular structures have also been visualized for the animal pathogen *P.*

aeruginosa (142), the plant pathogen *Pseudomonas syringae* (91) and the *Yersinia* spp. (129). The EM studies show that TTSAs from a wide range of pathogens share a common structure. The basal body structure is very similar to the flagellar basal body, and it is connected to an elongated extracellular hollow structure called the "needle" in animal pathogens and the "Hrp pilus" in plant pathogens (16). The needle displays a certain amount of heterogeneity in its features among the various pathogens having TTSSs. While the Hrp pilus of *P. syringae* is long and flexible, the MxiH and PrgI needles from *Shigella* and *Salmonella,* respectively, are short and relatively rigid. The EPEC needle has an additional filament attached to the needle called the "EspA filament" (112, 162, 171). In the flagellar apparatus, the hook is probably the equivalent of the needle (18). Except for the flagellar system these diverse TTSAs are believed to have a common function of translocating effector proteins into host cells for manipulating host functions (96, 112, 162, 171).

Comparison with bacterial flagella. The Gram-negative bacterial flagellum is composed of the non-motor structural elements and the motor elements (116). The non-motor basal body is composed of the MS ring, the rod, the L and P rings, the hook and associated hook–filament junction zones, and the filament with its distal cap (116). The motor consists of structural components embedded in the cell cytoplasmic membranes, including an ATPase that is driven by the proton motive force to promote the mechanical movement (116). Although there is much debate about the evolution of the TTSS, there is clearly an evolutionary relationship between the TTSS and the bacterial

flagellar system. In spite of only weak sequence similarities, a number of the components of the TTSS appear to be structurally and functionally homologous to those of the flagellar system.

Both TTSS and flagella share the ability to translocate bacterial proteins out of the bacterium. There are more than 20 proteins that contribute to form the TTSA and nearly all of them are essential for function (96). About 10 cytoplasmic or inner membrane proteins show sequence similarity to flagellar hook-basal body (HBB) proteins, while some others show no obvious sequence homology but share functional similarity. The TTSA and needle visually resemble the HBB with a 2-3nm inner channel that is similar to the inner channel of the flagellum (17, 126). External structural components and later effectors are translocated through the channel in a partially unfolded state because of the relatively small inner diameter. The hydrophobic translocator proteins of the TTSS are secreted and inserted into host membrane to open a path for later bacterial effectors to pass through into the cytoplasm of eukaryotic host cell. The insertion of a translocon pore into the host cell membrane is essential for later translocation of TTSS effectors. During assembly of the flagellum, new filament subunits are inserted directly under a cap like structure (136). Although there has been no cap identified in any TTSS, it is possible that the translocators might be functionally homologous to the flagellar cap FliD and the filament protein (FliC or flagellin). FliD allows insertion of flagellin at the flagellar tip which may be equivalent to tip complex mediated insertion of translocator proteins into the host cell membranes by the TTSS (187). FliD is a pentamer, while the TTSS tip

proteins LcrV from *Yersinia* and IpaD from *Shigella* were recently suggested to likely form a pentamer at the needle tip as well. This leads to the possibility that there is structural and functional homology between the tip complex and the flagellar cap (20, 101). Whether FliD has a TTSS homolog is still a much debated question.

4. Details of the type III secretion system from different Gram-negative pathogens

There are more than 25 different Gram-negative bacteria species utilizing a single or multiple TTSSs as key virulence determinants. The TTSS is used to deliver host-interfering bacterial effectors into the membrane and cytoplasm of their host cells in a single injection step. Quite a few important Gram-negative human pathogens require the TTSS for manipulating their host cells. This can lead to invasion of the host cells, killing of these targets, or specialized forms of adherence/colonization, depending upon the pathogen and its specific TTSS. Below are descriptions of some of these pathogens and the unique features of their TTSSs.

4a. *Shigella flexneri*

Structure of the *Shigella* type III secretion appratus (TTSA). The first TTSA structure was reported from *S. typhimurium* in 1998 (112). In 1999, Blocker *et al.* proposed that the TTSA of *S. flexneri* is composed of a needle, a transmembrane neck and a cytoplasmic bulb based on EM visualization (16). In 2000, Tamano *et al.* isolated and

purified the intact TTSA from *S. flexneri* (171). Purified TTSA complexes were analyzed by SDS-PAGE to separate the component proteins (17, 171) and identify them by immunoblot analysis. MxiD, MxiG, MxiJ and MxiH were identified as major components of the TTSA. MxiH is polymerized to form the external needle and the other proteins are proposed to be part of the basal structure (171).

The basal structure is composed of two rings with 31.6 ± 0.3 nm in length (171). The upper ring is 9.5 ± 0.9 nm wide and 15.0 ± 1.3 nm thick, while the lower ring is 26.1 ± 1.3 nm wide and 11.2 ± 0.2 nm thick (171). Multiple copies of MxiD, MxiG, MxiJ and MxiM appear to form the two stacked rings of the basal body (131, 132)(Figure. 2). MxiD was proposed to form the upper ring doublet embedded in the bacterial outer membrane (17). MxiD was hypothesized to project downward from the outer membrane, traverse the peptidoglycan layer and extend to the inner membrane (131, 132). MxiG and MxiJ were previously reported as integral inner membrane proteins (6, 7). Thus, Blocker *et al*. proposed that MxiG and MxiJ form rings in the inner membrane. Soon after, MxiM was also identified as part of the basal structure (161). MxiM is a lipoprotein that is attached to the inner surface of the outer ring doublet via its acyl moiety, where it interacts with MxiD in the outer membrane and stabilizes MxiJ in the inner membrane (161). The proposed positions of MxiD, MxiG, MxiJ and MxiM are shown in Figure 2. Further comparison to the flagellar system led to the identification of flagellar C-rod (cytoplasmic rod) counterparts in the *Shigella* TTSA. The flagellar C-rod is a macromolecular structure

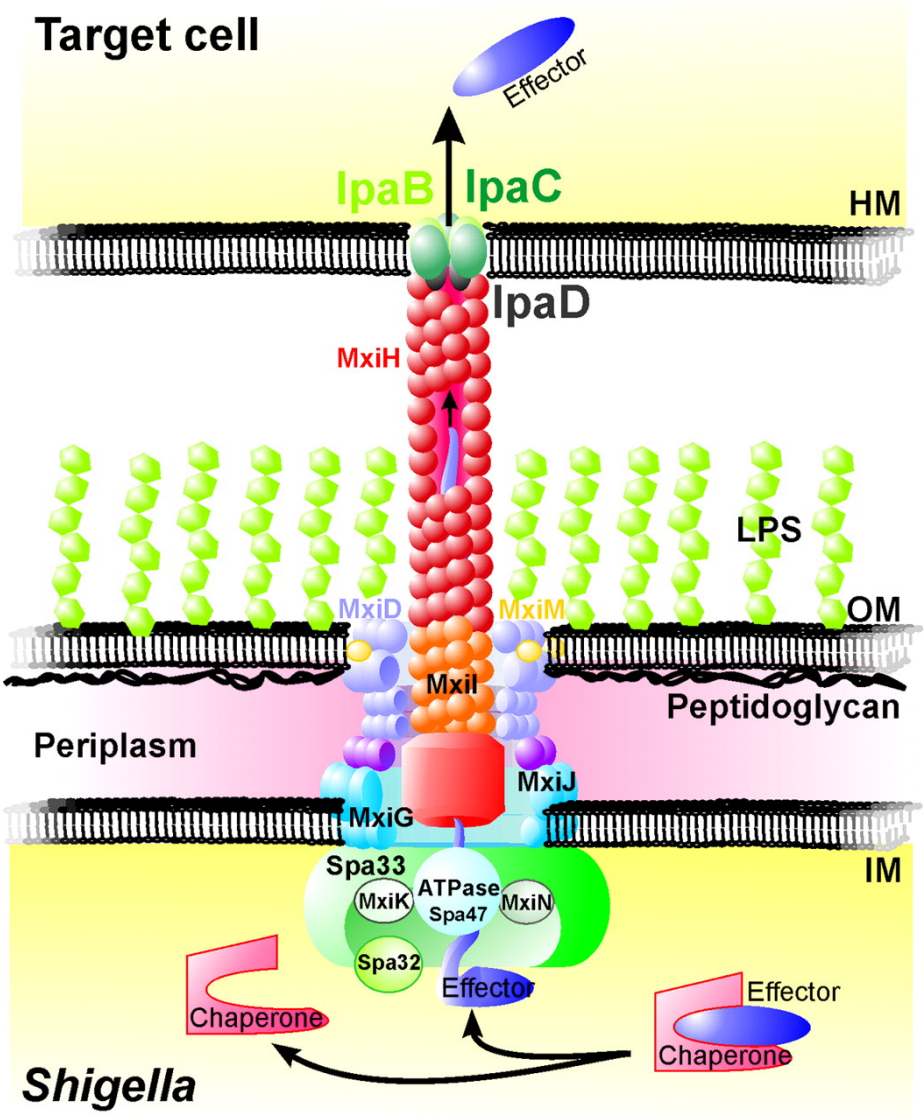

Figure 2. Diagram of the *S. flexneri* Mxi-Spa TTSS. The basal body spans the bacterial inner and outer membranes. The hollow needle is exposed with a tip complex formed by IpaD at its top. Direct contact with host cell triggers the secretion of the IpaB/C translocon (160). (HM: host membrane; LPS: lipopolysaccharide; OM: outer membrane; IM: inner membrane)

on the cytoplasmic side of the basal body structure (17, 18). The components appear to have homologs in *S. flexneri* TTSS *spa* locus (64, 135). The Spa proteins were proposed to be the putative C-rod components in the *Shigella* TTSA complex based on sequence homology even though these proteins could not be identified in the isolated needle complexes (17). The putative *Shigella* C-rod components are cytoplasmic membrane-associated proteins that presumably control secretion of other TTSA components. Similar homologs were identified in the *S. typhimurium* SPI1 TTSA (135). Recently, it was demonstrated that Spa33 is, in fact, a C-rod component of the *Shigella* TTSA (127). It was shown that Spa33 interacts with MxiG and MxiJ in the basal body, and with Spa47 (the ATPase which is homologous to the flagellar ATPase, FliI) which is proposed to power type III secretion (18, 127).

More detailed studies were reported on the extracellular components of TTSA in recent years. Cryo-EM results showed that the *Shigella* needle is a hollow structure with a channel having a 2-3nm inner diameter, a 7nm outer diameter, and a length of 50-60nm (38). MxiH was identified as a major needle component, whereas MxiI was termed as a minor needle component since deletion of either of the proteins resulted in needleless TTSAs. Later, it was suggested that MxiI forms the periplasmic rod structure to which the MxiH needle is attached, however, whether the rod structure exists is still a debated question since so far there is no conclusive visualization of the rod (18, 172). MxiH is polymerized in a helical fashion with 5.6 subunits per turn and a 24 Å pitch (38). Later research on the MxiH monomeric structure and cryo-EM needle imaging suggests that the

major axis of MxiH monomers lines up with the major axis of the needle, while the head domain of the protein is surface exposed and the N-terminal and C-terminal tails are likely inside with the C terminus buried in the wall (55).

Invasion plasmid antigen (Ipa) proteins. Five antigenic *Shigella* proteins were consistently observed through immunoblot analysis using convalescent serum from recovered shigellosis patients (86, 106, 121, 133, 158). The largest protein was identified as IcsA and was encoded on the virulence plasmid outside the 37-kb locus that is essential for *Shigella* invasion. The other four proteins were indeed encoded within the invasion locus and were originally called *a* (78 kDa), *b* (62 kDa), *c* (43 kDa) and *d* (38 kDa). The locus was identified as the *ipa* locus by Buysse *et al.* when they named the genes invasion plasmid antigens (*ipa*) A-D in the order of molecular mass for the encoded proteins (25). IpaA-D were encoded in a single operon, the *ipaBCDA* operon (12).

Inactivation of *ipaB, C* or *D* resulted in a negative Serény test, abolished contact hemolysis, and eliminated invasion of epithelial cells. Complementation with a wild-type copy of the genes restored virulence capacity. IpaB, C and D were thus identified as the main effectors for *Shigella* invasion (124). Deletion of *ipaA* did not affect the invasive ability of *S. flexneri* (13, 124), although later studies showed that *ipaA*-null mutant is unable to induce rearrangements of host cytoskeleton following invasion, which compromises bacterial cell to cell spread (175). It was reported that IpaA binds viniculin,

and may be involved in the efficient resolution of filopodia and lamellopodia following uptake of the bacteria by epithelial cells.

IpaB plays a critical role in cellular invasion (32). Together with IpaC, it forms a translocon pore in the host membrane, which is the first step for injecting later bacterial effectors into host cytoplasm. IpaB, along with IpaC, has also been implicated in lysis of the phagocytic vacuole following cellular uptake (11, 94). It was also demonstrated that IpaB, in conjunction with IpaD, is involved in the proper control of type III secretion (122). Deletion of either *ipaB* or *ipaD* results in massive, uncontrolled secretion of the remaining Ipa proteins. Although IpaD is the only Ipa protein initially found present on the *Shigella* surface, addition of the bile salt deoxycolate (DOC) can induce the stable colocalization of IpaB on the *Shigella* surface with IpaD. This may represent the first step of T3SS induction (63, 137). IpaB and IpaD together appear to regulate secretion from the *Shigella* surface prior to receiving a secretion signal triggering later effector secretion.

IpaB and IpaC are hydrophobic proteins that are predicted to contain transmembrane helices that allow them to insert into target cell membranes (83, 113). They exist in the bacterial cytoplasm independently bound to the chaperone protein IpgC prior to their secretion (123). Upon receiving the host cell contact signal, secretion is activated, causing the release of IpaB and IpaC from IpgC, which allows them to enter and exit the *Shigella* TTSA. Following their secretion, IpaB and IpaC combine to form a pore complex within the host cell cytoplasmic membrane (123, 138).

In addition to controlling secretion, IpaD has been shown to aid the insertion of the translocon pore into eukaryotic membranes (146). Formation of the IpaB-C pore thus represents final assembly of a molecular conduit with IpaD and the B-C complex linking the bacterial cytoplasm to the epithelial cell cytoplasm. The full conduit is composed of the TTSS basal body which spans bacterial inner and outer membranes, the external needle, the tip complex IpaD and the IpaB-C pore complex that spans the host membrane. This allows direct translocation of later effector proteins from the bacterial cytoplasm into the host cell cytoplasm. IpaA is among the 20 or so proteins translocated into the host cytoplasm (156, 176). Since IpaB, C and D are necessary for translocation of proteins into the host cell, they have been termed the "translocators", while the proteins that are injected into host cell cytoplasm to alter host cell function are termed "effectors" of invasion (3, 4). It cannot be ruled out that IpaB, C and D also have effector functions since IpaB is known to trigger apoptosis in macrophages by activating caspase 1 and IpaC is directly involved in mediating entry into epithelial cells (173, 193).

4b. TTSS in other Gram-negative bacteria – comparison with the *S. flexneri* TTSS

Salmonella typhimurium *Salmonella* spp. cause a variety of diseases ranging from gastroenteritis to bacteremia and enteric fever (96). Some *Salmonella* are limited to a particular host like *S. typhi* which only cause systemic typhoid fever in humans. Others, like *S. typhimurium* and *S. enteritidis,* have a broader host range causing a variety of

diseases, depending on the host (140). *Salmonella* gastroenteritis occurs through contaminated food and water (78, 79). In contrast with *Shigella*, *Salmonella* is not as stable when exposed to the low gastric pH. As a result, a much higher infectious dose of $\geq 10^4$ organisms is required for human infection (29, 60). *Salmonella* has long been a model system for studying bacterial invasion of epithelial cells.

Salmonella species contain two TTSSs encoded by two different chromosomal loci, termed SPI-1 and SPI-2 (*Salmonella* Pathogenecity Islands) (70). These two TTSSs play very different roles in pathogenesis of *Salmonella*. The TTSS encoded by SPI-1 is similar to the *Shigella* TTSS and the *Burkholderia pseudomallei* Bsa TTSS, which is required for the initial invasion of intestinal mucosal cells, whereas the one encoded by SPI-2 is required for survival in macrophages and in the establishment of systemic infection (70, 96).

After ingestion, *Salmonella* reaches the intestine where they invade the intestinal epithelia after transcytosis across M-cells (33). There is also evidence that *Salmonella* can invade the epithelial cells surrounding the M-cells directly from the apical surface (45, 170). *Shigella,* on the other hand, invades only via the basal surface. After crossing the M-cell, *Salmonella* is taken up by underlying macrophages (45). Once in the macrophages, the bacteria can either multiply within the resulting phagosomal vacuole or can induce macrophage apoptosis, which allows bacterial release at the basal surface of the mucosal epithelium. Survival within the macrophages is mediated by the TTSS encoded by SPI-2 while macrophage apoptosis is mediated by SPI-1 TTSS (45, 96). The

invasion of the epithelial cell at their basal surface is also mediated by the TTSS encoded by SPI-1 (96, 168). As with *Shigella, Salmonella* invasion of host cells is accompanied by membrane ruffling at the site of host cell contact caused by major rearrangement of the actin cytoskeleton (66).

The structure of the *Salmonella* SP-I TTSS needle component PrgI was solved in 2007 (182). PrgI from *Salmonella*, MxiH from *Shigella* and BsaL from *Burkholderia* all have a similar overall two helix bundle architecture with a tight Pro-X-X-Pro linker/turn (55, 191), suggesting a helical packing for the *Salmonella* needle that is similar to that of the previously described *Shigella* needle. The initial protein secreted by *Salmonella* SPI-1 TTSS are called Sips (*Salmonella* invasion proteins), which are homologous to the *Shigella* Ipa proteins and *B. pseudomallei* Bip proteins. SipD and IpaD have significant amino acid sequence similarity especially at their C-termini which is believed to be essential for anchoring these proteins at the needle tip. SipB, SipC and SipD are required for invasion like their *Shigella* homologs IpaB, IpaC and IpaD, while SipA is expendable for this process (104, 105). After host cell contact, SipB and SipC are secreted through the *Salmonella* TTSA and inserted into the target membrane to form the translocon pore (45, 71). Mutations in *sipB, sipC* and *sipD* individually prevent the translocation of SipB and SipC into the host cell, indicating that all three proteins are required for translocon formation (45), as is the case for their counterparts in *Shigella*.

Burkholderia pseudomallei *B. pseudomallei* is the causative agent of mellioidosis, an illness that can manifest itself in humans as an acute, sub-acute or chronic infection

(52). Melioidosis can be an acute lung infection, systemic blood stream infection or chronic suppurative abscesses (28). Infection by this saprophytic bacterium is endemic to southeastern Asia and northern Australia, and has the potential for global spread (52). Acute mellioidosis is a potentially fatal septicemic infection, while the sub-acute form of the disease can lead to the formation of systemic abscesses in multiple organ systems (49). Asymptomatic infections can progress to clinical mellioidosis as is often observed in endemic regions (51). Acute and sub-acute mellioidosis can also give rise to *B. pseudomallei* latency and the potential for delayed, and often fatal, relapse despite appropriate antibiotic therapy during the initial infection (31, 49). *B. pseudomallei* are found in contaminated water and soil, from which humans and animals eventually become infected through direct contact with the organism (27). Humans can also be infected through inhalation of dust containing the organism. Person-to-person transmission has also been reported (28). *B. pseudomallei* and its close relative *Burkholderia mallei* (causative agent of glanders) are considered important bioterrorism agents due to their ready world-wide availability and their ability to be transmitted by aerosol (167). No vaccine is currently available against this organism.

Several virulence factors have been implicated in the pathogenesis of *B. pseudomallei*, including a polysaccharide capsule, secreted hemolysins, lipases, proteases and siderophores (153). It was reported that *B. pseudomallei* has at least 3 different loci that encode putative TTSSs (152). One of the loci, the *bsa* (*Burkholderia* secretion apparatus), is encoded within a recently identified pathogenicity island that is similar to

those encoded by the *Shigella* virulence plasmid (the Mxi/Spa TTSS) and the *Salmonella* pathogenicity island SPI-1 (Inv/Spa TTSS) (167). The importance of the *bsa* TTSS for *B. pseudomallei* virulence and pathogenesis is not yet entirely clear; however, it has been predicted to be an important aspect of *B. pseudomallei* pathogenesis by contributing to cellular invasion and survival in macrophages (102). Furthermore, Stevens *et al.* showed that the *bsa* TTSS is critical for *B. pseudomallei*'s ability to invade and replicate in J774.2 murine macrophages and for vacuolar escape following host cell invasion (167).

The *bsa* locus encodes homologs of *Salmonella* and *Shigella* type III translocators: BipB (SipB in *Salmonella*, IpaB in *Shigella*), BipC (SipC in *Salmonella*, IpaC in *Shigella*) and BipD (SipD in *Salmonella*, IpaD in *Shigella*). Mutations in BipD showed defects in cellular invasion, intracellular replication, endocytic vacuolar escape and actin cytosleleton rearrangements (166). BipD has also been shown to be required for replication in murine macrophage-like cells. Although there is no direct evidence to demonstrate the existence of BipD at *B. pseudomallei* needle tip, the recently solved structure of BipD shows similar overall dumbbell shape with IpaD and LcrV of *Yersinia,* suggesting that BipD probably behaves like its homologs (57, 101).

***Yersinia* spp.** The pathogenic *Yersinia* spp. for humans are *Y. pestis, Y. pseudotuberculosis and Y. enterocolitica* (26). *Y. enterocolitica* and Y. *pseudotuberculosis* cause a normally self-limiting form of gastroenteritis and are transmitted through contaminated food and water (39). Infection in this case is caused by invasion of the intestinal tract and intestinal lymphoid tissues (39). *Y. pestis,* which is

transmitted either through a flea bite or through airborne or droplet infection, is the causative agent of plague, an acute illness with high mortality (21, 181).

Y. enterocolitica and *Y. pseudotuberculosis* cause gastroenteritis and usually gain entry into the host through the fecal-oral route. Like *Shigella* spp., these bacteria survive passage through the stomach and reach the small intestine (43, 181) where they cross the mucosal barrier via the M cells and are released at the basal surface of the intestinal epithelium (80, 87). *Yersinia* is capable of limited survival and multiplication within macrophages (89). Thus, migrating phagocytes transport the bacteria to local lymphoid tissue where they induce inflammation and cause the symptoms of gastroenteritis. These bacteria can multiply extracellularly to avoid host immune defenses by blocking subsequent uptake by phagocytes via their TTSS.

Y. pestis infections are transmitted through flea bites and result in bubonic or septicemia plague (21, 181). Typical symptoms of bubonic plague are headache, fever and swelling of lymph nodes, whereas in septicemic plague the infection directly proceeds to the blood stream without going through the lymph node phase (181). The disease can also be transmitted as droplet infection leading to pneumonic plague which is an acute pulmonary infection (21). Unlike *Y. pseudotuberculosis* and *Y. enterocolitica*, *Y. pestis* travels directly from the blood stream to the liver and spleen where it avoids phagocytosis via its TTSS (181). Accumulation of massive numbers of bacteria causes necrosis and eventually damages spleen and liver tissue (9, 23).

Although the pathogenic *Yersinia* spp. have different modes of transmission, they all require the TTSS for their virulence (44, 181). Proteins called Yop (*Yersinia* outer proteins which are homologs of *Shigella* Ipa proteins) and LcrV (protective V antigen, homolog of *Shigella* IpaD) are secreted via their TTSS and are essential for *Yersinia* virulence (181). In Y. *pseudotuberculosis* and *Y. enterocolitica*, TTSS is not required for initial invasion. The bacteria can establish infection in associated lymphatic tissues without the TTSS-encoding plasmid (87, 88, 181). Similarly studies showed that *Y. pestis* can establish initial infection in mice without TTSS (87, 88, 181). After initial infection, however, the plasmid-cured *Yersinia* spp. are cleared more rapidly by phagocytes. It was later demonstrated that inhibition of phagocytosis depends on the TTSS (82).

The TTSA in *Yersinia* spp. consists of a basal body structure located within the bacterial membranes and an external needle like the *Shigella* and *Salmonella* TTSSs. The secreted proteins, the Yops, were first identified a part of *Yersinia* membrane preparations. They are encoded on the virulence plasmid along with TTSA structural components like the needle protein YscF and its chaperones YscE and YscG. Expression and secretion of the Yops can be induced by a shift in temperature to 37^{o}C coupled with Ca^{2+} depletion in the growth medium (43).

Upon host cell contact, the *Yersinia* TTSA allows direct translocation of virulence proteins into the target cell though the translocon pore formed by the translocator proteins YopB and YopD (43). Pore formation is aided by another translocator, the needle tip protein LcrV (40, 42). LcrV and YopD also have a regulatory role in type III secretion

(67, 130). LcrV forms a distinct structure at the tip of the *Yersinia* TTS needle, where it controls insertion of YopB and YopD into the target membrane (129). The functional equivalents of YopB, YopD and LcrV in *S. flexneri* are IpaB, IpaC and IpaD, respectively.

Pseudomonas aeruginosa *P. aeruginosa* is an opportunistic pathogen that causes severe infections in immuno-compromised individuals and secondary infections in burn patients and cystic fibrosis patients (19). *P. aeruginosa* has a large arsenal of virulence determinants including at least six different secretion systems. The TTSSs of *P. aeruginosa* and *Yersinia* spp. are highly similar and several type III secreted proteins within the two systems share considerable sequence homology. Crystal structures of *Yersinia* needle protein YscF bound with its chaperones YscE and YscG and *P. aeruginosa* needle protein PscF bound with its chaperones PscE and PscG were recently revealed, and they are structurally very similar (151, 169). Needle tip proteins PcrV and LcrV from *P. aeruginosa* and *Yersinia* spp., respectively, are genetically exchangeable, as are some other secreted proteins, without leading to a loss of function (20, 68). Translocators PopB/D (from *P. aeruginosa*) and YopB/D (from *Yersinia* spp.) are also very similar.

***Bordetella* spp.** The *Bordetella* subspecies *B. pertussis*, *B. parapertussis* and *B. bronchiseptica* cause respiratory infections in mammals (189). *B. pertussis* only infects humans and is the causative agent of the acute and highly contagious disease known as whooping cough or pertussis (47). *B. parapertussis* causes a pertussis-like syndrome in

humans, but it can also infect sheep (47, 48, 149). *B. bronchiseptica* is 99% identical at the DNA sequence level to *B. pertussis* and, in fact, *B. pertussis* is considered to be a human-adapted variant of *B. bronchiseptica* (98, 147). Unlike *B. pertussis* and *B. parapertussis*, *B. bronchiseptica* infects a wide variety of mammals, including mice, guinea pigs and rabbits (46, 74). Approximately 80 to 90% of kennel cough cases are also caused by *B. bronchiseptica*. Pertussis incidence has remained high in recent years, even among vaccinated populations (1, 73, 93). Forty million children are infected worldwide each year with 300,000 deaths reported, primarily in infants (2, 58). Adolescents and adults are a significant reservoir. About 26% of adults with coughing illness show evidence of infection (2, 120).

B. pertussis infects the respiratory epithelium of humans. It is spread by aerosols or by direct contact with an infected person. It produces a large number of virulence factors that play important roles in its pathogenesis (189). At the first stage of the infection, the bacteria colonize the host ciliated respiratory epithelia, causing symptoms that are common cold-like such as inflammation of the nose, sneezing, watering eyes, sore throat, fever, and cough. The symptoms disappear later but the dry cough of the patient becomes more persistent and intense because of the airway ciliated epithelial cells are killed by secreted bacterial toxins. The patient struggles for air when the coughing becomes extremely intense. The sharp intake of breath sounds like a “whoop” when air is forced through the narrowed glottis. Vomiting, cyanosis, and apnea may occur after the cough.

The recurrence decreases later, but can last for several weeks. The disease is especially serious in infants, causing pneumonia, seizures, encephalopathy and even death.

The *Bordetella* TTSS was discovered in late 1990s (189) and it is essential for *Bordetella* pathogenesis (178, 188, 189). The TTSS of *B. bronchiseptica* is most closely related to the *Yersinia* and *P. aeruginosa* TTSSs (92). The translocator proteins, BopB and BopD of *B. bronchiseptica*, which are homologs of *Yersinia* YopB and YopD and *P. aeruginosa* PopB and PopD, share sequence similarity with them (129). LcrV and PcrV are orthologs having similar function and similar tip complex structures and their genes reside at the same position in the ORFs (22, 76, 77). No LcrV and PcrV homolog was found in the *Bordetella* TTSS (188), however, a 22 kDa protein, Bsp22 (*Bordetella* secreted protein, 22 kDa) is encoded in the operon at the position at which *lcrV* and *pcrV* are found. Bsp22 has no sequence similarities to any known TTS proteins, including LcrV and PcrV.

Bsp22 is the most abundant *Bordetella* TTSS secretion protein (188). Although the exact function of Bsp22 has not been elucidated, experimental results suggest that it is not targeted directly into host cell membranes and may be localized at the bacterial surface (188). The effect of Bsp22 on type III associated phenotypes raises the possibility that it is involved in targeting TTSS effector proteins into host cells (188). Like LcrV and PcrV, it may function by directing translocon pore formation in host cell membranes (65, 69, 76, 77, 117). Thus, it is possible that Bsp22 is the functional homolog of LcrV and PcrV in *Bordetella* forming the tip complex and controlling TTS.

Enteropathogenic *E. coli* (EPEC) EPEC is one of the leading causes of diarrhea in the developing world (34, 59). Their infections are distinguished by adhesion to epithelial cells in the small intestine and formation of characteristic lesions having considerable cystoskeletal rearrangement and causing damage to mucosal epithelium (34). After initial loose adherence to epithelial cells, the EPEC TTSS mediates the contact and communication with the host cell. At the site of contact, the epithelium forms an elongated pedestal-like structure that harbors the bacterium at its top. The pedestal consists of numerous cytoskeletal proteins like actin, α-actinin and ezrin (154). Formation of the A/E (attachment and effacement) lesion requires the EPEC adhesin intimin and the EPEC TTSS which is composed of a basal structure, a needle and an extension attached to the needle called the EspA filament (162). The adhesin binds to Tir (translocated intimin receptor) which is translocated through the TTSS and inserted into the target cell membrane to serve as the receptor for intimin (108, 109). Type III secreted proteins EspA, EspB and EspD are translocated directly into the target cell cytoplasm and are required for signal transduction within the host cell (108, 109, 154). Although it forms an elongated filament, EspA is most likely the IpaD equivalent while EspB and D are the translocon equivalents of IpaB and IpaC, respectively.

The TTSA of *Shigella* is assembled before the initiation of type III secretion. The TTS effector and translocator proteins are synthesized and stored in the bacterial cytoplasm prior to TTS activation when they are bound to their chaperones for preventing premature secretion. The *Shigella* TTSS is normally activated *in vivo* by direct contact

with host cell, whereupon a rapid burst of secretion takes place. It was not known until recently how the TTSA assembly, especially the external needle and tip. Cordes *et al.* have demonstrated that the *Shigella* needle is a helical assembly of MxiH monomers (38). In this study, we determine the atomic structure of needle protein BsaL from *B. pseudomallei* that is the first atomic structure of needle protein monomer, which gives insight into the structure and assembly of TTSS needle in general. Structure of IpaD was solved later and this previously known translocator protein was found to localize at the needle tip before TTS initiation (63, 101). The position of IpaD suggests a direct interaction between MxiH and IpaD. We test this interaction by NMR spectroscopy, identify specific MxiH residues involved and propose binding model of the needle and the tip in this study. It is not known how the signal to activate TTS travels. We also investigate the role of tip protein IpaD in TTS activation.

CHAPTER 2: Materials and Methods

Materials

Shigella flexneri 2a strain 2457T was obtained from A. T. Maurelli. *Shigella flexneri* strain SH116 containing the non-polar *mxiH* null mutations were acquired from Dr. A. Allaoui (Université Libre de Bruxelles, Bruxelles, Belgium), *Burkholderia pseudomallei* K96243 genomic DNA was obtained from Dr. D. DeShazer (The United States Army Medical Research Institute for Infectious Diseases). Henle (INT) 407 human intestinal epithelial cells were from ATCC. These cells were cultured in Eagle's modified minimal essential medium (Fisher Scientific, St. Louis, MO) which was supplemented with 10% newborn calf serum (Life Technologies, Gaithersburg, MD) and grown at 37^{o}C with 5% CO_2. All other culture media and supplies were obtained from Fisher Scientific (St. Louis, MO). Taq polymerase and PCR Supermix High Fidelity were purchased from Invitrogen (Carlsbad, CA). Oligonucleotide primers were purchased from Integrated DNA Technologies (Coralville, IA). The plasmids pET22b, pET15b, Clonables 2x Ligation Premix, *E. coli* NovaBlue cells, *E. coli* BL21(DE3) and Tuner (DE3) cells were from Novagen (Madison, WI). Restriction enzymes were from New England Biolabs (Ipswich, MA). ^{15}N-Ammonium chloride (99% pure), $^{13}C_6$-glucose (99% pure), ^{15}N L-Alanine (95-99%), ^{15}N L-Valine (95-99%), ^{15}N L-Leucine (95-99%), ^{15}N L-Isoleucine (95-99%) and Deuterium Oxide (99%) were from Cambridge Isotope Laboratories, Inc. (Andover, MA). Iminodiacetic acid Sepharose was from Sigma Chemical Company (St. Louis,

MO). BME Vitamins solution 100× was from Sigma Chemical Company (St. Louis, MO). All other solutions and chemicals were reagent grade and were purchased from either Sigma Chemical Co. (St. Louis, MO) or Fisher Scientific (St. Louis, MO).

Buffers and Reagents

See Appendix A

Bacterial strains, media and growth conditions

Shigella flexneri strains were grown at 37 ^{o}C on Trypticase Soy Agar (TSA) containing 0.025% Congo red with appropriate antibiotics for selection of the virulence and complementation plasmids. Bacteria that retained the virulence plasmid appeared as red colonies on these TSA plates. These colonies were inoculated into Trypticase Soy Broth (TSB) containing 50 μg/ml of kanamycin and 100 μg/ml of Ampicillin as necessary. TSB broth cultures were grown at 37^{o}C with shaking at 200 rpm.

Cloning of *bsaL* and *bsaL* mutants from *Burkholderia pseudomallei* K96243 for protein expression

The *B. pseudomallei* gene *bsaL* with a C-terminal truncation (5 amino acids deleted from the C-terminus, Δ5) was amplified by PCR directly from the genomic DNA (strain K96243). A primer to the 5' region of *bsaL* containing a GAGAGA sequence and start codon encoded in an NdeI site and a primer to the 3' region of the gene with a XhoI site

was used. The resulting PCR products were digested with NdeI and XhoI and ligated into NdeI/XhoI digested pET22b (Novagen) for protein expression, which encodes six tandem histidine residues at the C-terminus of the proteins for easy purification. The resulting plasmids were transformed into *E. coli* protein expression strain Tuner (DE3) (Novagen).

Purification of Recombinant protein BsaL Δ5

Recombinant proteins were purified via a C-terminal His_6 tag by nickel-chelation chromatography. Briefly, the cells were grown in LB medium at 37^{o}C, 200 rpm. Protein expression was induced at OD_{600} ~0.5 using IPTG for exactly 3 hrs. The cells were harvested by centrifugation at 4^{o}C. The cell pellet was resuspended in binding buffer. The cells were sonicated and the solution clarified by centrifugation at 20,000g for 20 mins. BsaL was purified in its soluble form from the *E. coli* cytoplasm and thus did not require refolding steps. After centrifugation the supernatant fraction was applied to nickel affinity iminodiacetic acid sepharose (Sigma) column. The protein was eluted with elution buffer. The fractions contatining the protein of interest, as determined by separation on 17% SDS-PAGE gel, were collected. Fractions containing recombinant protein were pooled and dialyzed into 10mM Na-phosphate, 10mM NaCl, pH 7.0.

Expression of isotopic labeled recombinant BsaL Δ5 in minimal media for NMR spectroscopy

To obtain uniformly ^{15}N, or ^{15}N,^{13}C-labeled proteins, the *E. coli* expression strain was grown in minimal media supplemented with ^{15}N NH_4Cl, or ^{15}N NH_4Cl and ^{13}C-glucose as the sole nitrogen and carbon sources, respectively. After reaching mid-log phase, bacteria were induced to produce protein with 1 mM IPTG and grown at 15 ^{o}C overnight. Bacteria were collected, resuspended in IMAC binding buffer, sonicated, and the cellular debris removed by centrifugation. Recombinant protein was purified via His_6 tag by IMAC chromatography as described above. Fractions were pooled and dialyzed into appropriate buffers (see above) and the protein concentration was estimated by UV absorbance at 280 nm.

NMR spectroscopy and structure determination for BsaL Δ5

NMR data were acquired at 25 °C on a Bruker Avance 800 MHz and a Varian Inova 600 MHz NMR spectrometers, both equipped with cryogenic triple-resonance probes. Resonance assignments were obtained from 2D ^{1}H–^{15}N HSQC and ^{1}H–^{13}C-HMQC and the following 3D datasets: HNCA, HNCO, CBCA(CO)NH, ^{15}N-edited NOESY-HSQC (t_{mix} 120 ms) and ^{13}C-edited HMQC-NOESY (t_{mix} 120 ms) (81, 118). NMR data were processed using NMRPipe and analyzed using NMRView (56, 99). Inter-proton distance restraints were obtained from the NOESY datasets above and were classified based on peak volumes into upper bounds of 2.7, 3.5, 4.5 and 5.5 Å and lower bound of 1.8 Å. Based on the secondary chemical shifts, the backbone dihedral angles of residues in helix α1 and α2 were restrained to $\Phi=-60(\pm20)°$ and $\psi=-60(\pm20)°$ (185). Additional negative

restraints were imposed on non-glycine residues based on the chemical shifts (185). Structure calculations and refinement were done as follows. An initial set of 200 structures were generated by torsion angle dynamics using CYANA, and 100 structures with the lowest target functions were further refined by molecular dynamics and simulated annealing in vacuo using AMBER7 with the ff99 force field (84). From this, a set of 50 structures with the lowest energies were further refined in AMBER7 with the generalized Born (GB) potential (50). Twenty structures with the lowest AMBER energies were analyzed by PROCHECK and graphics were made using MOLMOL and PyMOL (111, 115).

Cloning of *mxiH* and *mxiH* mutants for protein expression

Plasmid pWPSF4*mxiH* was used as a template for PCR reactions intended to clone the *mxiH* gene for overexpression in *E. coli*. A primer to the 5' region of *mxiH* containing a GAGAGA sequence and start codon encoded in an NdeI site and a primer to the 3' region of the gene with a XhoI site was used. The resulting PCR products were digested with NdeI and XhoI and ligated into NdeI/XhoI digested pET22b (Novagen) which encodes a six tandem histidine residues at the C-terminus of the proteins. Plasmids carrying mutation in the *mxiH* gene were first converted into C-terminal truncations (5 amino acids deleted from the C-terminus, Δ5) by PCR before being utilized as templates for cloning into pET22b for protein expression. The resulting plasmids were transformed into the *E. coli* protein expression strain Tuner (DE3) (Novagen).

Purification of Recombinant protein MxiH Δ5

The protein expression *E.coli* Tuner (DE3) (Novagen) cells were grown in LB medium at 37℃, 200 rpm. Protein expression was induced at OD600 ~0.5 using IPTG for exactly 3 hrs. The cells were harvested by centrifugation at 4℃. The cell pellet was resuspended in binding buffer. The cells were sonicated and the solution clarified by centrifugation at 20,000g for 20 mins. MxiH had to be purified from inclusion bodies in the presence of 6 M urea. After sonication, the cell pellet was solubilized in HisBIND binding buffer containing 6M urea and centrifuged again to remove insoluble components. Recombinant proteins were purified via a C-terminal His6 tag by nickel-chelation chromatography as described above. The protein was eluted with HisBIND elute buffer containing 6 M urea. The fractions containing the protein were determined by separation on 17% SDS-PAGE gel, collected, pooled and then step-dialyzed against PBS to gradually remove the urea (4 M, 2 M, 1 M, 0.5 M and 0 M urea) at 4℃. The recombinant protein was then dialyzed into 10 mM Na-phosphate, 10mM NaCl, pH 7.0.

Examining MxiH folding by Circular dichroism spectroscopy

A Jasco J720 spectropolarimeter (Jasco Inc., Easton, MD) was used for Far UV CD spectra and thermal unfolding at 222 nm. Far UV Spectra were recorded from 190nm to 260nm at a scan rate of 15-20 nm/min using a 0.1 cm path length cell. Spectra were

acquired in duplicate and averaged. The thermal-induced unfolding curves were acquired using a 0.1 cm path length cell with a temperature ramping rate of 15° C/h. The MxiH Δ 5 concentration was between 40 and 80 μM in all the cases. Deconvolution of CD spectra was achieved through analysis with DICHROWEB (104, 188). The unfolding transitions were analyzed using Jasco Spectral ManagerTM software.

Expression of isotopic labeled recombinant MxiH Δ 5 in minimal media for NMR spectroscopy

To obtain uniformly ^{15}N, or ^{15}N,^{13}C-labeled proteins, expression strain *E. coli* was grown in minimal media supplemented with ^{15}N NH_4Cl, or ^{15}N NH_4Cl and ^{13}C-glucose (see above). After reaching mid-log phase, bacteria were induced to produce protein with 1 mM IPTG and grown at 15 ^{o}C overnight. Bacteria were collected, resuspended in IMAC binding buffer, sonicated, and the cellular debris removed by centrifugation. Soluble recombinant MxiH Δ 5 can be acquired because of low temperature growth. Recombinant protein was purified via His_6 tag by IMAC chromatography as described above. Fractions were pooled and dialyzed into appropriate buffers (see above) and the protein concentration was estimated by UV absorbance at 280 nm.

NMR spectroscopy and backbone assignment of MxiH Δ 5

NMR data were acquired at 25 °C on a Bruker Avance 800 MHz NMR spectrometer equipped with cryogenic triple-resonance probe. Backbone resonance assignments were

obtained from 2D $^{1}H–^{15}N$ HSQC and the following 3D datasets: HNCA, CBCA(CO)NH and HNCACB acquired using a 0.8 mM $^{15}N,^{13}C$-MxiH sample as described for BsaL. NMR data were processed using NMRPipe and analyzed using NMRView (14, 56, 81, 99).

Purification of recombinant IpaD

Recombinant full length IpaD in pET15b with an N-terminal His tag was cloned in the lab before and used for protein expression and purification in *E. coli* protein expression strain BL21 (DE3) (Novagen). Recombinant proteins were purified by nickel-chelation chromatography as described above. After sonication, the solution was clarified by centrifugation at 20,000g for 20 min and the supernatant was applied to the nickel-chelation column. The fractions containing IpaD were determined by separation on 12% SDS-PAGE gel, collected, pooled and then dialyzed into 10mM Na-phosphate, 10mM NaCl, pH 7.0 NMR buffer.

NMR chemical shift mapping of the interaction between MxiH and IpaD

Uniformly ^{15}N-labeled MxiH and unlabeled IpaD were dissolved in NMR buffer (10 mM sodium phosphate, pH 6.0, 10 mM NaCl, 10% D_2O, and 90% H_2O). NMR data were acquired at 25 °C on a Bruker Avance 800 MHz spectrometer fitted with a cryogenic triple-resonance probe and a Z-axis pulse field gradient. NMR data were processed using NMRPipe and analyzed using NMRView (56, 99). Chemical shift mapping was done by

acquiring two-dimensional ^{1}H-^{15}N HSQC at MxiH: IpaD molar ratios of 0.5, 1, 2, 4, and 8. Both IpaD and MxiH were dialyzed into the same buffer prior to titration to assure that the chemical shift changes were only due to protein-protein interactions and not to changes in solution condition upon mixing.

Cloning of *mxiH* mutants for expression in *S. flexneri mxiH* null strain SH116

The plasmid pRK*mxiH* was used as a template in PCR reactions to create all the *mxiH* mutants. The PCR primers used are listed in the Appendix. Using pRK*mxiH* as a template, point mutations were made by means of inverse PCR using High fidelity PCR supermix and specific primers. The primers have a GAGAGA sequence, a restriction site and 18 bases past the point mutation. The following PCR conditions were used: [95^{o}C, 2 min] (1 cycle); [95^{o}C, 50 s; 54^{o}C, 45 s; 72^{o}C, 4 min] (35 cycles); [72^{o}C, 10 min] (1 cycle). The PCR products were digested with appropriate restriction enzymes, intramolecularly ligated and then electroporated into *S. flexneri* SH116. For inducible expression of *mxiH* in SH116, the gene was subcloned into the pKT1001 (171) where the NdeI site was removed and the EcoRI-HindIII polylinker region replaced with that from pWPsf (146). The resulting plasmid was named pRK2*mxiH*.

Preparation of mxiHΔ5 Mutants for Expression in *E. coli* Tuner (DE3)

To produce MxiH in its monomeric form, five residues were genetically deleted from the C terminus of the protein. The resulting mutant $mxiH^{C\Delta5}$ genes were copied from the

corresponding plasmids containing *mxiH* mutants created as described above by PCR. A 5'-primer containing GAGAGA, an NdeI restriction site, and the first 18 bases of *mxiH* and a 3'-primer containing GAGAGA, a XhoI restriction site, and the last 18 bases of *mxiH* excluding the stop codon and the last 5 amino acids were used. The PCR product was digested with NdeI and XhoI and ligated into correspondingly digested pET22b, and the ligated product was transformed into *E. coli* NovaBlue. Double-stranded sequencing was performed on each new mutant *mxiH*$^{C\Delta5}$ gene to confirm that only the desired mutation was incorporated. The resulting plasmids were used to transform *E. coli* Tuner (DE3) (Novagen). This strain was used for purification of the mutant MxiH$^{C\Delta5}$ proteins as described above.

Cloning of *ipaD* mutants for expression in *S. flexneri ipaD* null strain SF622

The plasmid pwpsf4*ipaD* was used as a template in PCR reactions to create all the *ipaD* mutants. The PCR primers used are listed in the appendix. Using pwpsf4*ipaD* as a template, point mutations were made in a similar way as described above for making *mxiH* mutant. The PCR products were digested with appropriate restriction enzymes, intramolecularly ligated and then electroporated into *S. flexneri* SF622 (146).

Cloning of *ipaD* mutants for protein expression

Plasmid pwpsf4*ipaD* was used as a template for subsequent PCR reactions designed to generate IpaD mutants. A primer recognizing the 5' region lacking the first 38 amino

acids of *ipaD*, but having a GAGAGA sequence and start codon encoded within an NdeI site together with a primer to the 3' region deleting the last 11 residues of the *ipaD* gene, but containing a stop condon and an XhoI site was used. The resulting PCR products were digested with NdeI and XhoI and ligated into NdeI/XhoI digested pET22b (Novagen), which encodes six tandem histidine residues (His_6Tag) at the C-terminus of the proteins. Plasmids carrying the *ipaD* gene or mutated *ipaD* genes were first converted into N-terminal and C-terminal truncations by PCR before being used as templates for cloning into pET22b for protein expression. The resulting plasmids were transformed into *E. coli* protein expression strain BL21(DE3) (Novagen).

Western blot analysis

The obtained proteins were electrophoretically separated by standard acrylamide SDS-PAGE gel (17% for BsaL and MxiH; 12% for IpaD; 10% for IpaB and IpaC). After that, the proteins were electrophoretically transferred from SDS-PAGE gels to PVDF membranes using a Trans-Blot SD Semi-Dry Transfer Cell (Bio-Rad Inc., Hercules, CA) for 45 min at a constant voltage of 15V. After transfer, the membrane was incubated in blocking buffer (LI-COR Biosciences) with shaking for at least 1 hour at room temperature. The blocked membrane was then incubated with a solution containing primary antibodies. The primary antibody was allowed to incubate with the membrane room temperature for at least one hr with gentle shaking. Following this incubation step, the membrane was rinsed three times with PBS containing 0.1%Tween-20 for 5 min.

Membrane was incubated in the secondary antibodies for 1 hr at room temperature with continuous shaking. The membrane was then rinsed three times with PBS containing 0.1%Tween-20 for 5 min, and then rinsed with PBS. The blot was examined in a ODYSSEY Infrared Imaging System (LI-COR Biosciences) until a suitable image was obtained.

Assay of overnight Ipa secretion in *Shigella* mutants

Wild type and mutant strains were inoculated into 10 ml Trypticase Soy Broth (TSB) with 50 μg/ml kanamycin and 100 μg/ml ampicillin. The cultures were incubated overnight at 37^{o}C at 200 rpm. The cultures were clarified by centrifugation and trichloroacetic acid (TCA) was added to the culture supernatant to a final concentration of 10%. The proteins were incubated on ice for 30 min to allow for affinity binding of the proteins to the solid state matrix. The beads were then collected by centrifugation at 10,000 rpm in a SS34 rotor. The resulting pellet was washed once with 10 ml 5% TCA followed by two washes with 20 ml ice-cold 100% acetone. Proteins were resuspended in 50 μl SDS-PAGE sample buffer and 15 μl of this sample was separated on 10% SDS-PAGE gel and visualized by Coomasie blue staining.

Assay of Congo red (CR) induction of TTSS secretion in *Shigella*

Bacteria were inoculated into 10 ml TSB with appropriate selective antibiotics and incubated with shaking at 37^{o}C. Upon reaching an O.D.$_{600}$ ~ 1.0, 1 ml of the bacteria were

collected by centrifugation and then resuspended in 500 µl cold phosphate buffer at pH 7.2. After adding 5 µl Congo red solution (3.5mg/ml in phosphate buffer), the bacteria were incubated at 37^{o}C for 12 min without shaking. After centrifugation, the bacterial pellet was discarded and the supernatant was clarified by passing through Spin-X® columns. SDS sample buffer and DTT were added and 15 µl of the sample was separated on a 10% SDS-PAGE gel.

Growth and maintenance of Henle 407 epithelial cells, preparation of cell culture plates

Henle 407 intestinal epithelial cells (ATCC# CCL6) were grown in Minimal Essential Medium Eagle (Modified) containing Earle's Salts, L-glutamine, sodium bicarbonate, and phenol red (MEME). This medium was supplemented with 1% antibiotic solution (10,000 U/ml penicillin and 10 mg/ml streptomycin in 0.9% NaCl, Sigma Chemical Co., St. Louis, MO) and 10% newborn calf serum (MEME-CS). The cells were grown in 5% CO_2:95% air at 37^{o}C and fed by replacement of media twice a week with MEME-CS. Cells were allowed to grow to confluence and then passaged as follows: The cells in one 25 cm^2 flask were rinsed once with 3 ml of solution A and treated with 3 ml 0.25% trypsin (GIBCO-BRL, Grand Island, NY) for 5 min to allow the monolayer to lift from the flask. The trypsinized flasks were agitated to free the cells from the substrate, and this solution was pipetted up and down ten times to produce a single-cell suspension. Three ml of MEME-CS was added to the single cell suspension, and 1 ml of this solution

was added to each of six new 25 cm^2 flasks containing 5 ml of MEME-CS. The newly passaged cells were replenished with fresh MEME-CS the next day. In order to prepare cell culture plates for invasion assays the above procedure was followed up to the trypsin incubation step. During the trypsin incubation, 500 μl of MEME-CS was added to each well of a sterile 24 well tissue culture plate. Once the monolayer was observed to lift from the surface of the flask with gentle agitation, 3 ml of MEM-CS was added and the solution pipetted vigorously to produce a single cell suspension of epithelial cells. Two drops of the cell suspension was added to each of the 24 wells, stirred in a figure eight motion, and placed in the tissue culture incubator at 37°C for 12 hours prior to initiation of experiments. This places approximately 5×10^4 cells per well.

Assay of bacterial entry into cultured epithelial cells

S. flexneri invasion of Henle 407 cells was monitored using a standard gentamycin-protection assay as described (145). Pre-confluent monolayers of Henle 407 cells were seeded into 24-well plates and grown overnight at 37°C. SH116 harboring the desired *mxiH*-containing plasmid or SF622 harboring the desired *ipaD*-containing plasmid was grown in trypticase soy broth (TSB) containing ampicillin and kanamycin to an A_{600} of 0.4 to 0.6. The bacteria were then added to the wells and incubated with the cells for 30 min at 37°C to allow for invasion. After incubation, free bacteria were removed by aspiration and the cells washed with MEM containing 5% calf serum and 50 μg/ml gentamycin. The cells were incubated in the final gentamycin wash for 1 hour to

kill adherent, non-internalized bacteria and rinsed with MEME. After aspiration of all the MEME, cells were lysed and immobilized by overlaying them with 250 μl 0.5% agarose in water. The agarose was then overlaid with 0.5% agar containing 2× LB medium. After overnight incubation at 37^{o}C, internalized bacteria formed subsurface colonies that were quantified.

Contact-mediated hemolysis of sheep red blood cells

Contact-mediated hemolysis was measured as described by Blocker *et al*. (16). Briefly, *S. flexneri* were grown overnight on TSA-Congo red plates and a single red colony was used to inoculate TSB. The bacteria were grown to mid-log phase at 37^{o}C, 200 rpm. The bacterial cells were collected by centrifugation at 4^{o}C at 4000 rpm and resuspended in PBS at 1/40th the original volume. Sheep red blood cells (RBCs) were washed and resuspended in PBS at a concentration of 1 x 10^{10} cells/ml. RBCs and bacteria (50 μl each) were added to wells of microtiter plates and the plates centrifuged at 2200 × g for 15 min at 25^{o}C. The plates were then incubated at 37^{o}C for 1.5 hrs. The cells were resuspended by adding 90 μl cold PBS and the plates were centrifuged again at 2200 × g at 15^{o}C for 15 min. The supernatant fraction (100 μl) was transferred to a second microtiter plate and the absorbance of the released hemoglobin measured as the absorbance at 545 nm using a mitrotiter plate reader (μQuant plate reader, Biotech Instruments, Highland Park, VT).

Purification of long TTSA needle from *S. flexneri*

mxiH gene was cloned into the IPTG inducible plasmid pRK2 and was over expressed in *mxiH* null strain (*mxiH*pRK2/SH116). Over expression of *mxiH* gave rise to assembly of extremely long needles up to 500nm. This strain was inoculated into TSB containing kanamycin, ampicillin and 1mm IPTG and grown overnight at 37^{o}C. The cells were harvested by centrifugation, and resuspended in 1/30th volume ice-cold phosphate buffered saline (PBS), pH 7.2. The cell suspension was passed vigorously through a syringe with an 18 gauge needle to shear the needle complexes. The supernatant containing the needle complexes was clarified by centrifugation at 4^{o}C and 4000 rpm for 10 min first and then at 13000 rpm for 15 min twice.

Visualization of purified needles by transmission electron microscopy (TEM)

A 5 µl drop of the needle sample was placed on Parafilm. Carbon-formvar coated copper grids (Electron Microscopy Sciences) were floated on the sample with the carbon-coated side placed face down on the sample. Grids were incubated with the sample in this manner for 5 min to allow for adsorption of the sample. The grids were then washed twice with 20 µl PBS and 20 µl dH2O. The grids prepared above were floated on a 10 µl drop of 2% uranyl acetate in water for negative staining. Staining for 10-12 minutes gave the best contrast for visualization. After staining, the grids were blotted on edge against a Whatman filter paper to remove excess uranyl acetate. The grids were allowed to dry completely overnight before visualization under the microscope.

Electron micrographs were taken using a 1200 JEM 1200 EX II transmission electron microscope (Microscopy and Analytical Imaging Center, University of Kansas) at an electron acceleration voltage of 80 KeV for visualization.

Fluorescence polarization (FP) spectroscopy for measuring the interaction of IpaD with FITC-DOC

Fluorescein-4-isothiocyanate-labeled DOC (FITC-DOC) was prepared by Dr. Ken Stensrud in Department of Chemistry, University of Kansas. FP measurements were obtained using a Beacon fluorescence polarimeter (Panvera Corp.). FP measures the rotational diffusion of a fluorescent molecule. Large molecules rotate slower than small ones resulting in higher polarization value. When fluorescent FITC-DOC binds to nonfluorescent IpaD the molecular volume of the fluorescent species will increase, thus an increased mP value. A constant concentration of FITC-DOC (30-50 nM) in PBS was mixed with increasing concentrations of IpaD (μM range). The change in FP was monitored as a change in millipolarization units (ΔmP) and was plotted as a function of IpaD concentration.

Immunofluoresence microscopy for the presence of IpaD at *Shigella* surface

S. flexneri were grown to early log phase in TSB with or without 2.5 mM DOC. The bacteria were collected by centrifugation at 4000 rpm for 10 min and washed twice with PBS. They were resuspended in 4% (v/v) formaldehyde in PBS and were dry fixed to slides. After being blocked with 1% BSA in PBS, the bacteria were labeled with

monoclonal mouse anti-IpaD antibodies and Alexa Fluor 488 goat anti-mouse IgG. Imaging was performed using a Yokugawa-type spinning disk confocal attached to an Olympus IX-81 microscope, alternately using either the 473-nm laser line with a 505 to 530 band-pass emission filter (Alexa 488) or a 561-nm laser line with a 580-520 band-pass emission filter (Alexa 568).

NMR spectroscopy and backbone assignment of IpaD$^{38-321}$

37 amino acids at the N-terminus and 11 amino acids at the C-terminus of IpaD were truncated by PCR using pwpsf4*ipaD* as template. A primer to the 5' region containing a GAGAGA sequence and start codon encoded in an NdeI site and a primer to the 3' region of the gene with a XhoI site was used. The resulting PCR products were digested with NdeI and XhoI and ligated into NdeI/XhoI digested pET22b (Novagen) for protein expression. The resulting plasmids were transformed into *E. coli* protein expression strain BL21 (DE3) (Novagen).

Uniformly ^{2}H-, ^{15}N-, ^{13}C-labeled proteins were obtained by growing the expression strain *E. coli* BL21 (DE3) in minimal media with D_2O instead of H_2O supplemented with ^{15}N-NH_4Cl and ^{2}H-, ^{13}C-glucose as the nitrogen and carbon sources. An overnight culture of *E. coli* BL21 (DE3) with pET22bIpaD$^{38-321}$ in LB was harvested and the bacteria were inoculated into minimal media with D_2O in the next morning. After grown at 37 ^{o}C for 45 min, the bacteria were induced to produce protein with 1 mM IPTG and grown for another 6 hours before harvest. The bacteria were then collected, resuspended in IMAC

binding buffer, sonicated, and the cellular debris removed by centrifugation. Recombinant protein was purified via His_6 tag by IMAC chromatography as described above. Fractions were pooled and dialyzed into 10 mM sodium phosphate pH 7.0 with 10 mM NaCl buffer and the protein concentration was estimated by UV absorbance at 280 nm.

Uniformly ^{2}H-, ^{15}N-, ^{13}C-labeled proteins were dissolved in NMR buffer (10 mM sodium phosphate pH 7.0, 10 mM NaCl, 10% D_2O, and 90% H_2O). NMR data were acquired at 30°C on a Bruker Avance 800 MHz spectrometer fitted with a cryogenic triple-resonance probe and a Z-axis pulse field gradient. NMR data were processed using NMRPipe and analyzed using NMRView. Backbone resonances were assigned using ^{1}H-^{15}N TROSY and TROSY-based HNCA and HNCACB.

NMR chemical shift perturbation for the interaction between IpaD and deoxycholate (DOC)

Uniformly ^{15}N-labeled $IpaD^{38-321}$ was purified and dissolved in NMR buffer (10 mM sodium phosphate, pH 7.0, 10 mM NaCl, 10% D_2O, and 90% H_2O). NMR ^{1}H-^{15}N TROSY data were acquired at 30 °C on a Bruker Avance 800 MHz spectrometer fitted with a cryogenic triple-resonance probe and a Z-axis pulse field gradient. NMR data were processed using NMRPipe and analyzed using NMRView. Two-dimensional ^{1}H-^{15}N TROSY spectrum of free IpaD was collected, and then spectra of IpaD bound with DOC were acquired at DOC: IpaD molar ratios of 1, 3 and 6. Chemical shift mapping was done by overlaying the ^{1}H-^{15}N TROSY spectra described above.

CHAPTER 3: Solution Structure of Monomeric BsaL, the Type III Secretion Needle Protein of *Burkholderia pseudomallei*

Introduction

B. pseudomallei is the causative agent of mellioidosis, an illness that can manifest itself in humans as an acute, sub-acute or chronic infection (52). Mellioidosis is endemic to southeastern Asia and northern Australia, and has the potential for global spread (52). Asymptomatic infections can progress to clinical mellioidosis (51) and acute and sub-acute disease can give rise to *B. pseudomallei* latency and the potential for delayed relapse (31, 49). *B. pseudomallei* and *B. mallei* (glanders) are considered bioterrorism threats due to their world-wide availability and their ability to be transmitted by aerosol (167). Both organisms are on the CDC and USDA select agent list and require special handling due to the dangerous human and zoonotic infectious they can cause.

Many Gram-negative bacterial plant and animal pathogens, including a number of potential bioterrorism agents, use type III secretion systems (TTSSs) as their key virulence factors for the subversion of target eukaryotic cell functions (96). A better understanding of all aspects of type III secretion would be useful for improving both public health and national security. *B. pseudomallei* possesses at least one genetic region that encodes a TTSS resembling that of the plant pathogens *Ralstonia solanacearum* and *Xanthomonas* spp (167). A separate TTSS (the *bsa* locus) encoded within a recently identified *B. pseudomallei* pathogenicity island is similar to those encoded by the *Shigella*

virulence plasmid (the Mxi/Spa TTSS) and *Salmonella* pathogenicity island SPI-1 (Inv/Spa TTSS) (167). The importance of the Bsa TTSS for *B. pseudomallei* virulence and pathogenesis is not yet entirely clear, however, Stevens *et al.* showed that it is critical for invasion of *B. pseudomallei* and replication in J774.2 murine macrophages and for vacuolar escape within host cells (167).

The TTSA of Gram-negative bacterial pathogens is a macromolecular protein assembly that allows physical contact between the pathogen and its target cell (96). The TTSA functions like a syringe, wherein bacterial TTSS translocator proteins are delivered directly into the host cell membrane to form a translocon pore through which other proteins are then translocated into the host cytoplasm (18). A major component of the TTSA is an external needle that extends from a basal structure and forms a conduit for translocating proteins into the target cell. For *B. pseudomallei*, the TTSA needle is formed by the assembly of multiple copies of a single protein, BsaL, which is a homologue of MxiH in *Shigella*, PrgI in *Salmonella*, YscF in *Yersinia*, and other putative type III needle proteins (see Figure 3).

The *Shigella* MxiH needle, for which more extensive data are available, consists of a tube-like structure with a 70 Å outer and a 25 Å inner diameter channel that extends 500 Å from the base of the TTSA (38). A similar structure exists at the surface of *Salmonella*, *Yersinia* and *P. aeruginosa* (103, 119, 142). The *Shigella* needle monomer (MxiH) is arranged in a helical pattern with 24 Å pitch and 5.6 units per turn (37). Recent mutational analysis has implicated MxiH in controlling the induction of TTS in *Shigella*

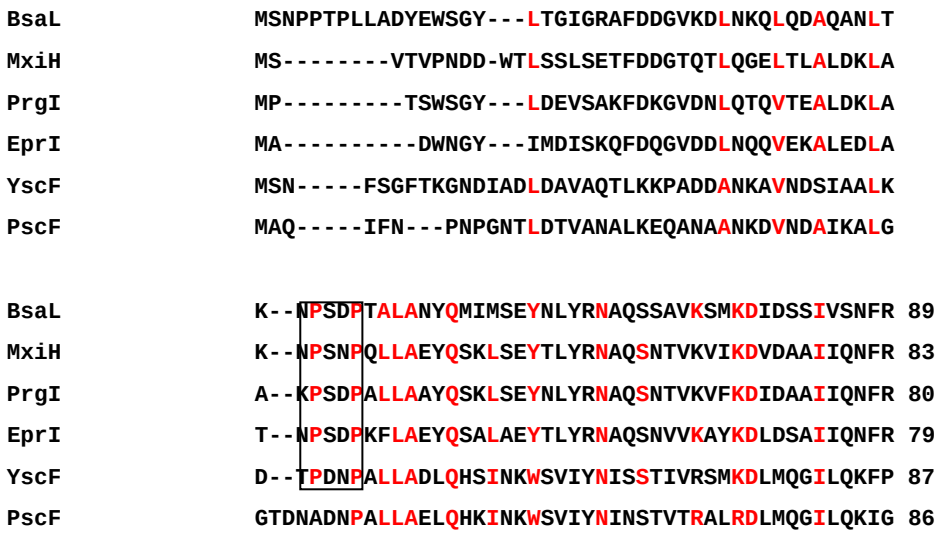

Figure 3. The TTSS needle proteins of different bacteria show sequence conservation, especially within the core structure where helix α1 and α2 of BsaL are located. The conserved P-X-X-P motif that forms the inter-helical turn in BsaL is boxed. The residues at the interface of the BsaL helix α-1 and α-2, which are involved in stabilizing the structure of the core domain, are conserved among bacterial species (marked in red). Conserved and identical residues are in red. Sequences are from Swiss-Prot, and the bacterial species and its associated needle protein are: *B. pseudomallei* (BsaL), *S. flexneri* (MxiH), *S. typhimurium* (PrgI), *E. coli* O157:H7 (EprI), *Y. pestis* (YscF), and *P. aeruginosa* (PscF).

with related findings reported for YscF of *Yersinia pestis* (107, 174). These reports implicate the TTSA needle and associated extracellular proteins in sensing host cell contact and the transmission of TTS signals.

Sequence alignment of the needle proteins from various bacterial species shows higher sequence conservation in the middle part of the proteins relative to their amino-terminal regions (Figure 3). Secondary structure predictions indicate a predominantly α-helical secondary content with some possible β-strand structure (54, 107). Circular dichroism (CD) spectroscopy confirms the α-helical content of the *Shigella* needle protein MxiH as well as PrgI and BsaL (54). Because of the potential for needle monomer self-association or aggregation, handling recombinant needle proteins *in vitro* must be considered carefully (150). Previous studies have shown that short C-terminal deletions render at least some TTSA needle proteins unable to polymerize on the bacterial surface (107). Such deletions yielded soluble and monomeric forms of MxiH and PrgI, as well as BsaL (54). These needle protein monomers retain all of their native secondary structure and tend to display readily reversible thermal unfolding (54).

The three-dimensional atomic structure of BsaL was the first to be solved for any of the TTSA needle proteins and this finding is the subject of this chapter. The high-resolution solution structure of the monomeric needle protein of *B. pseudomallei*, BsaL lacking its five C-terminal residues (BsaLΔ5), was determined by nuclear magnetic resonance (NMR) spectroscopy (191). This protein monomer is composed of two well-defined helices within the central portion of the protein's primary sequence, and

flanked by residues that appear to adopt a partial α-helical conformation. The NMR data rule out the possibility of an internal β-strand and provide insight into the possible sites of the monomer–monomer interactions that are likely to be needed to form the *B. pseudomallei* Bsa TTSA needle. The atomic structure of BsaL and its sequence homology with other TTSA needle proteins suggest potentially unique structural dynamics that could be linked with a universal mechanism for control of type III secretion in diverse Gram-negative bacterial pathogens.

Results

Preparation of BsaLΔ5 for structural analysis. Recombinant *B. pseudomallei* BsaLΔ5 lacking five C-terminal residues and possessing a His_6 C-terminal tag was purified by Ni^{2+}-chelation chromatography as described in Chapter 2. CD spectroscopy indicated that BsaLΔ5 is rich in α-helical secondary structure (approximately 70%) and is similar, in this respect, to MxiHΔ5 and PrgIΔ5 (Dr. Roma Kenjale, unpublished results) (54). The 2D $^{1}H–^{15}N$ heteronuclear single quantum coherence (HSQC) spectrum of recombinant BsaLΔ5 (Figure 4) showed a narrow ^{1}H chemical shift range with well-dispersed peaks, consistent with the likelihood that this protein contains a high degree of α-helical structure. Because of the high degree of solubility and apparently well-defined structural content of BsaLΔ5, it was a prime candidate for structure determination using NMR spectroscopy.

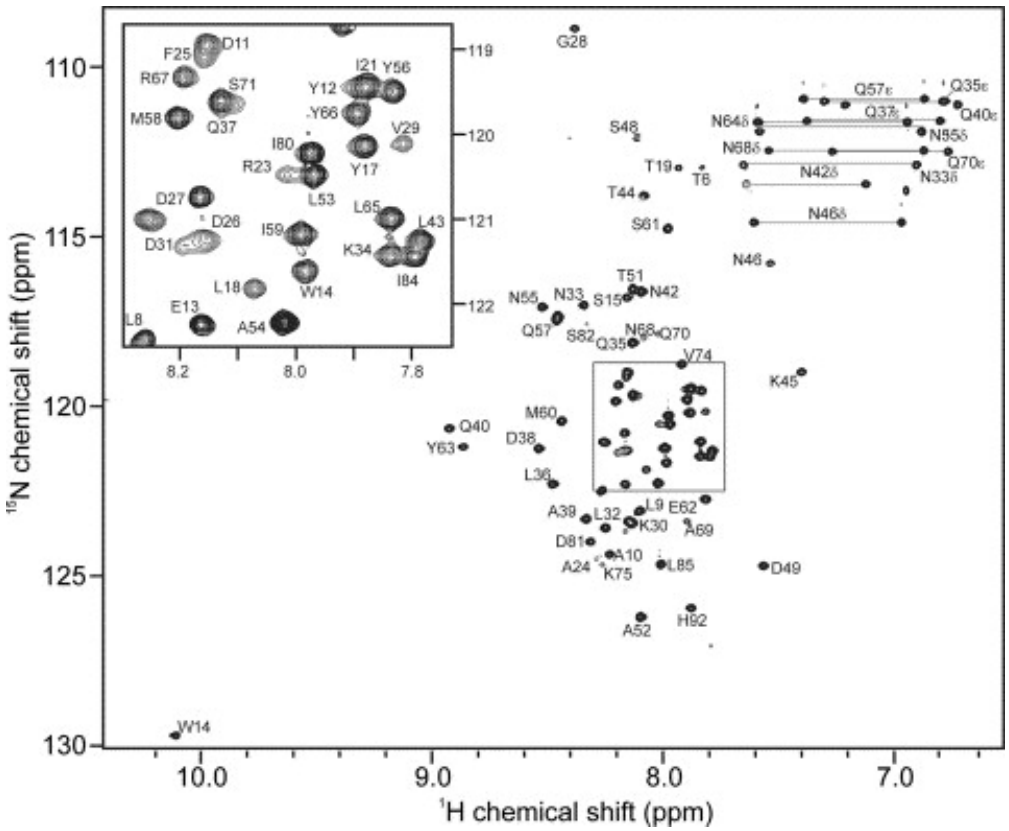

Figure 4. The 2D NMR ^{1}H–^{15}N correlation spectrum (HSQC) of the recombinant ^{15}N-labeled BsaLΔ5. The HSQC showed well-dispersed peaks and a narrow proton chemical shift range of about 1.5 ppm, suggesting a predominantly helical structure. Assignments are indicated, and the insert shows the blow-up of the central portion of the spectrum (boxed) (191).

NMR spectroscopy of BsaL$^{\Delta 5}$. Analysis of 3-D HNCA, CBCA(CO)NH, HNCO, ^{13}C-edited HMQC-NOESY, and ^{15}N-edited NOESY-HSQC experiments afforded near complete sequence-specific backbone and side-chain resonance assignments of BsaLΔ5 (81, 118). Ser2 and three residues at the C terminus, Met77–Asp79, are missing from the ^{1}H–^{15}N HSQC spectrum due to exchange broadening and could not be assigned. The His residues in the C-terminal His_6-tag are disordered, as determined by secondary chemical shifts in the random coil range, and ^{15}N and ^{13}C NOESY peaks that showed only strong intraresidue nuclear Overhauser effect (NOE) peaks. Analysis of the H^{α}, C^{α}, C^{β}, and C′ secondary chemical shifts suggested the presence of two well-defined helices in BsaL$^{\Delta 5}$ (Figure 5) (185). This was further confirmed by the NOE patterns, such as $H_i^N - to - H_{i+2}^N$, (where i=residue number), $H_i^{\alpha} - to - H_{i+3}^{\beta}$, and $H_i^{\alpha} - to - H_{i+4}^N$ NOEs, suggesting that these helices adopt a regular α-helical conformation.

The central portion of BsaLΔ5 forms a two-helix bundle. Structure calculation and refinement using CYANA and AMBER yielded well-converged structures (Figure 6a), with low energies and low distance and dihedral angle restraint violations (Table 1). A total of 716 NOE-derived distance restraints and 67 φ and 33 ψ dihedral angle restraints were used in the structure calculation (Table 1). PROCHECK analysis of the ensemble of 20 low energy structures showed that more than 99% of the residues are within the allowed region of the Ramachandran plot (Table 1). The central portion of BsaLΔ5, spanning from K30 to N68, forms the highly structured core domain of this

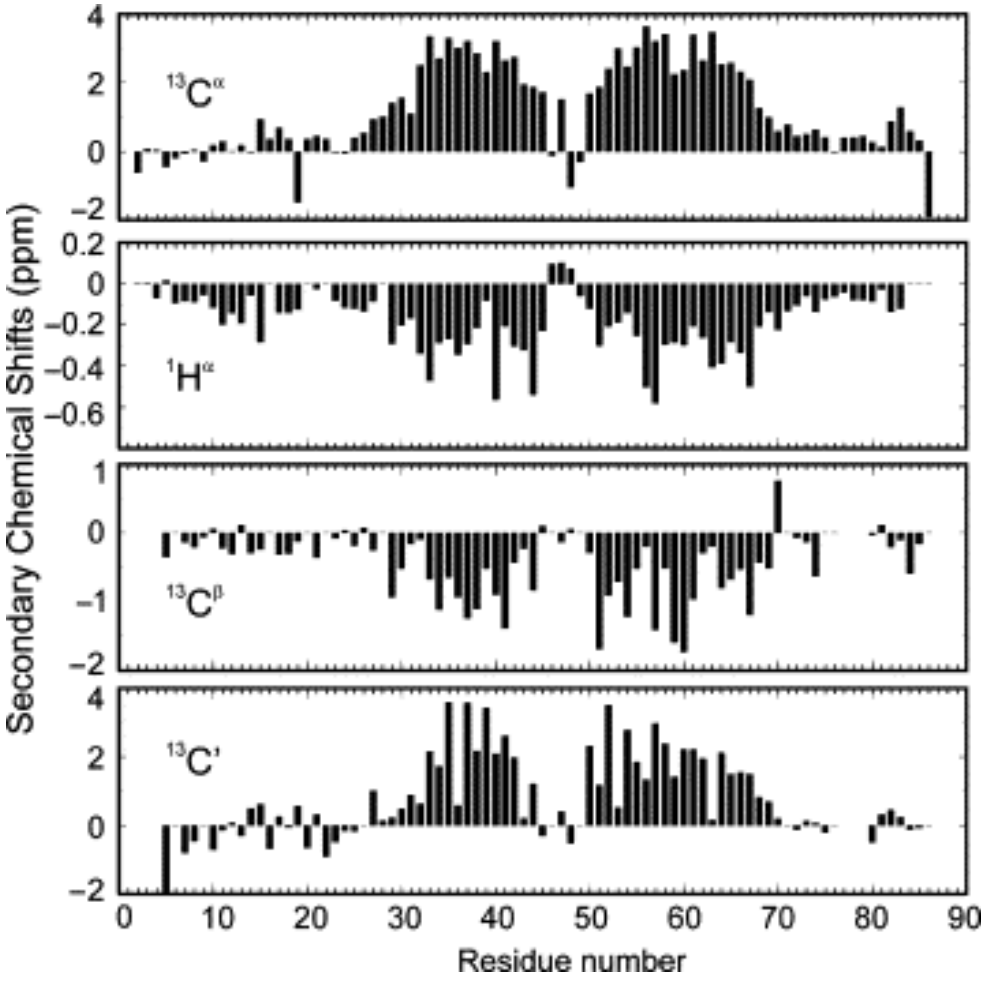

Figure 5. Secondary chemical shift index. Secondary chemical shifts obtained by subtracting the random coil $^{13}C\alpha$, $^{1}H\alpha$, $^{13}C\beta$, and $^{13}C'$ chemical shift values from those observed in the protein indicate the presence of two well-defined helices in the middle of the protein (191).

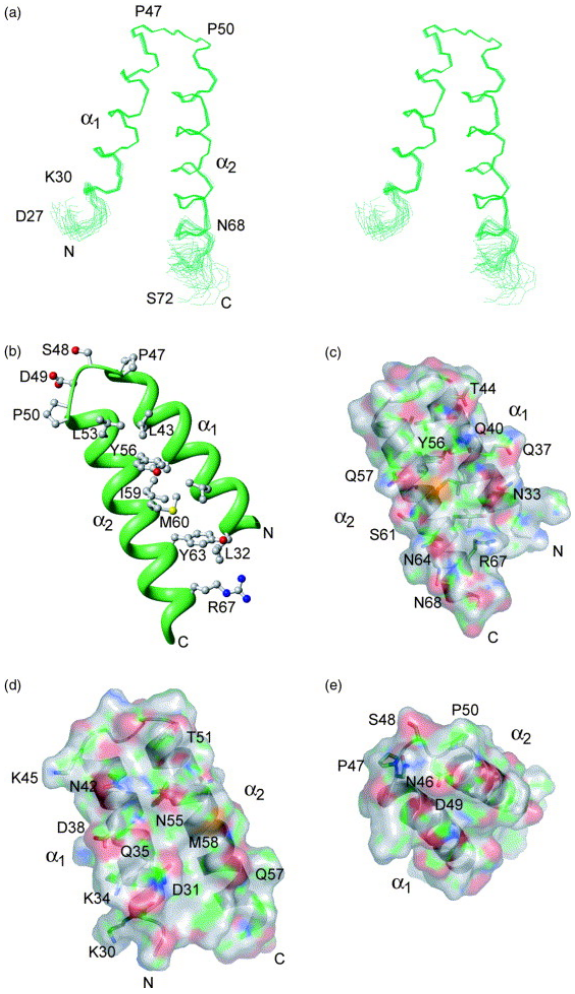

Figure 6. **NMR structures of BsaLΔ5.** (a) Stereo view of the 20 lowest energy NMR structures of BsaLΔ5 showing residues Asp27–Ser72. Residues Lys30–Asn68 form the well-defined core domain of BsaLΔ5. The rest of the molecule does not adopt a single conformation. (b) Ribbon diagram of the lowest energy NMR structure of BsaLΔ5, showing the residues that form the hydrophobic contacts at the interface of helix α1 and α2. (c–e) Surface representations showing the polar residues that line the surfaces of the core domain of BsaLΔ5. The side-chain functional groups of residues on the surface are colored as follows: amides blue, carboxyls and hydroxyls red, methylenes green, and the methionine sulfur atoms orange (191).

Table 1. Number of restraints for BsaLΔ5 (residues M1-I85) and the core domain (residues K30-N68), and structure statistics for the 20 low energy structures of BsaLΔ5.

	K30-N68	M1-I85		K30-N68
A. Number of restraints			B. Structure statistics (20 structures)	
Total distance restraints	582	716	RMSb deviation from the mean structure (K30-N68)	
Intraresidue (i,i) a	116	133	Backbone atoms (N,Cα,C′) (Å)	0.37
Sequential (i,i+1)	127	193	All heavy atoms (Å)	0.88
Medium range (2≤|i−j|≤4)	217	267	Violation analysis	
Long range (|i−j|>4)	122	123	Maximum dihedral angle (deg.)	2.4
Total dihedral angle restraints	67	100	Maximum distance (Å)	0.28
Phi	34	67	Energies	
Psi	33	33	Mean AMBER energy (kcal/mol)	-3183
			Mean restraint energy (kcal/mol)	37
			Deviation from idealized geometry	
			Bond lengths (Å)	0.0100±0.0001
			Bond angles (deg.)	2.43±0.02
			PROCHECK statistics	
			Most favorable (%)	87.2
			Additionally allowed (%)	12.3
			Generously allowed (%)	0.4
			Disallowed (%)	0.1

a i,j=residue number.

b RMS, root-mean-square.

needle protein monomer, with two well-defined helices joined by an ordered, four-residue PSDP turn. More than 80% of the assigned NOEs and nearly all of the long-range NOEs are found within this core domain, yielding an average of about 15 restraints per residue (Table 1). Helix α1 has five helical turns and spans residues K30–N46. This is followed by a highly ordered linker composed of Pro47-Ser-Asp-Pro, which immediately connects with the seven-turn helix α2 spanning residues T51–N68.

The helix α1-α2 interface is stabilized by hydrophobic interaction. The BsaLΔ5 core domain is stabilized by hydrophobic interactions (Figure 6), mediated by residues that are also conserved among needle proteins (Figure 3). The hydrophobic side of the amphiphatic helix α1 forms direct contact with the hydrophobic side of the second helix (Figure 6b). The two helices pack at an angle of −66°, and the interface is formed by the hydrophobic interactions of L32, L36, A39, and L43 on helix α1 with Y63, M60, I59, Y56, L53, and A52 on helix α2. The aromatic rings of Y56 and Y63 are stabilized by hydrophobic contacts. The Y56 ring is sandwiched between the hydrophobic side-chains of L43 and M60, and forms additional contacts with the methylene groups of Q40 and Q67. Similarly, the Y63 ring is wedged between L36 and the methylene groups of R67 with additional contacts to side-chains of L32 and Q64.

The surface of the core domain is lined with polar residues. The surfaces of the core domain are dominated by polar groups (Figure 6c–6e). One side is lined with polar residues: Q40, Q37, N33 on helix α1 and Q57, S61, Q64, and N68 on helix α2 (Figure 6c). In addition, the hydroxyl groups of Y56 and Y63 are pointed toward the surface and

contribute to the overall polarity of this side (Figure 6c). N68 is conserved among needle proteins (Figure 3), however, it does not participate in hydrophobic contacts at the helix α1-α2 interface, suggesting that it might be involved in functions other than stabilizing the core domain. The other side of BsaLΔ5 (Figure 6d) is also lined with polar residues: K30, D31, K34, Q35, D38, N42, and K45 on helix α1 and T51, N55, Q57, and the hydroxyl group of Y66 on helix α2. The linker between helix α1 and α2 is also polar, comprised of S48 and D49 and near to N46 at the end of helix α1 (Figure 6e). The polar nature of the helix-turn-helix core domain of BsaLΔ5 suggests that this domain is solvent-exposed in the needle apparatus.

Significance of two *trans* proline residues at the interhelical turn of BsaLΔ5. The two proline residues located at the center turn of BsaLΔ5, P47 and P50, are in a *trans* conformation, as evidenced by strong NOEs from the proline Hδ protons to the Hα protons of the preceding residues, N46 and D49, respectively. The *trans* conformation of these two Pro residues constrains the orientation of the two helices, α1 and α2, so that they must be positioned next to each other. That is, they must assume a structure that is very close to the final global fold of the core domain of the needle protein. These two Pro residues are highly conserved among TTSA needle proteins in diverse bacterial species (Figure 3). The constraining action of these two Pro residues suggests a role in the folding of all these needle protein homologues and may provide an explanation for the reversible unfolding of the protein *in vitro* (54).

Terminal residues flank the core domain and are likely to be in partial-helical conformations. The first seven residues of BsaLΔ5 are unstructured. These residues have no apparent secondary structures from chemical shifts and show only intraresidue NOEs. Based on sequential NOE patterns, the three Pro residues in this region, P4, P5, and P7, are all in *trans* conformation, with a minor *cis* conformation also observed for P4. The regions flanking the well-defined core domain of BsaLΔ5, A10 to G28 at the N terminus and S71 to I84 at the C terminus, are partially ordered. They exhibit medium-range NOE patterns that are more characteristic of α-helical structures. For example, residues from L9 to G28 and S71 to I84 showed a consistent pattern of $H_i^{\alpha} - to - H_{i+3}^{\beta}$ NOEs with weaker intensities compared to the corresponding $H_i^{\alpha} - to - H_{i+3}^{\beta}$ NOEs found in helix α 1 and α2. There are also sequential $H_i^{N} - to - H_{i+1}^{N}$ NOEs found from L8 to G28, and for some of the residues between S71 to I84, again with weaker intensities compared to those found in helix α1 and α2. It is not possible to ascertain the presence (or absence) of weak $H_i^{N} - to - H_{i+1}^{N}$ NOEs between S71 and I84 with the available NMR data due to spectral overlap. The NOE patterns suggest the regions flanking the core domain are not completely disordered, but are more likely to be in partial-helical conformations.

No β-hairpin in BsaLΔ5. In the absence of high-resolution structural data for the needle proteins of the TTSA, the *Salmonella* flagellar filament, FliC, was used to predict the structure of the needle proteins of the TTSA (54, 107). This secondary structure prediction suggested the presence of a β-hairpin in the needle proteins corresponding to residues Y63-Q70 of BsaLΔ5. This is not supported by the NMR data. The secondary

chemical shifts, NOE patterns, and NMR structure indicate that Y63–Q70 forms the C-terminal part of helix α2 and cannot be in a β-hairpin conformation. Based on the sequence similarity, other needle proteins are also likely to fail to have a β-hairpin in this region (Figure 3).

Discussion

The bacterial TTSA consists of a basal body that spans the inner and outer membranes of Gram-negative bacteria and an external needle formed by the polymerization of multiple copies of a single type of protein into a tube-like helical structure (18). These substructures give rise to an apparatus that is capable of delivering bacterial proteins into eukaryotic cells for the subversion of normal cellular functions. Upon assembly, the needle apparatus forms a 25 Å diameter channel that is used for translocating bacterial effector proteins into the host cell membrane and cytoplasm. For high-resolution structural determination of monomeric needle proteins, it was necessary to consider potential problems that could arise from the intermolecular protein–protein interaction of recombinant needle subunits. Such issues probably contribute to the lack of high-resolution structures for any TTSS needle protein until recently. Deletion of the C-terminal five residues of the needle proteins MxiH from *Shigella*, PrgI from *Salmonella*, and BsaL results in the production of monomeric forms of these proteins (54, 150). Monomers produced in this way retain extensive native secondary structure, as determined by biophysical characterization, thus allowing high-resolution structure

determination of these needle protein monomers. The central portions of the sequences of several needle proteins show strong sequence conservation (Figure 3) and all of those purified as monomers appear to have very similar secondary structures that are rich in α-helical content (Dr. Roma Kenjale, unpublished results). It was expected that structure determination for any one of the needle proteins would provide a significant contribution to the current understanding of how needle protein structure correlates with its biophysical properties, its polymerization into type III secretion needles, and possibly its role in pathogenesis.

Recombinant BsaLΔ5 showed ideal characteristics needed for NMR-based structure determination. BsaLΔ5 displayed near-millimolar solubility and well-dispersed peaks in the 2D $^{1}H–^{15}N$ HSQC spectrum (Figure 4), making it highly suitable for NMR structural characterization. Analysis of secondary chemical shifts clearly identified two well-defined helices (Figure 5) and further analysis of the NOESY datasets yielded a good number of distance restraints (Table 1), which allowed for atomic-level structure determination with good structural statistics.

As a monomer, the central portion of BsaLΔ5 forms a well-structured, two-helix bundle. The first seven residues are completely disordered and the regions flanking the well-structured core domain are partially ordered. This is reflected in a higher number of distance restraints, averaging about 15 restraints per residue within the central region. In contrast, the flanking regions showed medium-range NOEs that are characteristic of α-helical structures. The NMR structure of BsaLΔ5 (Figure 6) supports the CD data

showing that this needle protein is predominantly α-helical. PrgI and MxiH appear to have similar structures (55, 182). The data presented here do not, however, support the previous suggestion that there may be a β-hairpin within the C-terminal half of these needle proteins. The core domain is stabilized by hydrophobic interaction and the surface is lined with polar residues, suggesting that this part of the needle protein is solvent exposed when incorporated into the needle apparatus.

The two-helix bundle is a common structural feature of many proteins, and a search using DALI yielded at least 52 proteins that are structurally homologous to the core domain of BsaLΔ5 (95) (Table 2). These proteins contain helix-turn-helix structures that can be superimposed with the core domain of BsaLΔ5 with a root-mean-square deviation (RMSD) of 2.0 Å or better. Table 2 contains a wide variety of proteins, including membrane proteins, enzymes, chaperones, and transcription factors found in eukaryotes, bacteria, and viruses. These proteins can be involved in cell adhesion, gene regulation, signaling, and metabolism. What is noteworthy is the lack of sequence identity among these proteins. Of the 52 proteins, 42 had sequence identity below 10% with the highest identity being a designed protein (23%). There is structural homology with another TTSS protein, YscE, of *Y. pestis* which had a backbone RMSD value of 1.9 Å and 14% sequence identity with the BsaLΔ5 core domain (144). YscE is a TTSS chaperone that, together with another protein, YscG, forms a stable ternary complex with the *Yersinia* needle protein, YscF. This interaction prevents premature polymerization of the needle protein in the bacterial cytoplasm (169).

Table 2. List of proteins that are structurally homologous to the core domain of BsaL (residues K30-N68) obtained using the search program DALI. The core domain of BsaL showed a structural homology with the TTS chaperone YscE (in bold below).

PDB ID	RMSD* Å	ID† %	Functional Class	Protein Name, Source
1H6O	1.1	9	Telomere binding	Telomeric Repeat Binding Factor 1, *Homo sapiens*
2MHR	1.2	10	Oxygen binding	Myohemerythrin, *Themiste zostericola*
1P68	1.4	23	Designed	De Novo Designed Protein, Synthetic
1RJ1	1.4	0	Protein binding	Invertase Inhibitor, *Nicotiana tabacum*
1R9S	1.5	15	Transcription	NA-Directed RNA Polymerase II, Synthetic
1U89	1.5	10	Structural	Talin 1 Fragment, *Mus musculus*
1EYY	1.6	5	Oxidoreductase	Aldehyde Dehydrogenase, *Vibrio harveyi*
1FOH	1.6	9	Flavin	Phenol Hydroxylase, *Trichosporon cutaneum*
1BL8	1.7	5	Membrane	Potassium Channel Protein Mutant, *Streptomyces lividans*
1EGU	1.7	3	Lyase	Hyaluronate Lyase, *Streptococcus pneumoniae*
1KMI	1.7	5	Signaling	Chemotaxis Protein CheY, *Escherichia coli*
1ORQ	1.7	2	Membrane	Fab Light Chain 6e1 Fab Heavy Chain, *Mus musculus*
1RW9	1.7	3	Lyase	Chondroitin Ac Lyase, *Arthrobacter aurescens*
1SKV	1.7	5	Unknown	Hypothetical 7.5 KDa Protein, *Sulfolobus* virus-like particle
1UJW	1.7	10	Transport	Vitamin B12 Receptor, *Escherichia coli*
1EK9	1.8	10	Membrane	Outer Membrane Protein TolC, *Escherichia coli*
1NKD	1.8	7	Transcription	N Rop Protein, *Escherichia coli*
1U7L	1.8	5	Structural	Vacuolar ATP Synthase Subunit C, *Saccharomyces cerevisiae*
1VCS	1.8	13	Transport	Vesicle Transport Homolog, *Mus musculus*
1YC9	1.8	17	Membrane	Multidrug Resistance Protein (VceC), *Vibrio cholerae*
1DOV	1.9	10	Cell Adhesion	Alpha-Catenin Fragment, *Mus musculus*
1FPO	1.9	5	Chaperone	Chaperone Protein Hscb (Hsc20) Mutant, *Escherichia coli*
1I4D	1.9	10	Signaling	Arfaptin 2 Fragment (Partner of Rac), *Homo sapiens*
1LRE	1.9	8	Cell surface	Receptor-Associated Protein Fragment, *Homo sapiens*
1QSD	1.9	18	Chaperone	ß-Tubulin Binding Post-Chaperonin Cofactor, *Saccharomyces cerevisiae*
1UPG	1.9	10	Transcription	Transcriptional Repressor Tram, *Agrobacterium tumefaciens*
1VMG	1.9	12	Hydrolase	Hypothetical Protein, *Sulfolobus solfataricus*
1WDZ	1.9	10	Signaling	Insulin Receptor Substrate P53 Fragment, *Homo sapiens*

1XVH	1.9	11	Cell adhesion	Hypothetical Protein, *Staphylococcus aureus*
1Y2O	1.9	10	Signaling	Bai1-Associated Protein 2 Isoform 1, *Homo sapiens*
1YF2	1.9	3	Hydrolase regulator	Type I Restriction-Modification Enzyme, *Methanocaldococcus jannaschii*
1ZHC	1.9	2	Unknown	Hypothetical Protein, *Helicobacter pylori*
1ZW0	**1.9**	**14**	**Chaperone**	**Type III Secretion Protein YscE, *Yersinia pestis***
2A65	1.9	5	Transport	Na(+):Neurotransmitter Symporter, *Aquifex aeolicus*
1CXZ	2.0	3	Signaling	His-Tagged Transforming Protein RhoA, *Homo sapiens*
1D2M	2.0	7	Hydrolase	Excinuclease Abc Subunit B (UvrB), *Thermus thermophilus*
1DL2	2.0	8	Hydrolase	Class I Alpha-1,2-Mannosidase, *Saccharomyces cerevisiae*
1GRJ	2.0	5	Transcription	N Grea Transcript Cleavage Factor, *Escherichia coli*
1GW5	2.0	10	Endocytosis	Adaptor-Related Protein Complex Subunit, *Mus musculus*
1GWC	2.0	3	Transferase	Glutathione S-Transferase TSI-1, *Aegilops tauschii*
1HUW	2.0	7	Hormone	Human Growth Hormone Mutant, *Homo sapiens*
1K04	2.0	12	Transferase	Focal Adhesion Kinase 1 (Fadk 1), *Homo sapiens*
1KON	2.0	11	Unknown	Protein YebC, *Escherichia coli*
1LF6	2.0	5	Hydrolase	Glucoamylase, *Thermoanaerobacterium spp.*
1LNQ	2.0	2	Metal transport	Potassium Channel Related, *Methanothermobacter spp.*
1SF9	2.0	13	Unknown	Hypothetical Protein, *Bacillus subtilis*
1X8Z	2.0	13	Protein binding	Invertase/Pectin Methylesterase Inhibitor, *Arabidopsis spp.*
1YKE	2.0	10	Gene regulation	RNA Polymerase II Mediator Complex Protein MED7, *Saccharomyces cerevisiae*
1Z1W	2.0	0	Hydrolase	Tricorn Protease Interacting Factor F3, *Thermoplasma spp.*
2B7M	2.0	3	Endocytosis	Exocyst Complex Component Exo70, *Saccharomyces spp*
2BDE	2.0	16	DNA Binding	Cytosolic IMP-GMP 5'-Nucleotidase, *Legionella pneumophila*
2C2A	2.0	5	Transferase	Histidine Kinase, *Thermotoga maritime*

*RMSD, Root-mean-square deviation of the backbone atoms.

†ID, Percent sequence identity between the fragment of the matched protein that aligned with the core domain of BsaL (K38-N68).

CHAPTER 4: Identification of the MxiH Needle Protein Residues Responsible for Anchoring Invasion Plasmid Antigen D (IpaD) to the Type III Secretion Needle Tip

Introduction

The pathogenesis of *Shigella flexneri* requires a functional type III secretion apparatus (TTSA) to provide a conduit for injecting host-altering effector proteins into the membrane and cytoplasm of the target cell (45). Type III secretion systems (TTSSs) are a shared virulence determinant for many Gram-negative animal and plant pathogens.They are used to subvert normal cellular functions (24, 92). The *Shigella* TTSA is composed of a basal body that spans both bacterial membranes and an exposed needle that is a polymer of MxiH. The needle is 50 nm in length, has an outer diameter of 7.0 nm, and possesses an inner channel that is 2.0-3.0 nm in diameter (17, 38).

Invasion plasmid antigen D (IpaD) was recently discovered to localize to the tip of the TTSA needle where it controls type III secretion (TTS) and directs the insertion of the translocator proteins IpaB and IpaC into the host cell membrane (63, 146). From its position at the TTSA needle tip, IpaD is initially responsible for recruiting and stably maintaining IpaB to this site in the presence of bile salts (137). This step in *Shigella* TTS will be discussed more thoroughly in Chapter 5, however, it is clear in this series of events that interactions between IpaD and MxiH that are responsible for tip complex stabilization are critical for *Shigella* pathogenesis (63, 137).

The high resolution crystal structures of MxiH and IpaD were recently reported (55, 100). MxiH monomers possess a helix-turn-helix head group with an elongated C-terminal helix (55). The head group is stabilized by hydrophobic contacts between residues at the interface between the two helices that flank a central PSNP loop (55). The MxiH structure resembles the *B. pseudomallei* needle monomer (BsaL) structure which was the first in this protein class to be determined.

The TTSA needle appears to pack by polar contacts between the individual MxiH monomers with the PSNP loop facing outward and upward relative to the central channel (55). In contrast to MxiH, IpaD has a more complex structure that resembles a dumbbell in its shape (101). IpaD has a central coiled-coil that defines the handle of the dumbbell and is flanked at each end by distinct N- and C-terminal domains (101). This shape defines the tip proteins as a unique class and appears to be important for IpaD localization at the tip of the needle (62, 63). Based on *in silico* modeling of the *Yersinia* tip complex protein LcrV on the reconstructed *Shigella* MxiH needle tip, the LcrV N-terminal globular domain and the C-terminal end of the coiled-coil both have a role in docking LcrV on the needle (55). Although the IpaD structure shows that its N-terminal domain can mimic a MxiH molecule and thereby serve to chaperone the C-terminal coil in the bacterial cytoplasm by preventing the premature association of MxiH and IpaD, how IpaD docks onto the MxiH needle could not be resolved even after the structure of the two proteins became available (101). Nevertheless, interactions in addition to those that dictate needle assembly would be expected to be involved in maintaining IpaD at the

needle tip. Therefore, the structural basis for the interaction between MxiH and IpaD was explored.

The data presented here show that specific residues within the MxiH head group are located at the MxiH-IpaD interface. These residues are needed for stable maintenance of IpaD at the TTSA needle tip but are distinct from those needed for needle assembly. The work presented here provides an initial step in understanding this important protein-protein interaction at the TTSA needle tip prior to receipt of any signal for TTS induction.

Results

MxiH binding to IpaD. IpaD localizes at the tip of the *Shigella* TTSA needle (63). Although it has been shown that the C-terminal coil of IpaD is required for its maintenance at the MxiH needle tip, no such data are available to directly demonstrate the structural role of the TTSA needle protein in the IpaD-MxiH interaction. Using fluorescence polarization (FP) analyses, we were able to detect *in vitro* protein-protein interactions between MxiH and IpaD (Figure 7). IpaD was labeled with fluoresesin maleimide (FM) at C322, which provides the only free thiol in IpaD. C322 is 10 residues away from the IpaD C-terminus, and it is this portion of IpaD that mediates its stable association with the *Shigella* TTSA needle tip (63). The initial polarization value for IpaD was 247.9 ± 0.7 mP, a high value that is consistent with the attachment of a fluorescent probe to a large (36.6-kDa) protein. FM-IpaD association with MxiH resulted in a

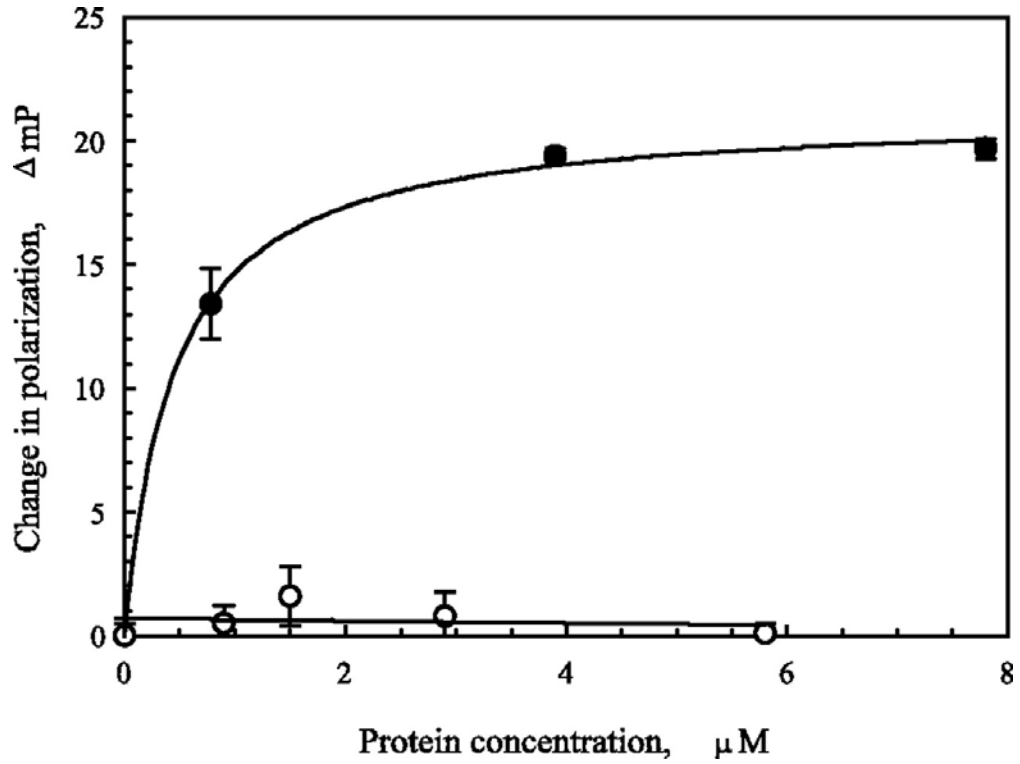

Figure 7. Interaction of IpaD with MxiH. FM-labeled IpaD (200 nM) was incubated with $MxiH^{C\Delta5}$ (closed circle) or IpgC (open circle). The change in the polarization value (ΔmP) of the FM-IpaD was measured as a function of MxiH concentration. Addition of anti-IpaD IgG resulted in a maximum ΔmP of 30.8 (n = 3) (190). These experiments were performed with the help of Dr. W. D. Picking.

measured increase of 21.2 mP whereas no change was seen upon the addition of the negative control protein IpgC, the chaperone for the translocator proteins IpaB and IpaC (Figure 7). Because the maximum mP achieved by the addition of anti-IpaD IgG is 30.8 mP, the change in polarization upon addition of MxiH appears to represent a significant change based on the fact that its mass is only one fourth that of IpaD. The fact that a detectable change is observed most likely stems from the previous observation that IpaD association with the MxiH needle involves the C-terminus of IpaD and this is near where the FM labeling occurs (63). The FP data presented here thus indicate that IpaD and MxiH interactions are detectable *in vitro*. Furthermore, the binding data suggest that the two proteins have an apparent dissociation constant (Kd) in the micromolar range (Figure 7).

Identification of MxiH$^{C\Delta5}$ residues interacting with IpaD by NMR spectroscopy.

We used NMR chemical shift mapping to identify the MxiH$^{C\Delta5}$ residues that contact IpaD based on the reasoning that the MxiH$^{C\Delta5}$-IpaD interaction should result in changes in the NMR resonances of MxiH$^{C\Delta5}$. Because the smaller MxiH$^{C\Delta5}$ (8.3 kDa) is more amenable to NMR characterization compared with IpaD, we titrated unlabeled IpaD into ^{15}N-labeled MxiH$^{C\Delta5}$ and monitored the changes in the chemical shifts of MxiH$^{C\Delta5}$ by acquiring several ^{15}N HSQC spectra with increasing amounts of IpaD. Indeed, there are NMR peaks of MxiH$^{C\Delta5}$ that shift upon adding IpaD (Figure 8). We assigned the resonances of free MxiH$^{C\Delta5}$ using standard three-dimensional NMR experiments (Figure 9). Assigning the NMR peaks of free MxiH$^{C\Delta5}$ was challenging because of the broad peaks between 7.8-8.5

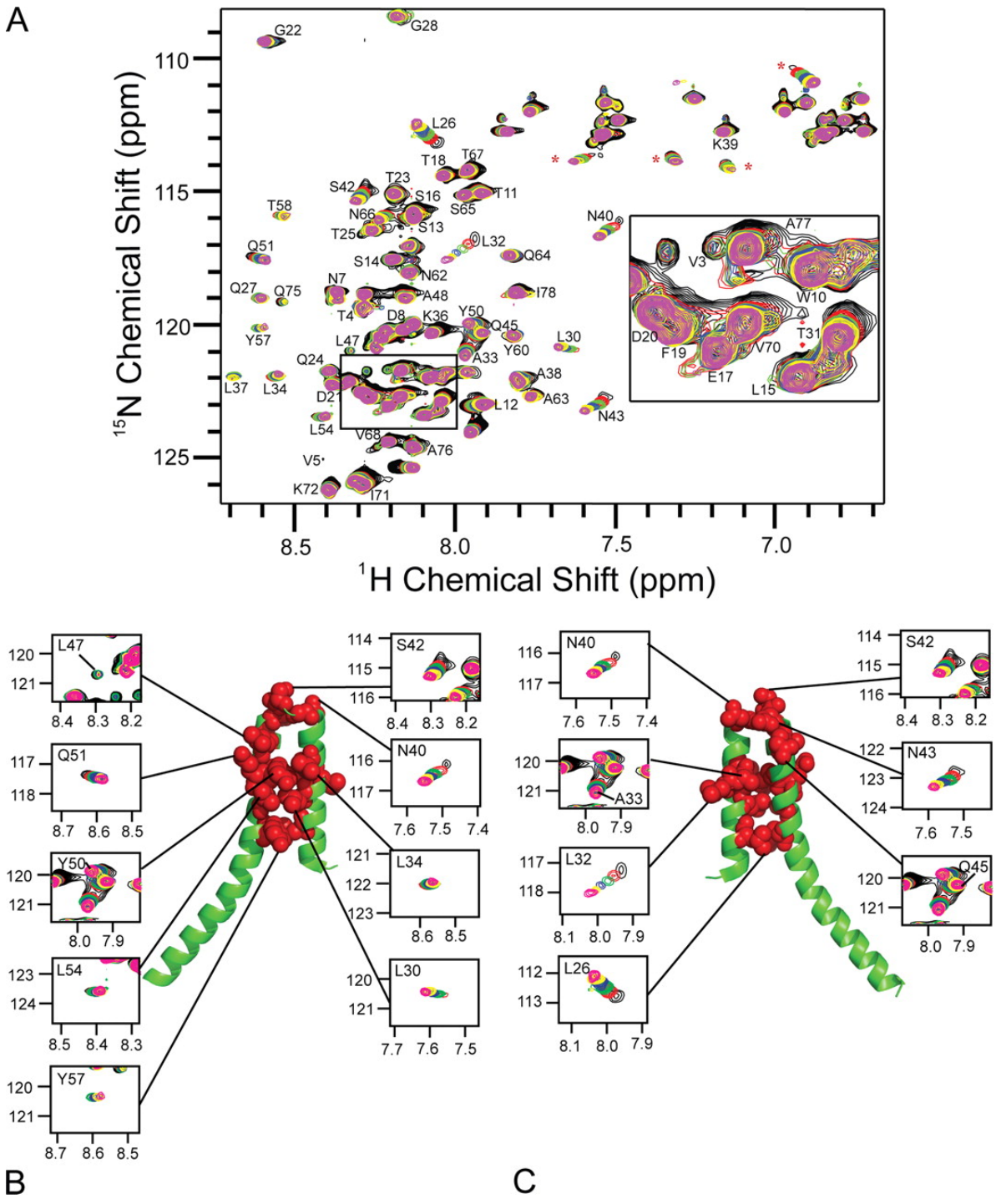
A
^{15}N Chemical Shift (ppm)
^{1}H Chemical Shift (ppm)
B
C

Figure 8. Identification of MxiH Residues That Interact with IpaD by NMR Spectroscopy (continued). A) Titration of ^{15}N-MxiH$^{C\Delta5}$ with increasing amounts of unlabeled IpaD. Overlay of six protein-nitrogen correlation spectra (^{15}N HSQC) at various MxiH$^{C\Delta5}$:IpaD molar ratios (*black*, 0; *red*, 0.5; *green*, 1.0; *blue*, 2.0; *yellow*, 4.0; *magenta*, 8.0). The actual MxiH$^{C\Delta5}$: IpaD concentrations used are as follows (in μM): *black* (800:0), *red* (320:160), *green* (200:200), *blue* (110:220), *yellow* (60:240), and *magenta* (30:250). Peaks with * could not be assigned because they did not show cross-peaks on the ^{13}C plane in the three-dimensional data sets (HNCA, CBCACONH, and HNCACB) used in the backbone assignments. The *insert* shows an expansion of a crowded region of the ^{15}N HSQC. MxiH$^{C\Delta5}$ contains a single tryptophan, and the side chain Trp-10 N$^{\varepsilon1}$ resonance (at ^{15}N = 129.375 and ^{1}H = 10.076) was not perturbed upon addition of IpaD and therefore is not shown. B) The HSQC peaks of individual residues affected by IpaD binding are shown separately for clarity. MxiH residues that are perturbed by IpaD are mapped on the surface of the crystal structure of MxiH (Protein Data Bank code 2CA5). C) The back side view of panel B is shown (190).

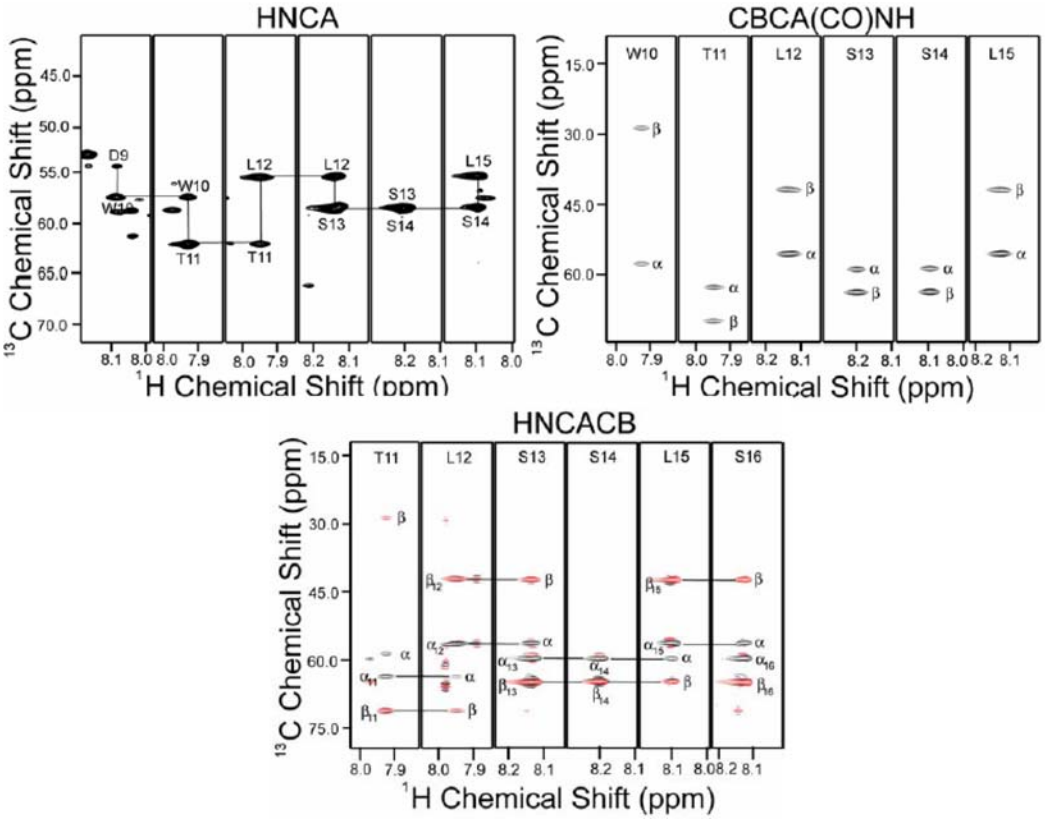

Figure 9. 3D NMR experiments of free MxiH$^{C\Delta5}$. A) HNCA spectra of MxiH, shown as ^{13}C, ^{1}H strips for residues W10-L15. Each strip shows the Cα of the current residue and the Cα of the preceding residue. HNCA, together with CBCA(CO)NH and HNCACB, confirms the backbone assignments for W10-L15. The backbone assignments for the rest of the protein were obtained in a similar manner. B) CBCA(CO)NH spectra of MxiH, shown as ^{13}C, ^{1}H strips for residues W10-L15. CBCA(CO)NH shows the Cα and Cβ of the preceeding residue together with backbone amide of the current residue. C) HNCACB spectra of MxiH, shown as ^{13}C, ^{1}H strips, for residues T11-S16. Each strip shows the Cα and Cβ of the preceeding and current residue and the amide resonances of the current residue. The Cα and Cβ have opposite phases (shown as black and red peaks). The spectra were acquired using a 0.8 mM ^{15}N, ^{13}C-MxiH$^{C\Delta5}$ at 800 MHz and 25°C (190).

ppm in the center of the two-dimensional ^{15}N HSQC spectra (Figure 8A). The narrow proton chemical shift range is consistent with the predominantly α-helical structure of $MxiH^{C\Delta5}$. The disordered N-terminal 19 residues in the X-ray structure of $MxiH^{C\Delta5}$ most likely also contribute to the broad peaks between 7.8-8.5 ppm (55). Nevertheless, using three-dimensional HNCA, CBCA(CO)NH, and HNCACB (Figure 9), we assigned 62 of 78 backbone amides of $MxiH^{C\Delta5}$.

Upon adding IpaD to labeled $MxiH^{C\Delta5}$, many of the $MxiH^{C\Delta5}$ chemical shift peaks were perturbed. Further addition of IpaD changed peak positions even more, indicating that binding was in fast exchange NMR time scale. This behavior is consistent with the micromolar binding affinity obtained in fluorescence polarization experiments. The peaks of the PSNP loop residues (N40, S42, N43, and Q45) and the head group residues (L26, L30, L32, A33, L34, Y50, Q51, L54, and Y57) clearly shifted to a different part of the spectrum (Figure 8). The latter set of residues form a contiguous surface (Figure 8B and 8C) when mapped on the X-ray crystal structure of $MxiH^{C\Delta5}$ (55). The side chains of L30, L34, Y50, Q51, L54, and Y57 form one face of the contiguous surface (Figure 8B), and the side chains of L26, L32, and A33 are on the "backside" (Figure 8C). Therefore, it is likely that the main site of IpaD binding on $MxiH^{C\Delta5}$ is the surface formed by residues in the contiguous surface and the PSNP loop.

***In Vivo* analysis of MxiH mutant strains.** NMR chemical shift mapping of the MxiH homolog from *Burkholderia pseudomallei*, BsaL, showed that the BsaL residues equivalent to MxiH L30, L54, and Y57 are part of the needle monomer-monomer surface

contact (141). Therefore, we propose that there are two overlapping sites on MxiH: one for IpaD binding and another for MxiH binding and that the L30-L54-Y57 surface (see Figure 8B) is common for both IpaD and MxiH binding. Hence, MxiH mutations were designed to disrupt IpaD binding while attempting to maintain the MxiH-MxiH association. Thus, not all residues that showed chemical shift changes upon IpaD addition were mutated. Residue Q51 was previously mutated (Table 3) and it had no effect on IpaD association with the *Shigella* surface (63, 107). Mutation of S42 was also shown to have no effect on MxiH function (107). Residues that are not conserved among needle proteins from different pathogens were not mutated since the side chain composition at these positions does not appear to be critical. This was the case for L26, L32, A33, and Q45 (55, 182). Where NMR assignments were lacking, mutations were not introduced because subsequent interpretation of the data would be difficult. Most importantly, those residues that appeared to have a role in the packing of MxiH monomers were not mutated because the mutations would be expected to disrupt needle assembly (141). Therefore, we did not mutate the MxiH residues L30, L54, Y57 which appear to be necessary for MxiH-MxiH contacts. In contrast, L47 showed minor chemical shift changes; however, it is next to the PSNP loop and near Y50. Likewise, it is invariant among the needle proteins of *Shigella*, *Salmonella*, and *Burkholderia*. In the MxiH monomer structure, the side chain of L47 (which is on helix 2) is oriented toward the surface of the two-helix bundle (Figure 8B) (55). This suggests that L47 is not needed in maintaining the hydrophobic core that dictates the overall fold of the MxiH structure and thus may be

Table 3. MxiH mutants used in this study

Mutants[a]	**Reason for selection**[b]
$MxiH^{L34A}$	Minor chemical shift, somewhat conserved
$MxiH^{N40A}$	Major chemical shift, somewhat conserved
$MxiH^{N43A}$	Major chemical shift, conserved
$MxiH^{N43K}$	Same as above, introduces bulky charged group
$MxiH^{L47A}$	Minor chemical shift, highly conserved
$MxiH^{L47D}$	Same as above, introduces charged group
$MxiH^{Y50F}$	Major chemical shift, highly conserved, preserves phenyl ring
$MxiH^{Y50L}$	Same as above, eliminates phenyl ring, preserves hydrophobic side chain
$MxiH^{Q51A}$	Previously shown to retain function and does not interfere with IpaD localization at needle tip (63, 107)

a) Mutations were introduced into full-length MxiH for complementation analysis using *S. flexneri* SH116. A $MxiH^{C\Delta5}$ version with a C-terminal His_6 was then made for L47A, L47D, Y50F, Y50L, and Q51A for generation of recombinant protein in *E. coli* BL21 (DE3). The recombinant protein was used for analyzing interactions with FM-labeled IpaD by fluorescence polarization

b) Chemical shifts refer to the NMR shifts described in Fig. 11. Conserved is a measure of the sequence conservation seen among MxiH and its needle protein homologues from *Salmonella typhimurium* (PrgI) and *B. pseudomallei* (BsaL)

involved in IpaD binding. Therefore, L47 was mutated to determine its potential role in anchoring IpaD to the *Shigella* TTSA needle tip. N40 and N43 of the MxiH PSNP loop and L34, L47, and Y50 of the contiguous surface were selected for site-specific mutations. Mutations were introduced to give MxiH^{L34A}, MxiH^{N40A}, MxiH^{N43A}, MxiH^{N43K}, MxiH^{L47A}, MxiH^{L47D}, MxiH^{Y50F}, MxiH^{Y50L}, and MxiH^{Q51A} (Table 3). For residues N43, L47, and Y50, two substitutions per residue were introduced to explore the importance of side chain composition in needle tip association. MxiH^{N43A} and MxiH^{N43K} were designed to test the impact of replacing a polar residue with either a smaller nonpolar or a somewhat larger and positively charged residue. MxiH^{Y50F} maintained the phenyl ring while MxiH^{Y50L} maintained a hydrophobic side chain. In contrast, the MxiH^{L47A} mutation decreased the length of the hydrophobic side chain while MxiH^{L47D} changed the polarity of the region by adding a negative charge.

The ability of the MxiH mutants to complement the *S. flexneri mxiH* null strain SH116 was assessed using established phenotypic assays with the data summarized in Table 4 (63). First, invasion of Henle 407 cells and contact-mediated hemolysis were used to assess the proper introduction of IpaB/IpaC translocons into targeted cells, which is dependent upon IpaD localization to the TTSA needle tip (17, 63, 137, 146). Second, overnight secretion of Ipa proteins was used to provide a measure of functional needle formation. Excessive overnight secretion can provide a measure of the loss of IpaD at the needle tip because an *ipaD* null mutant and IpaD mutants that fail to localize at the needle tip are known to be hypersecretive (63, 122, 146). Lastly, induced (rapid) secretion of Ipa

Table 4. Phenotype of MxiH mutants

Mutant strain[a]	**Exposed IpaD/MxiH**[b]	**Invasion**[c]	**Hemolysis**[d]	**Uninduced/induced secretion**[e]
Wild type	+/+	100 ± 7[f]	100 ± 14[g]	+/++
mxiH null	–/–	<1 ± 1	2 ± 1	–/–
MxiH$^{C\Delta5}$	–/–	0 ± 0	0 ± 0	–/–
ipaD null	–/+	0 ± 0	0 ± 0	+++/–
MxiH^{L34A}	+/+	44 ± 10	22 ± 5	+/++
MxiH^{N40A}	+/+	82 ± 5	17 ± 3	+/++
MxiH^{N43A}	+/+	77 ± 7	25 ± 3	+/++
MxiH^{N43K}	50%/+	8 ± 3	2 ± 2	++/+
MxiH^{L47A}	–/+	<1 ± 1	2 ± 1	+++/–
MxiH^{L47D}	–/+	<1 ± 1	1 ± 0	+++/–
MxiH^{Y50F}	20%/+	57 ± 8	9 ± 2	++/+
MxiH^{Y50L}	50%/+	51 ± 6	12 ± 2	++/+
MxiH^{Q51A}	+/+	97 ± 8	106 ± 5	++/++

Table 4. Phenotype of MxiH mutants (continued)

a) Wild type is pRKMxiH/SH116, the *mxiH* null mutant strain is SH116, and the *ipaD* null mutant is SF622. All other strains are SH116 transformed with the plasmid encoding one of the MxiH point mutants as described here.

b) Surface localization of IpaD and MxiH was determined by immunofluorescence microscopy. At least 100 bacteria in each of three randomly selected fields were counted ($n = 3$). In most cases, surface localization was either seen on all bacteria or none in a given field. For some mutants, reduced overall fluorescence was visualized and a reduced number of bacteria were seen with IpaD on their surfaces. In these cases, an approximate percentage of cells having surface IpaD is given.

c) Invasion is relative to pRKMxiH/SH116 ± S.D. ($n = 3$).

d) Contact-mediated hemolysis is relative to pRKMxiH/SH116 ± S.D. ($n = 3$).

e) Uninduced secretion is the secretion of TTSS proteins (IpaB and IpaC) into the culture medium during overnight growth. Induced secretion is the secretion of TTSS proteins by bacteria after a 30-min incubation with Congo red (63, 107).

f) Raw value of invasion of Henle cells by pRKMxiH/SH116 is 237 ± 15 colonies.

g) Raw value of contact-mediated hemolysis of pRKMxiH/SH116 is 2.8 ± 0.02 (A_{545}).

proteins into culture supernatants upon adding Congo red was examined because this activity is lost in *ipaD* null mutants and it thus correlates with the loss of IpaD at the TTSA needle tip (63). In contrast, loss of needle polymerization results in no Ipa secretion or detection of MxiH on the bacterial surface (63, 107, 137). Therefore, if a MxiH mutant fails to maintain IpaD at the needle tip, there will be no invasion, no contact hemolysis, uncontrolled overnight secretion, a loss of Congo red-induced Ipa protein secretion, and no IpaD detected on the bacterial surface (63). Because the MxiH mutants were designed not to interfere with MxiH polymerization, however, MxiH should be detected on the *Shigella* surface and overexpression of *mxiH* should give rise to the formation of long versions of the TTSA needle that can be sheared from the bacterial surface and visualized by transmission electron microscopy (TEM) with negative staining. The phenotypes of the *mxiH* mutant strains are presented in Table 4.

N40 and N43, which are part of the PSNP loop, were mutated because they showed some of the largest chemical shift perturbations upon addition of IpaD (Figure 8). Previous results concluded that the polar residues in the PSNP region can tolerate mutation to Ala and still give rise to functional needle tip complexes (107). Likewise, although contact-mediated hemolysis was reduced for N40A and N43A, these mutations had minimal effects on needle tip complex formation as determined by surface localization of IpaD (Table 4). In contrast, mutation of N43 into the somewhat larger and basic residue Lys decreased needle tip complex formation (Table 4). The decreased ability for this strain to stably maintain IpaD at the needle tip (50% reduction) resulted in a lack

of secretion control as well as loss of the ability for *Shigella* to invade Henle 407 cells and lyse erythrocytes (Table 4). Thus, the PSNP loop interacts directly with IpaD and is required for the formation of the MxiH-IpaD tip complex.

Adjacent to the PSNP loop, L34, L47, Y50, and Q51 form a contiguous surface on the two-helix bundle and were perturbed upon adding IpaD (Figure 8B). Although the chemical shift of L34 was small, it lies within the contiguous surface, suggesting that L34 could contribute to IpaD binding. Indeed, the L34A mutation partially reduced invasion and hemolysis, suggesting that it has a minor effect on IpaD binding to the needle. Q51A has been characterized and found to have only a partial defect in secretion control, indicating a minor deficiency in IpaD affinity for MxiH (107). In contrast to L34 and Q51, mutation of L47 and Y50 had significant consequences with regard to *S. flexneri* phenotype and the observed interactions with IpaD *in vitro*. It is also noteworthy that L47 and Y50 are highly conserved among the needle proteins from different species. Both L47A and L47D mutants abolished IpaD surface presentation, resulting in a noninvasive, nonhemolytic strain that completely lacks secretion control (Table 4). These mutations, however, did not affect MxiH-MxiH interactions since they were capable of needle formation as detected by immunofluorescence microscopy (Table 4) as well as electron microscopy (see Figure 10A for L47D). When recombinant $MxiH^{C\Delta5}$ proteins possessing mutations at L47 were prepared so that their interaction with FM-labeled IpaD could be monitored *in vitro* by FP analysis, a detectable decrease in binding to IpaD was observed (Table 5). Thus, L47 is critical for IpaD-MxiH binding and the proper assembly of IpaD

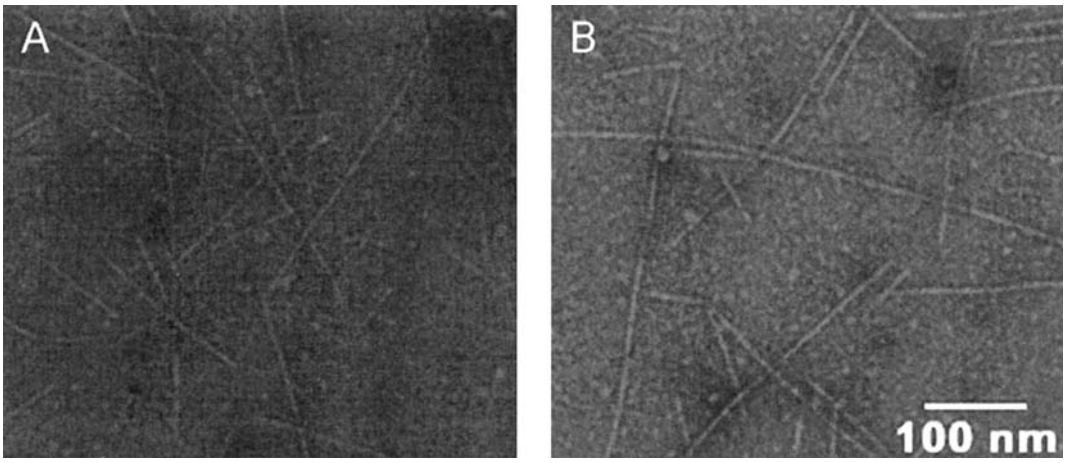

Figure 10. Transmission electron micrographs of sheared needles from *S. flexneri* SH116 expressing MxiH^{L47D} (*A*) or MxiH^{Y50F} (*B*) from a pRK2 plasmid. Needles were sheared from bacteria in log phase by passage through a 25-gauge needle. The needles were applied to carbon-coated Formvar grids and negatively stained with 2% uranyl acetate (190).

Table 5. Association of MxiH mutant proteins with FM-IpaD by fluorescence polarization.

Mutant protein	Maximum observed ΔmP[a]	Apparent dissociation constant[b]
Wild type	24.6 ± 2.0	0.48
$MxiH^{L47A}$	7.8 ± 0.7	2.47
$MxiH^{L47D}$	–1.7 ± 0.9	ND
$MxiH^{Y50F}$	7.6 ± 0.4	1.30
$MxiH^{Y50L}$	12.8 ± 0.8	2.48
$MxiH^{Q51A}$	24.7 ± 0.9	0.65

[a] The change in polarization is presented in millipolarization units

[b] The apparent dissociation constant was determined using 25 nM FM-IpaD using Sigmaplot®

ND – not determined

at the needle tip. Y50 is near L47 on helix α2 and its phenyl ring forms a network of hydrophobic contacts with residues on helix α1 that contribute to the stability of the two-helix bundle (55). The hydroxyl group of Y50 is pointed toward the MxiH surface and is not involved in any intramolecular contacts (55). Therefore, the Y50 hydroxyl group is not required in stabilizing the overall fold of the MxiH two-helix bundle. Structurally, a Phe or Leu in this position would be expected to maintain the hydrophobic core and the overall fold of the two-helix bundle, yet Y50 is invariant among the needle proteins of *Shigella, Salmonella*, and *Burkholderia*. Thus, the mutations Y50F and Y50L were made and the phenotypes of each mutant strain determined (Table 4). Y50L and Y50F resulted in a 50-80% reduction in IpaD surface presentation, which negatively affects invasion, hemolysis, and secretion control (Table 4). Both Y50F and Y50L, however, form stable needles *in vivo* when examined by either immunofluorescence (Table 4) or electron microscopy (Figure 10). As with L47, the recombinant $MxiH^{C\Delta5}$ proteins possessing the Y50 mutations were purified to examine their binding interaction with FM-labeled IpaD. Indeed, like the L47 mutants, the Y50 mutants have a noticeable increase in the apparent dissociation constant, with Y50F being 3-fold higher and Y50L being 5-fold higher (Table 5). Thus, although the hydroxyl group has a role in the stable maintenance of IpaD at the TTSA needle tip, the hydrophobic interaction mediated by the phenyl ring appears to contribute more substantially to the *in vitro* interaction between IpaD and $MxiH^{C\Delta5}$. Taken together, the data indicate that key residues of the contiguous face and those of the PNSP loop of MxiH contribute to the proper binding, maintenance,

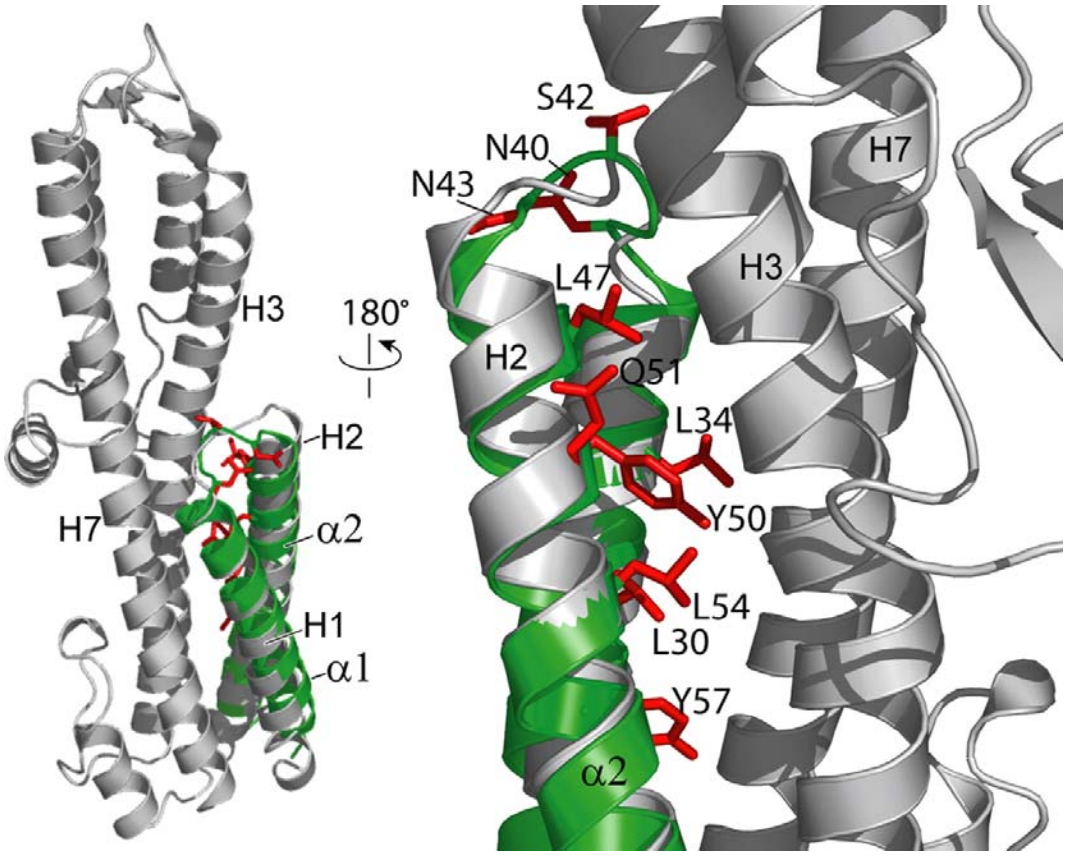

Figure 11. Model of MxiH-IpaD binding. Left) The two-helix bundle of MxiH (*green*, α1 and α2) can be superimposed with helices H1 and H2 of IpaD (*gray*) with a C^{α} root mean square deviation of 3.2 Å. Right) The MxiH-IpaD binding interface is expanded, and the figure is rotated by 180° relative to the orientation in the left panel. The side chains of MxiH residues (L30, L34, Y50, L54, Y57) that experienced NMR chemical shift perturbation upon titration of IpaD as well as L47 are all oriented toward helices H3 and H7 of IpaD. The loop residues (N40, S42, and N43, *red*) also showed chemical shift perturbations (190).

and function of the MxiH-IpaD tip complex (Figure 11).

Discussion

Previously, we have shown that the C-terminal coil of IpaD is required for its association with the MxiH needle and that the N-terminal globular domain is external to the needle (63). Modeling using the recently solved individual crystal structures of MxiH and IpaD, however, was unable to explain how IpaD docks at the top of the MxiH needle other than that the orientation is likely to be the same as that predicted for LcrV (55, 101, 129). Based on the MxiH and IpaD crystal structures, Johnson *et al.* proposed a model for the interaction of MxiH with IpaD based on the fact that the IpaD N-terminal domain is structurally similar to MxiH and therefore could serve as an intramolecular cytoplasmic chaperone that prevents the interaction of IpaD with MxiH prior to IpaD's recruitment to the bacterial surface (101). The IpaD N-terminal helices H1 and H2 pack together in such a way that the MxiH structure can be superimposed on the MxiH two-helix bundle (α1 and α2) with a C^{α} root mean square deviation of 3.2 Å (Figure 11, left). This structural similarity is striking considering that the C^{α} root mean square deviation between the two needle homologs BsaL and MxiH is also 3.2 Å (182). This suggests that IpaD has a built-in surface that complements the size and shape of that portion of MxiH that is responsible for maintaining IpaD at the TTSA needle tip. The NMR chemical shift-mapping results provide the first biochemical data to support such a model in that the MxiH residues that are perturbed upon adding IpaD appear to form a contiguous face

(Figure 11, right) that may actually be contacting a yet unidentified surface on IpaD and this interaction is blocked in the bacterial cytoplasm by the presence of the IpaD N terminus. MxiH residues within the region capable of interacting with IpaD would include the side chains of L47 and Y50, which upon mutation in this study abolished or severely perturbed IpaD localization. Furthermore, in this model, the MxiH PSNP loop would directly contact helices H3 and H7 of IpaD. Such an interaction would be sterically impossible based upon the crystal structure of full-length IpaD unless the N-terminal domain were moved away upon tip complex assembly. Indeed, the chemical shifts of N40, S42, and N43 demonstrate an interaction between the PSNP loop and IpaD does exist, suggesting that it is possible that the N-terminal domain moves away upon tip complex assembly. Unfortunately, at this time it is impossible to predict how the N terminus (helix H1-H2') "swings away" during tip complex assembly to permit IpaD docking atop the MxiH needle. Because it has been postulated that the needle channel cannot accommodate a fully folded IpaD, it is possible that it travels through the needle channel in a partially unfolded manner and that refolding at the needle tip forces it to assume a conformation that is compatible with the MxiH-IpaD interactions demonstrated here (5, 55, 61). High resolution structures are also available for the MxiH/IpaD counterparts in *B. pseudomallei*, BsaL/BipD, and a similar BsaL-BipD binding model can be generated in which the two-helix bundle of BsaL can be superimposed to the N-terminal helices of BipD, also with a C^{α} root mean square deviation of 3.2 Å (Dr. Roberto De Guzman, unpublished results). The NMR structure of PrgI shows that it is

structurally homologous to MxiH and BsaL (182). The homology of SipD with BipD and IpaD suggests similarities in the structure of SipD. This suggests that the model of MxiH-IpaD or BsaL-BipD interaction might indicate a common feature of needle tip interaction for *Shigella*, *Salmonella*, and *Burkholderia* TTSAs.

CHAPTER 5: NMR Analysis of the Influence Deoxycholate (DOC) Binding has on the Structure of Invasion Plasmid Antigen D (IpaD) of *Shigella flexneri*

Introduction

Invasion Plasmid Antigen D (IpaD) has long been known as one of three translocators for the *Shigella* TTSS, which are essential for forming translocon pores in host cell membranes. These translocator pores (translocons) are required for triggering uptake by host cells and for later effector protein injection into the host cytoplasm. Although IpaB and IpaC are the translocator proteins that possess hydrophobic regions and are actually inserted into the eukaryotic membrane, IpaB/IpaC translocon pore formation depends on IpaD. How IpaD carries out this function was not known until it was recently discovered that IpaD is localized at the tip of the needle prior to type III secretion induction (63). Discovery of IpaD's position at the needle tip provided the first evidence that it serves as a conduit that connects the bacterial needle and the translocon pore embedded in the eukaryotic host membrane.

IpaD is a dumbbell shaped protein with two globular domains flanking a central coiled-coil that stabilizes the protein (100). The N-terminal globular domain of this 37 KDa protein consists of three α-helices and it most likely resides near the needle tip following IpaD placement at the TTSA needle tip. A long C-terminal α-helix extends the entire length of the protein and packs against a second long α-helix in the middle of the

protein. The second long helix is required for interaction with MxiH which helps to anchor IpaD at the needle tip (190). The distal globular domain is made of a few short α-helices and ß-strands that most likely point away from the needle tip (100, 137). Immunoelectron microscopy shows that only IpaD is presented at the needle tip prior to activation of the TTSS. The other two translocator proteins, IpaB and IpaC, are not seen at the needle tip at this early stage in TTSA biogenesis (63).

It has been known for some time that growing *Shigella* in Tryptic Soy Broth (TSB) containing bile salts increases *Shigella*'s adherence to and invasion of cultured HeLa cells (148). As mentioned above, IpaD is the only Ipa protein found exposed at the tip of the TTSA needle when *Shigella* are grown to log phase in TSB, however, when the bacteria are incubated in the presence of the bile salt deoxycholate (DOC), IpaB is recruited to the needle tip. The recruited IpaB is stably co-localized with IpaD at the needle tip to form a ternary complex consisting of MxiH, IpaD, and IpaB (137). As mentioned above, IpaB and IpaC form a translocon pore embedded in the host membrane which serves as the portal through which later effectors are injected directly into host cell cytoplasm. Because IpaB is hydrophobic and is known to bind to host membrane components involved in the bacteria entry process, the stable presence of IpaB at the TTSA needle tip may be essential for preparing the bacteria sensing host cell (90, 114, 164). IpaB recruitment to the needle tip is not accompanied by induction of TTS as determined by analysis of *Shigella* culture supernatants.

IpaD present at the TTSA needle tip is proposed to function as a sensor of environmental signals to trigger the first step of type III secretion. IpaB is recruited to the *Shigella* surface where it stably co-localizes with IpaD within minutes following DOC addition to the medium (137). Bile salts are natural detergents within the human small intestine and they represent an attractive environmental trigger for inducing IpaB localization to the TTSA needle tip as *Shigella* passes through the human small intestine. This would suggest that IpaB is the TTSS protein that senses actual host cell contact, perhaps by interacting with host membrane components, to trigger IpaC secretion into host cytoplasmic membrane where it and IpaB form the translocon pore. Our hypothesis is that bile salts bind directly to IpaD and this interaction causes a conformational change in IpaD that leads to the recruitment of IpaB to the bacterial surface.

IpaD is a stable and highly soluble protein that is convenient to work with *in vitro*. Fluorescence polarization (FP) experiments using unlabeled IpaD titrated into FITC-DOC were initially performed to demonstrate whether there is an interaction between DOC and IpaD (165). The polarization value of FITC-DOC increased upon the addition of IpaD, suggesting that they indeed interact. Molecular modeling suggested that DOC binds to the middle of the central coiled-coil of IpaD where the top of the N-terminus packs against the coiled-coil. NMR spectroscopy was also applied to examine this interaction by using unlabeled DOC titrated into ^{15}N-labeled IpaD. Chemical shift perturbation of IpaD ^{1}H-^{15}N correlation indicates the binding of DOC to IpaD also influences the protein's conformation. Backbone assignment of IpaD was made in order to identify the IpaD

residues potentially involved in this interaction. Identified IpaD residues that may be essential for DOC binding were chosen and mutated to potentially disturb DOC binding while not altering IpaD's stable presence at the TTSA needle tip.

Result

Deoxycholate interacts with IpaD based on florescence polarization measurements. When *S. flexneri* is grown to early log phase in TSB, IpaD is already present at the tip of the TTSA needles. IpaB and IpaC are not presented on the bacterial surface under these conditions. When DOC is added in the medium, IpaB (but not IpaC) was observed on the bacterial surface within 15 min where it co-localized with IpaD at the tip of the TTSA needle (C. Epler, manuscript submitted). Thus, we hypotheze that DOC binds to IpaD, causing a conformational change in the protein that promotes the mobilization of IpaB to the *Shigella* surface and, more specifically, the co-localization of IpaB with IpaD at the TTSA needle tip. This is not accompanied by full induction of type III secretion and this may represent the first discrete step in type III secretion induction.

To demonstrate that DOC's effects on the TTSS are due to the direct interaction between IpaD and DOC, fluorescence polarization (FP) measurements were used to measure the interaction *in vitro*. FP spectroscopy measures the rotational diffusion of a fluorescent molecule in solution. Small molecules rotate faster than large molecules in solution, which results in smaller polarization value. In contrast, large molecules have a larger polarization value. The association of a small fluorescent molecule with a larger

nonfluorescent molecule will result in an increase in the overall volume size of the fluorescent complex, thus leading to an increased polarization value. In this case, adding unlabeled IpaD into fluorescein-labeled DOC should result in a significant polarization value change since IpaD is a much larger molecule than DOC, thus providing a confident measure of the interaction. DOC was labeled with amine-reactive fluorescein-4-isothiocyanate after adding a diaminohexyl tether to the carboxyl group of DOC. This new DOC derivative, called FITC-DOC, was synthesized by Dr. Ken Stensrud (Department of Chemistry, University of Kansas) specifically so that the IpaD-DOC interaction could be examined *in vitro* by FP analysis. FITC-DOC was added into *Shigella* TSB medium to determine whether attachment of the fluorophore affected the biological activity. The FITC-DOC was still able to stimulate the recruitment of IpaB to the *Shigella* surface (165).

FP measurements were obtained using a Beacon fluorescence polarimeter (Panvera Corp.) with assistance from Dr. W. D. Picking and P. R. Adam (Department of Molecular Biosciences, University of Kansas). IpgC, the cytoplasmic chaperone for translocators IpaB and IpaC, served as the negative control in these experiments (Figure 12). A constant concentration of FITC-DOC (30 nM) in PBS was mixed with increasing concentrations of protein (μM range). The polarization value change of FITC-DOC was monitored as a change in millipolarization units (ΔmP) and plotted against protein concentration. The initial polarization value for FITC-deoxycholate was 27.5 mP, which is consistent with the relatively small size of FITC-DOC. When different proteins were

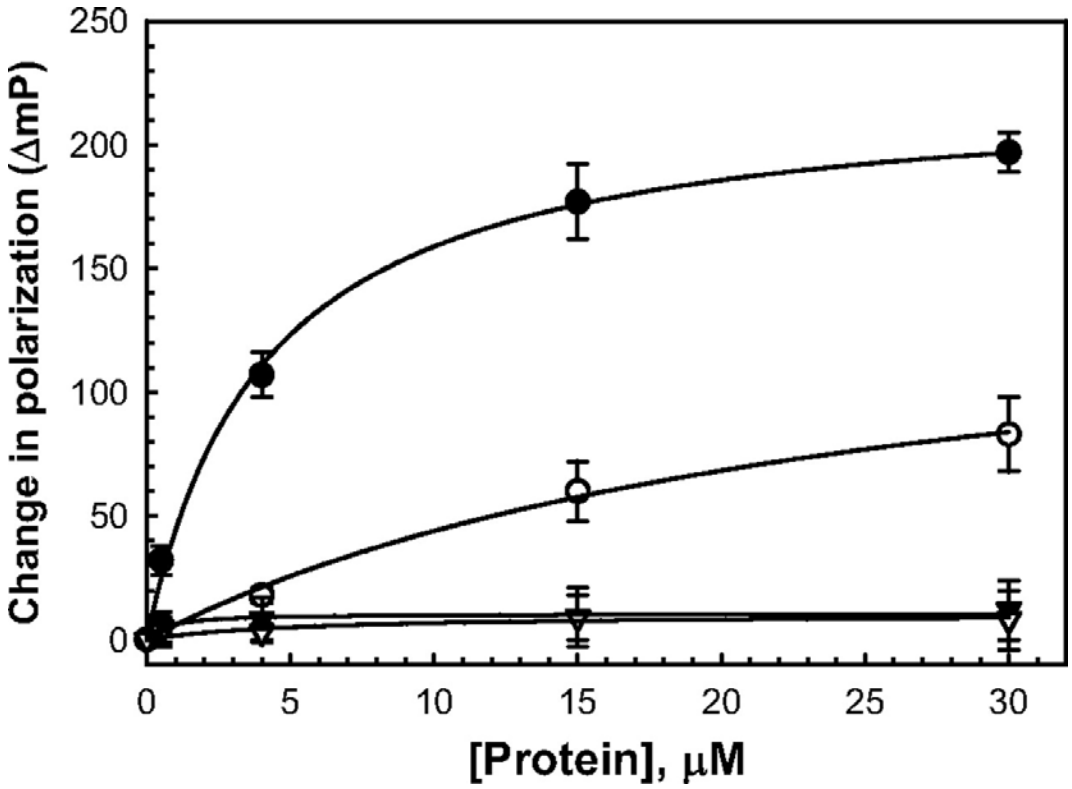

Figure 12. Fluorescent polarization change of FITC-DOC incubated with nonfluorescent IpaD. 30 nM FITC-DOC was incubated separately with nonfluorescent IpaD (closed circles), SipD (open circles), BipD (closed triangles), and IpgC (open triangles). IpgC is a *Shigella* cytoplasmic chaperone and was used here as a negative control. The starting mP for FITC-deoxycholate is 27.5 (FP experiments were performed by P. R. Adams and Dr. W. D. Picking) (165).

added into FITC-DOC solution, different polarization value changes were observed. The maximum increase of polarization value of FITC-DOC was with IpaD, which was about 250 mP units. When FITC-DOC was associated with SipD, the IpaD homolog from the enteric pathogen *Salmonella typhimurium*, there was also an increase of about 160 mP. In contrast, BipD, the IpaD homolog from the pulmonary pathogen *Burkholderia pseudomallei* did not seem to affect the polarization value of FITC-DOC, indicating that no interaction occurred with the purified BipD. These findings suggest that DOC interacts with IpaD to cause conformational changes in IpaD that may result in the recruitment of IpaB.

Molecular modeling defines the DOC binding site on IpaD. The FP measurements demonstrated that there is a direct interaction between DOC and IpaD, however, they do not provide information on where DOC binds to IpaD or identify and the amino acids of IpaD that are involved in the binding. Computational analyses were used to dock DOC onto the crystal structure of IpaD to help predict whether DOC consistently binds to IpaD and whether there is a likely binding pocket for this interaction. Dr. G. H. Lushington (Department of Chemistry, University of Kansas) performed these computational simulation experiments and the results are shown in Figure 13. Briefly, IpaD structures were imported into SYBYL from their native PDB format (PDB number 1HGU) to make the simulations. One hundred docked complexes that show the lowest energy level for each DOC-IpaD pair were then generated. From the

computational molecular docking analyses, it appears that the putative DOC IpaD binding site on IpaD

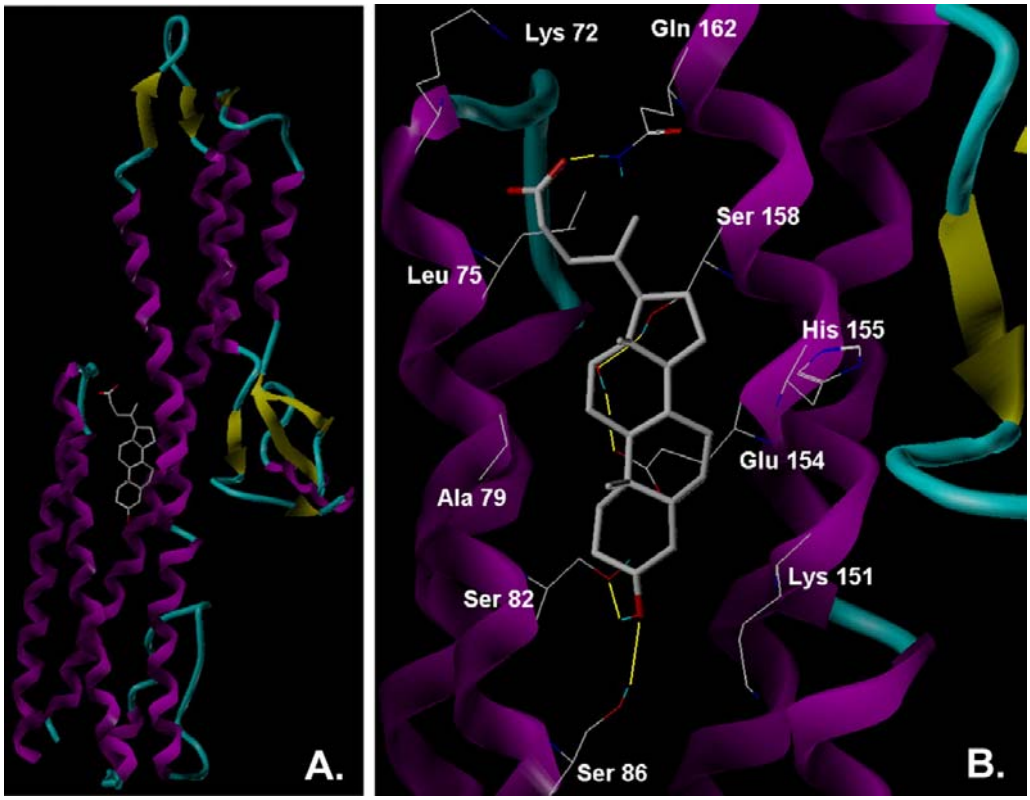

Figure 13. Computational simulated docking of deoxycholate onto the crystal structure of IpaD. α-helices of the ribbon structure of IpaD are shown in magenta, β-strands are shown in yellow and random coils were shown in light blue. A) DOC docked onto the ribbon structure of IpaD. B) Enlarged version of the binding pocket showing key residues of IpaD (L75, S82, E154, H155 and S158) that are essential for the interaction (165). Other residues that may contribute to the binding are also identified (computational simulation was done by Dr. G. H. Lushington).

is located on the central coiled-coil of the protein where the top of the N-terminal helix-turn-helix globular domain packs against the coiled-coil. Docking analyses using FITC-DOC as the ligand generated the same binding interaction, suggesting that it binds in the same way as unmodified DOC (data not shown). Within the IpaD coiled-coil, K151, E154, H155 and S158 appear to provide H-bonds as well as hydrophobic interactions and are essential for DOC binding (Figure 13). N-terminal globular domain residues L75 and S82 also seem to contribute to the interaction, however, additional docking simulations suggested that the IpaD N-terminal domain is not essential for the binding interaction because docking simulations using a truncated form of IpaD ($IpaD^{\Delta 1-120}$) resulted in the same binding model involving the central coiled-coil. This finding is consistent with FP measurements using recombinant $IpaD^{\Delta 1-120}$ that showed similar binding between FITC-DOC and $IpaD^{\Delta 1-120}$ as seen with FITC-DOC and full-length IpaD (Dr. W. D. Picking, unpublished results). The identification of a putative DOC binding site on IpaD now provides the basis for further molecular analyses.

Identification of IpaD residues interacting with deoxycholate by NMR Spectroscopy. Although computational simulations identify a putative binding pocket for the DOC-IpaD interaction, experimental information is still needed to determine whether this binding site is indeed real and to precisely identify the residues involved in the DOC binding event. NMR chemical shift mapping was used to identify the $MxiH^{C\Delta 5}$ residues that are responsible for anchoring IpaD at TTSA needle tip (see Chapter 4) and a similar

approach seemed feasible here for the identification of IpaD residues responsible for DOC binding.

a. NMR spectroscopy as a tool for identifying of protein residue involved in ligand interactions

Nuclear magnetic resonance (NMR) spectroscopy is a powerful technique for identifying molecular interactions and to measure the dynamics of a protein. In a ^{1}H-^{15}N HSQC (Heteronuclear Single Quantum Coherence) NMR spectrum, the NMR signal of an amide nitrogen is connected with the proton attached to it. This correlation of the amide proton and nitrogen results in a two-dimensional NMR spectrum that produces a single peak for every amide group that represents each residue in the protein of interest. The peak's position in the spectrum, which is defined by its ^{1}H and ^{15}N chemical shifts, provides information on the protein's primary sequence and secondary structure. The chemical shift changes when the local chemical environment of each nucleus changes, thus giving information on the local chemical environment surrounding the nucleus, and therefore structural information. Each protein has its own characteristic ^{1}H-^{15}N HSQC spectrum because of its sequence and structure. NMR chemical shift is useful in studying molecular interactions involving proteins. When a protein interacts with a binding partner, the residues that are affected by the binding interaction will have a different chemical environment, which results in changes in the corresponding NMR signals of the specific residues affected by the interaction. If the sequence specific assignment of the protein of interest is available, the shifted peaks indicate which amino acids in the protein are

affected by the binding. The residues that show chemical shift changes are deemed potentially involved in the binding interaction. These perturbed residues can be mapped onto the three dimensional structure of the protein to visualize the binding site.

b. Choice of NMR experiments for IpaD sequence assignment and chemical shift mapping

In order to map the residues showing chemical shift perturbation onto the three-dimensional crystal structure of IpaD, the backbone sequence assignment of the protein needs to be known. Unfortunately, the specific sequence assignment of a protein cannot be made directly from HSQC spectra. A number of additional three-dimensional NMR spectra have to be collected and analyzed. The 37-kDa IpaD is a relatively large protein for NMR experiments. A major problem for large proteins in NMR is signal overlap due to overcrowding of peaks in the NMR spectra. Another problem is that large proteins show poor resolution in NMR signals because of broadened peaks. Deuteration can be used to improve the quality of NMR signals by reducing overlap proton signals. Deuteration also improves the resolution of experiments by eliminating many proton-proton dipolar and scalar couplings. To introduce deuterium, the bacteria expressing the protein are grown in D_2O medium instead of H_2O medium (163). More importantly, the development of TROSY (transverse relaxation-optimised spectroscopy) based experiments help to cope with large size proteins in NMR spectroscopy (143). TROSY makes use of the interference of two different relaxation mechanisms that affect

the signal broadening by selecting the optimal case when the two relaxation mechanisms cancel each other out. The resulting peak is sharp and narrow in a spectrum, which reduces the overlap problem for large proteins. IpaD assignments can thus be obtained by using ^{1}H-^{15}N TROSY correlation and TROSY-based 3-dimentional experiments. This is the basis for identifying IpaD residues that are potentially involved in the DOC-IpaD interaction and which thus make up the binding site.

c. IpaD backbone sequence specific assignment

The initial HSQC spectrum of full length IpaD had broad peaks and major overlapping of peaks caused by the large size of the protein and its highly α-helical nature. In the crystal structure of IpaD, the first 37 residues and the last 11 residues of the protein were probably unstructured since there was no electron density detected for these in the IpaD crystal structure (100). A truncated version of IpaD based on the derivative used for determining the IpaD crystal structure was made in order to remove the unstructured ends to obtain better resolved NMR spectra. $IpaD^{38\text{-}321}$ lacking the first 37 and the last 11 amino acids of the protein was constructed with a C-terminal short His_6tag and put into pET22b for production and easy purification. Uniformly ^{2}H-, ^{15}N-, ^{13}C-labeled proteins were obtained by growing the expression strain *E. coli* BL21(DE3) in minimal media made with D_2O instead of H_2O and supplemented with ^{15}N-NH_4Cl and ^{2}H-, ^{13}C-glucose as the nitrogen and carbon sources, respectively. The deuterated sample was used for 3-D NMR data acquisition. Although protein production was reduced in the

D_2O medium compared with the H_2O medium, 500 ml of bacterial culture produced enough triple labeled IpaD$^{38-321}$ for NMR data collection (Figure 14).

Uniformly ^{2}H-, ^{15}N-, ^{13}C-labeled truncated IpaD was dissolved in NMR buffer for data collection. The data were acquired at 30 °C on a Bruker Avance 800 MHz spectrometer, processed using NMRPipe and analyzed using NMRView (56, 99). Backbone resonances of truncated IpaD were assigned using ^{1}H-^{15}N TROSY, TROSY-based 3-D HNCA and HNCACB (143).

^{15}N specific amino acid labeling was also used to obtain IpaD in which only a single type of amino acid in the protein was ^{15}N labeled. In this case, a single specific ^{15}N-labeled amino acid was added to minimal medium containing the other 19 unlabeled amino acids. The ^{15}N-amino acid labeled protein could be expressed and purified normally. On a ^{1}H-^{15}N TROSY spectrum only the labeled specific amino acids would show up but no others. IpaD labeled with ^{15}N-Alanine, ^{15}N-Valine, ^{15}N-Leucine, ^{15}N-Isoleucine, ^{15}N-Phenylalanine and ^{15}N-Tyrosine were produced separately and the ^{1}H-^{15}N TROSY spectrum for each of the single amino acid labeled IpaD$^{38-321}$ was collected for aiding in making backbone assignments (Figure 15).

The highly α-helical nature of IpaD, especially as part of an intramolecular coiled-coil, made sequence assignment challenging since NMR signals tend to appear in a very narrow proton range. Thus, peak overlapping, which is packed into a small region of the NMR spectrum, had to be resolved. In spite of this hurdle, the multiple NMR strategies used allowed us to assign 201 out of 284 residues in the truncated IpaD

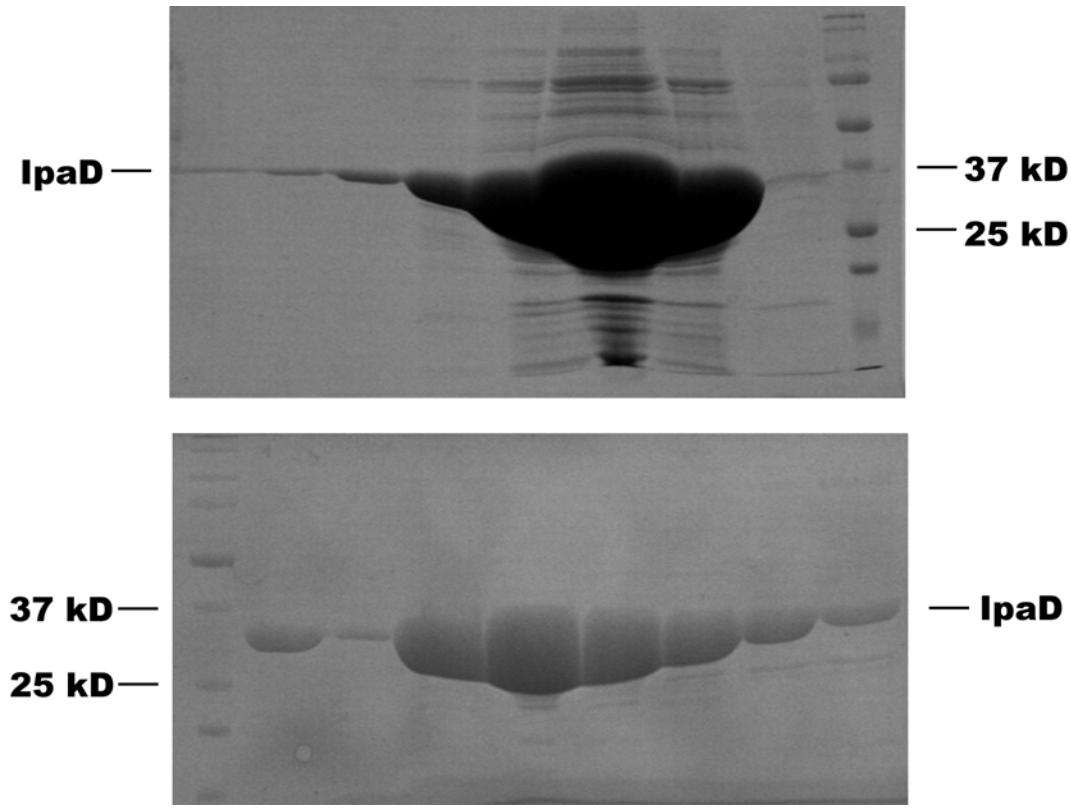

Figure 14. SDS-PAGE of isotopically labeled IpaD$^{38-321}$. Top: ^{15}N-labeled IpaD$^{38-321}$ expressed and purified from 500 ml H_2O minimal medium; Bottom: ^{2}H-, ^{15}N-, ^{13}C-labeled IpaD$^{38-321}$ expressed and purified from 500 ml D_2O minimal medium. 15 μl of protein sample from each 1.5ml fraction collected after nickel chelation affinity chromatography was loaded onto the 12% SDS-PAGE gel, and total of 10 fractions were collected while the protein was eluted from the resin.

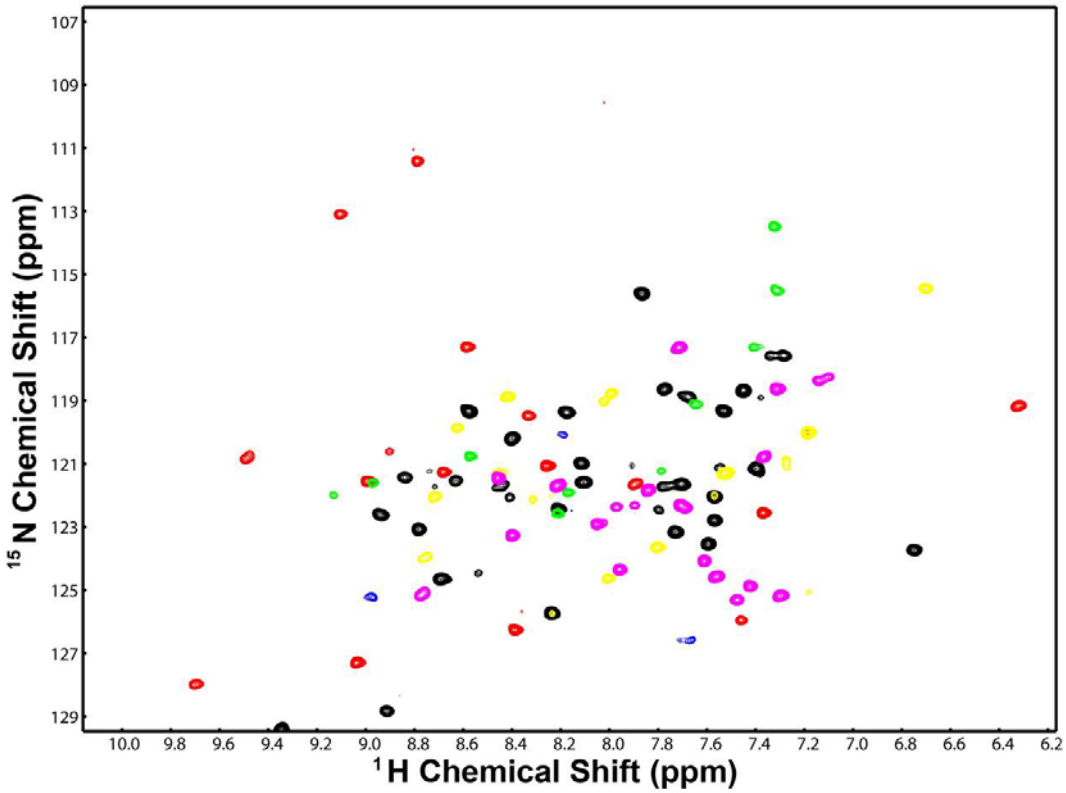

Figure 15. Overlay of the TROSY spectra of IpaD$^{38-321}$ containing specifically labeled amino acids. TROSY spectra of different labeled IpaD samples were collected at 30 °C on a Bruker Avance 800 MHz spectrometer (black, Leu; red, Val; blue, Phe; green, Tyr; yellow, Ile; magenta, Ala).

(Figure 16). The backbone sequence assignment of IpaD now provides the basis for interpreting chemical shift mapping data for identifying the IpaD residues involved in DOC binding.

d. Chemical shift mapping to identify the DOC binding site on IpaD

Based on the reasoning that the DOC-IpaD interaction should result in changes in the NMR resonances of the IpaD for amino acids whose chemical environments are changed by contact with the ligand, DOC was titrated into ^{15}N-labeled IpaD$^{38-321}$. The changes in the chemical shifts of IpaD were thus determined. Indeed, there are peaks in the IpaD ^{1}H-^{15}N TROSY spectrum that are perturbed upon the addition of DOC (Figure 17). The observation of chemical shift perturbations for IpaD when DOC is added confirms that DOC binds to IpaD and this is consistent with the FP data presented earlier. Interestingly, the characteristic chemical shift of the Trp side chain signal (bottom left corner of the spectrum) was perturbed, indicating that one of the four Trp residues in IpaD is potentially involved in DOC binding. It was later determined that the perturbed Trp side chain belongs to Trp177 using mutagenesis in combination with NMR spectroscopy (data not shown). Because there are no Trp residues within the expected DOC binding pocket, perturbation of the Trp177 chemical shift indicates that DOC binding could be inducing conformation changes in IpaD.

Several ^{15}N TROSY spectra with increasing amounts of DOC added to ^{15}N-labeled IpaD at a constant concentration were also acquired. Upon the addition of DOC into

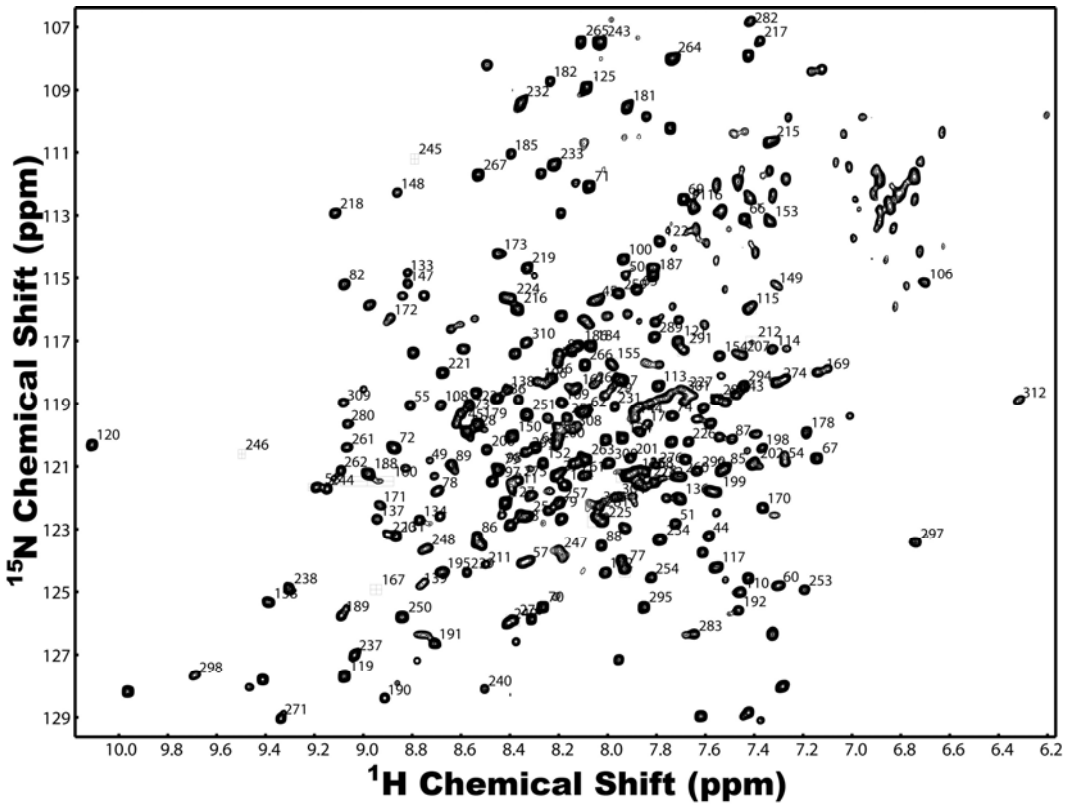

Figure 16. TROSY spectrum of IpaD$^{38-321}$ with its primary sequence assignment. Sequence assignment was made by collecting ^{1}H-^{15}N TROSY, TROSY-based 3-dimensional HNCA and HNCACB from uniformly ^{2}H-, ^{15}N-, ^{13}C-labeled IpaD$^{38-321}$. The data were acquired at 30 °C on a Bruker Avance 800 MHz spectrometer, processed using NMRPipe and analyzed using NMRView. Specific amino acid labeling (see Figure 15) was also used to help make the assignments.

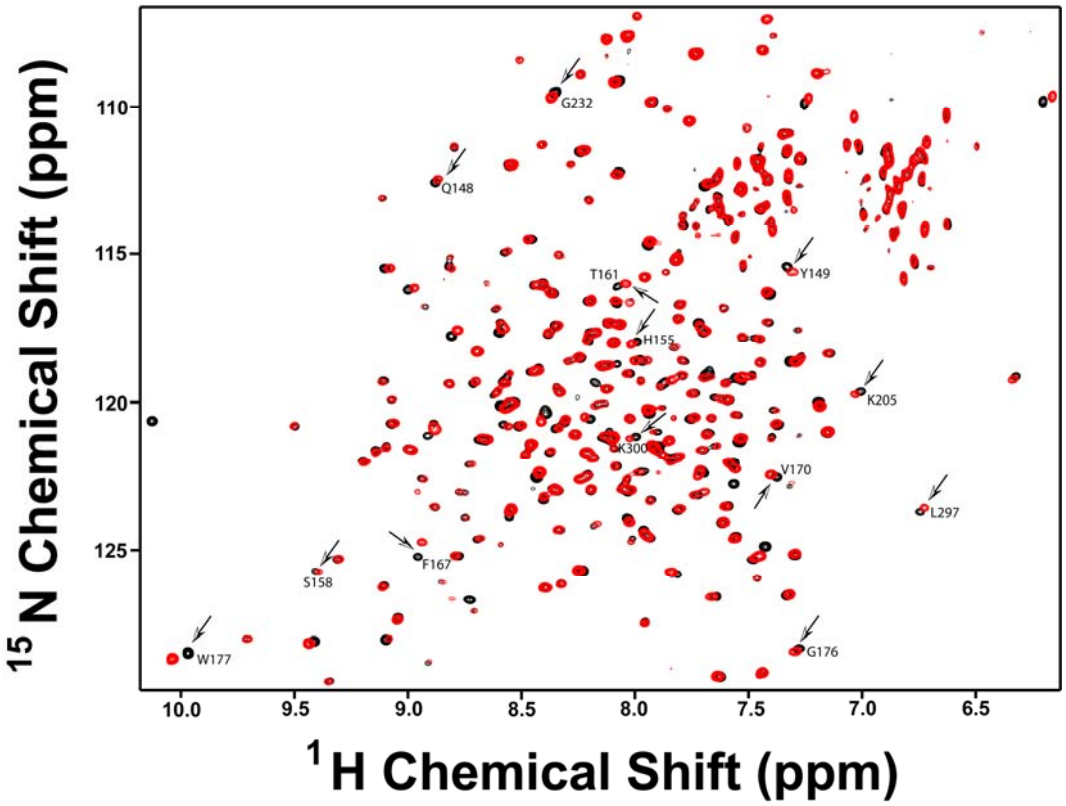

Figure 17. Chemical shift perturbation of ^{15}N-labeled IpaD$^{38-321}$ caused by adding DOC. The TROSY spectrum of free ^{15}N-labeled IpaD$^{38-321}$ (black) was overlaid with ^{15}N-labeled IpaD$^{38-321}$ bound to equal molar ratio of DOC (red). The chemical shifts of some IpaD residues were perturbed upon the binding of DOC, and some of the key residues are pointed with black arrows.

labeled IpaD, many IpaD peaks shifted. Further additions of DOC moved the peaks from their original positions even further, indicating that this binding interaction was in the fast exchange NMR time scale (Figure 18). This behavior is consistent with the micromolar binding affinity estimated from the FP experiments (Figure 12 and Figure 18).

Since the majority of the IpaD residues have been assigned based on the TROSY spectrum, most of the residues showing chemical shift perturbation can be identified. Those perturbed residues are listed in Table 6 and mapped onto the crystal structure of IpaD in Figure 19. The identified residues of IpaD for DOC-IpaD interaction from NMR chemical shift mapping are consistent with computational models of DOC docking. Several residues within the putative binding pocket identified via molecular modeling showed chemical shift changes upon the titration of DOC (see Figure 13). Key residues that are supposed to be involved in the binding interaction based on computational analyses, including S82 and S86 in the N-terminal globular domain and H155 and S158 in α-3 of the coiled-coil, showed chemical shift perturbations in these NMR experiments. K72, which is at the upper end of the binding pocket, also had a chemical shift change. Residues L150, Y153 and T161 are all in the predicted binding pocket and they showed chemical shift perturbations although they were not specifically pointed out in Figure 13. Interestingly, many IpaD residues in α-3 of the coiled-coil showed chemical shift perturbations although being higher on α-3 than E147. The perturbed α-3 residues extended all the way up to the distal domain along the helix. The short linker connecting the end of α-3 helix and the beginning of the distal domain consisting of G176, W177 and

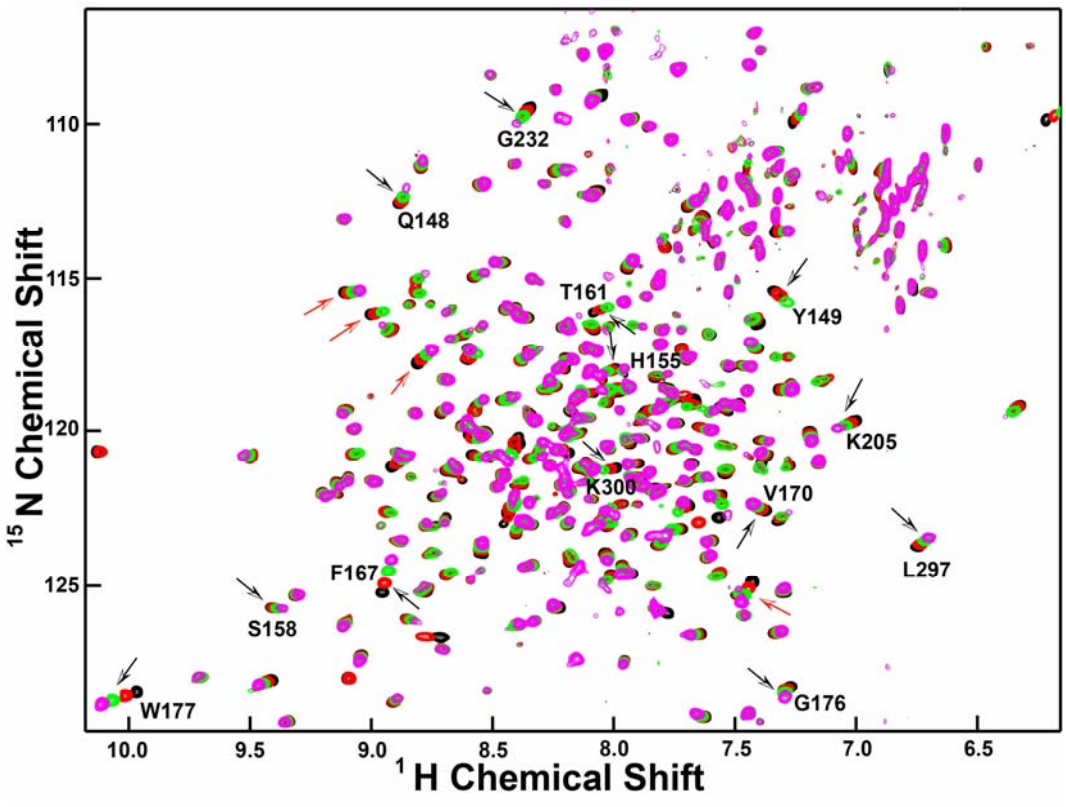

Figure 18. Titration of ^{15}N-labeled IpaD$^{38-321}$ with increasing amounts of DOC. Overlay of four protein-nitrogen correlation spectra (^{15}N TROSY) at various DOC:IpaD molar ratios (black, 0; red, 1.0; green, 3.0; magenta, 6.0). The actual DOC:IpaD concentrations used, repectively, are as follows (in μM): black (500:0), red (500:500), green (500:1500), and magenta (500:3000).

Table 6. IpaD residues identified as showing chemical shift perturbations upon titrating in DOC

N-terminal domain	T69, L70, T71, K72, S82, S86
α-3 of the coiled-coil	Q148, Y149, L150, Y153, H155, S158, T161, F167, V170, S172, S173
Linker between α-3 and the distal domain	G176, W177, I178
Distal domain	K189, L190, A198, E201, K205, Y206, Y212, N216, A223, N224, G232, T233, I234, K236, S238, V245, V246, M250
α-7 of the coiled-coil (C-terminal α-helix)	A274, F283, L297, Q299, K300, Y301, D309, V312

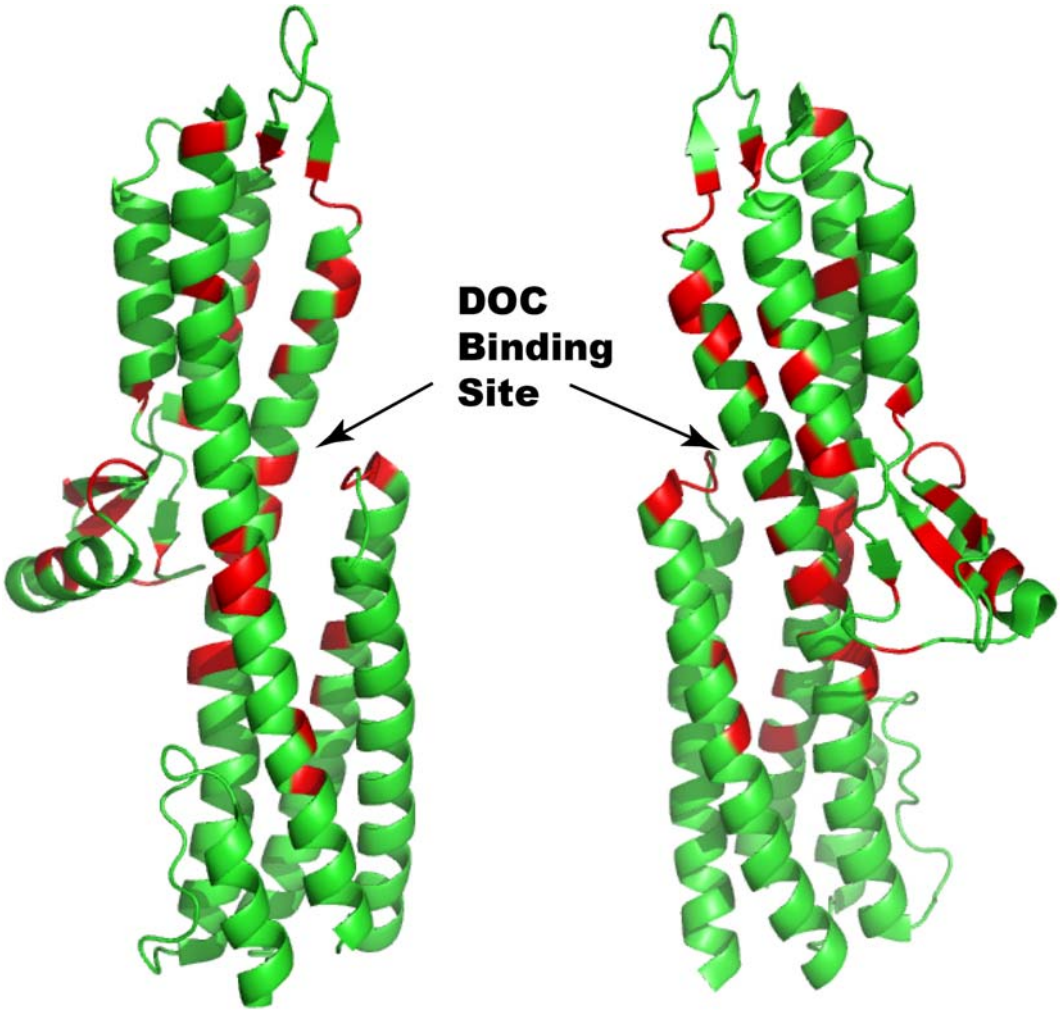

Figure 19. IpaD residues that are perturbed by DOC binding are mapped on the surface of the crystal structure of IpaD (Protein Data Bank code 2j0o). The ribbon structure of IpaD is shown in green, and the perturbed residues (listed in Table 6) are highlighted in red. Two pictures show opposite faces of the IpaD structure.

I178 are also perturbed upon DOC binding. The side chain signal of W177 showed significant chemical shift perturbation at the bottom left corner of the TROSY spectrum. Residues throughout the distal domain also had chemical shift changes, suggesting that DOC binding induces a global conformational change in the protein, which may be involved in the transient secretion induction (IpaB mobilization) and possibly the stable maintenance of IpaB at the TTSS needle tip following the addition of DOC to whole bacteria.

Mutagenesis studies of the IpaD residues that are suggested to interact with DOC by NMR spectroscopy. There are some residues in the IpaD N-terminal domain that are perturbed upon DOC binding, however, the N-terminal domain most likely does not reside next to the coiled-coil *in vivo* due to the steric hindrance expected to occur when IpaD is present at the needle tip. Thus, site-directed mutations were focused on the residues of the central coiled-coil which are proposed to be directly involved in DOC binding. Changes at S158 and K151 in the central coiled-coil had the most dramatic effect on IpaD-dependent invasion of cultured cells (Table 7). S158A resulted in an nearly 80% decrease in invasiveness and S158L (predicted to abolish DOC binding according to computer simulations) completely eliminated *Shigella* invasiveness. Experiments to more fully characterize these mutants are under way, however, S158A is also impaired in its ability to mobilize IpaB to the *Shigella* surface following DOC addition. In contrast, K151E resulted in a dramatic increase in *Shigella* invasiveness while being largely normal with respect to IpaD and IpaB presentation on the bacterial surface.

Table 7. The effect of selected IpaD mutations on *Shigella* invasiveness.

		IpaD exposed[b]		IpaB exposed[c]	
IpaD mutant	**Relative invasion[a]**	**-DOC**	**+DOC**	**-DOC**	**+DOC**
ipaD null strain (SF622)	0±0	0%	0%	0%	0%
Wildtype	100±8	100	100	0	95
S158A	**22±4**	**95**	**94**	**0**	**30**
S158L	**0±0**	**nd**	**nd**	**nd**	**nd**
N146Q	**21±3**	**nd**	**nd**	**nd**	**nd**
Y149F	**23±8**	**nd**	**nd**	**nd**	**nd**
N146Q/Y149F	**4±3**	**nd**	**nd**	**nd**	**nd**
K151E	**421±21**	**100**	**100**	**0**	**100**
E229K	58±9	80	77	0	22
K151E/E229K	0±0	28	13	0	18

Mutants made for this study are highlighted in bold and the number of bacteria having specific proteins on their surface was determined by immuno-fluorescence microscopy with help from C. Epler.

a) Invasion was measured using a standard gentamycin protection assay with the *S. flexneri ipaD* null strain SF622 serving as a negative control and SF622 making wild-type IpaD having 74±6 colonies per well (*n*=3).

b) IpaD staining was with monoclonal antibodies and [c]IpaB staining was with rabbit antisera. In both cases the value given is the percentage (%) of cells having the given protein on their surface.

nd = not yet determined.

Based on information revealed in solving the original crystal structure, there is a region consisting of four residues in the middle of helix α3 within the central coiled-coil of IpaD that develops a kink which could contribute to conformational changes that occur within the protein following ligand binding. Therefore, additional mutants were generated to stabilize the helical conformation within this region of α-3 to limit conformational change of IpaD, which may affect the recruitment of IpaB. The mutants N146Q, Y149F and N146Q/Y149F (Table 7) were generated to further stablilize the α-helix. In doing this, we expected that a reduction of flexibility in this region might affect the overall conformational change of IpaD. If such a structural change is important for IpaD-mediated virulence functions, these mutants should be noninvasive while retaining IpaD at the *Shigella* surface. N146Q and Y149F indeed have decreased *Shigella* invasiveness while the N146Q/Y149F double mutant almost abolishes the invasiveness (Table 7). These data suggest that helix α-3 does play a key role in signaling the first step in TTS induction. However, additional experiments, including NMR experiments, will need to be completed to fully understand the affect of the mutations. Meanwhile, examination of IpaD's presence on *Shigella* surface of these mutant strains and IpaB recruitment to the *Shigella* surface are ongoing.

Discussion

Fluorescence polarization (FP) measurements were initially used to show that FITC-DOC directly interacts with IpaD. Dr. G. Lushington (Director, KU Molecular Graphics and

Modeling Lab) then performed docking simulations to provide details on the putative IpaD binding pocket for DOC (see Figure 13). Molecular modeling predicted that DOC binds to a portion of the central coiled-coil where it associates with the turn of the N-terminal double helix. A truncated form of IpaD lacking its N-terminal domain ($IpaD^{\Delta 1\text{-}120}$) gave similar binding results.

A new construct encoding $IpaD^{38\text{-}321}$ (291 residues with His-tag) designed based on the IpaD form used to solve its crystal structure was used for the NMR studies. Over two thirds of the IpaD residues have been assigned using TROSY-based 3-D data collected on ^{2}H, ^{15}N, ^{13}C-labeled $IpaD^{38\text{-}321}$. In addition to the work presented, these IpaD assignments provide the basis for further studies on the structural dynamics of IpaD in the presence of other ligands or unlabeled proteins. We have identified a number of IpaD residues that are perturbed when titrated with unlabeled DOC (Figure 18 and Table 6). The perturbed residues are mapped onto the crystal structure of IpaD, which shows a pattern that is consistent with computer docking analyses. IpaD residues in the predicted DOC binding pocket, including Y149, H155, S158 and T161, are all perturbed upon DOC binding (Figure 19). While K151 has not yet been assigned, the residues perturbed by DOC binding flank this important amino acid. Furthermore, those residues altered by DOC binding extend from the DOC binding pocket and continue up α-3 (including F167, V170, G176 and W177) and eventually lead into the distal domain (Figure 19). Residues whose chemical enviroments are perturbed within the distal domain are presumably affected due to conformational changes in IpaD. From these studies, we show that NMR is providing a

precise map of the residues involved in DOC binding and strengthening arguments for exploring the role of the IpaD distal domain in IpaB recruitment and anchoring at the *Shigella* TTSA needle tip.

A potential conformational change was predicted by molecular modeling in the loop between α-1 and α-2 (Q67-K72) of the N-terminal domain following simulated DOC binding coupled with protein relaxation (see Figure 13)(Dr. G. Lushington). Because of our proposal that the IpaD N-terminus (α-1 and α-2) is replaced by the head domain of MxiH at the needle tip when IpaD is docked at the needle tip, we have not focused on this portion of the protein in this study (190). Nevertheless, the possibility that DOC binding may alter the IpaD-MxiH interface is intriguing from the stand point of how DOC may elicit signals that influence TTS events occurring within the TTSA.

Residues N146 to Y149 of helix α3 within the central coiled-coil of IpaD appear to develop a kink that may contribute to additional conformational changes within the protein. Therefore, the mutants in this study were mainly generated to alter DOC binding or stabilize the helical structure within this region of α-3. In doing this, we expected that the predicted DOC-induced IpaD conformational change would be compromised. N146Q and Y149F do partially decrease the *Shigella* invasiveness, while the N146Q/Y149F double mutant greatly reduces the invasiveness (Table 7), however, further investigation of IpaD's behavior on the bacterial surface and IpaB's recruitment to the *Shigella* surface is still needed for these mutants. Helix α-3 may play a key role in signaling for the first step in TTS induction and in accommodating the recruitment and maintence of IpaB at

the TTSA needle tip.

Based on our dynamics simulations and experimental results, we propose that IpaD undergoes a conformational change that allows IpaB to be recruited at the needle tip in a controlled manner. There are specific residues in IpaD that either interact with DOC directly or may be involved in conformational changes following DOC binding. Thus, our working hypothesis is that DOC induces this conformational change in IpaD to allow the controlled release of IpaB to give rise to a MxiH-IpaD-IpaB ternary complex.

CHAPTER 6: Discussion and Summary

Type III secretion is a tightly regulated process that is common among many Gram-negative pathogens. The TTSA is a complicated, protein-exporting nanomachine used to deliver bacterial effectors directly into a target eukaryotic host cell's membrane and cytosol. Phylogenetic analysis suggests that various TTSSs can be organized into five groups (75, 139, 177). The Ysc group includes the *Yersinia* Ysc TTSS, the *P. aeruginosa* Psc TTSS, and the *Bordetella* Bsc TTSS. The Hrp group includes *P. syringae* and *Erwinia* TTSSs. The Hrp2 group includes *Xanthomonas* and *Ralstonia* TTSSs and one of the two *Burkholderia* TTSSs. The Inv/Mxi/Spa group includes the *Samonella* SPI-1 TTSS, the *Shigella* TTSS and the *Burkholderia* Bsa TTSS. The Esa/Ssa group includes the TTSS of EPEC and the *Salmonella* SPI-2 TTSS. Among the 25 or so species of Gram-negative bacteria now known to possess a TTSS, there are more than 100 different effector proteins having a wide range of activities that interfere with the normal function of host regulatory proteins (41). Effector proteins from different bacteria can be very different in terms of structure and function, however, the TTSA is relatively well-conserved structurally and functionally (16, 53, 110, 112, 128, 134, 162, 171).

The TTSA is composed of about 25 different types of proteins, most of which are located adjacent to the bacterial inner membrane. First visualized by transmission electron microscopy (TEM) by Kubori *et al*. in *S. typhimurium*, the TTSA is a multifunctional protein complex that visually resembles a syringe and needle (112). Most of the TTSA

structural components are associated with the bacterial inner membrane which anchors the complex and provides the energy needed for translocation of later structural units, translocator proteins and effectors (160).

The major component of the extracellular portion of the TTSA is a needle assembled from multiple copies of a single protein. It is believed that needle monomers pass through the channel and polymerize at the growing distal end of the needle. Studies have shown that the needle proteins are critical for TTSS function and the null mutants are defective in secreting any virulence effectors (107). Needle proteins from a wide range of organisms share sequence similarities at key positions. Due to the efficient self-polymerizing nature of these proteins, structure determination was challenging, however, structures are now becoming available for a number of different needle monomers (55, 182, 191). Although different approaches have been used to obtain high-resolution structures for BsaL (*B. pseudomallei*) (191), MxiH (*S. flexneri*) (55), PrgI (*S. typhimurium*) (182), PscF (*P. aeruginosa*) (151) and YscF (*Y. pestis*) (169), common themes in the core needle monomer structure are apparent.

The NMR structure of BsaL was the first protein structure within the needle protein monomer class to be reported (191). BsaL is a helix-turn-helix with a tight PSDP turn. The N-terminal and C-terminal ends adopt partial helical features that flank a well-defined two helix bundle core. The two helix bundle is stabilized by hydrophobic interactions and the surface of the core domain is lined with polar residues that might be involved in the needle packing (Figure 20A). The crystal structure of *S. flexneri* MxiH

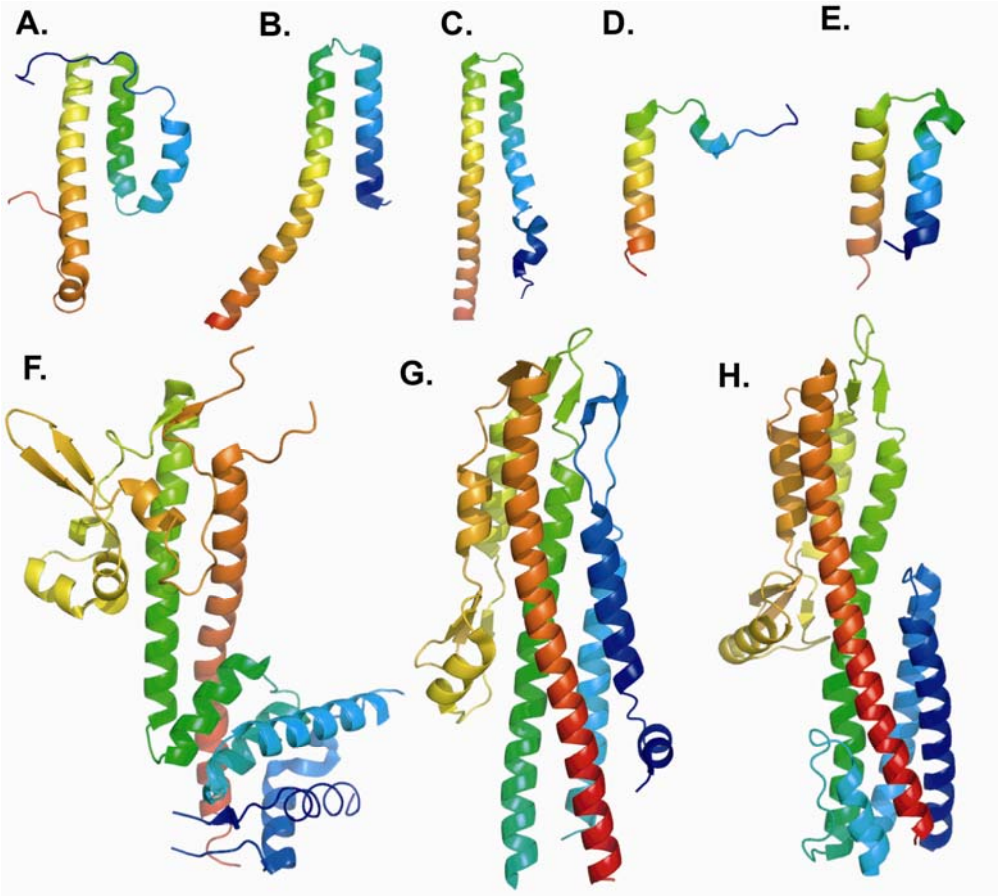

Figure 20. Structures of TTSS needle and tip proteins. Ribbon structures are shown for the needle protein monomers BsaL (PDB ID: 2g0u) from *B. pseudomallei* (A), MxiH (PDB ID: 2ca5) from *S. flexneri* (B), PrgI (PDB ID: 2jow) from *S. typhimurium* (C), PscF (PDB ID: 2uwj) from *P. aeruginosa* (D) and YscF (PDB ID: 2p58) from *Y. pestis* (E). Also shown are the structures of the needle tip proteins LcrV (PDB ID: 1r6f) from *Y. pestis* (F), BipD (PDB ID: 2j9t) from *B. pseudomallei* (G) and IpaD (PDB ID: 2j0o) from *S. flexneri* (H) (55, 57, 100, 151, 169, 182, 191).

shows a similar conformation, but it has a longer C-terminal helix (Figure 20B) (55). The NMR structure of PrgI revealed a two helix bundle with flexible ends similar to the structures of BsaL and MxiH, however, the electrostatic surfaces of PrgI appear to differ from those of BsaL or MxiH (Figure 20C) (182). The latter finding suggests that electrostatic interactions are important contributing factors in needle assembly. The purified needle proteins of *P. aeruginosa* and *Y. pestis* behave differently from BsaL, MixH and PrgI (151, 169). Deleting a small number of C-terminal residues does not lead to readily purified monomers for these proteins. The partial structure of *P. aeruginosa* PscF was only solved crystallographically when it was bound to its chaperones PscE and PscG (151). In this ternary complex, the first 54 residues of PscF were deleted to generate a crystal that was diffractable with high resolution (Figure 20D). The C-terminal 31 residues of PscF in the complex form an extended coil and a short helix that is similar with the C-terminal helix of MxiH. The PscE/F/G ternary complex may provide an indication as to how bacteria can prevent needle monomers from prematurely self-polymerizing in the bacterial cytoplasm, however, no chaperones have been reported for BsaL, MxiH, or PrgI.

The crystal structure of *Y. pestis* needle protein YscF in complex with its chaperones YscE and YscG was recently published by Sun. *et al* (169). It is worth noting that although the first 49 residues of YscF displayed no electron density within its ternary complex, residue 50-87 did adopt a helix-turn-helix structure (Figure 20E). The two helices of YscF are joined by a five-residue linker from I64 to N68, which differs from

the previous reported needle monomer structures which all have a short four-residue Pro-X-X-Pro turn.

The atomic structures of needle proteins have provided a basis for explaining biological data related to the phenotypes of needle protein mutants, however, empirical data on how needle monomers interact with each other for needle assembly and how relatively large proteins are able to traverse these needles are still lacking (107, 169). Furthermore, how or even whether this portion of the TTSA is structurally altered during the process of protein secretion is still unclear. Nonuniformity in needle length, both for isolated needles and needles reconstituted *in vitro*, make crystallization of assembled needles unlikely.

Available models of needle assembly have been generated by docking the crystal structure of the MxiH monomer into a 16 Å cryo-EM electron density map of the *S. flexneri* needle (55). Since the N terminus of the MxiH monomer is not visible in the published crystal structure, a helical structure for this part of the molecule was assumed for this model. The major axis of the monomer was in line with the major axis of the needle (Figure 21). The orientation of this model is in agreement with the functionally- and structurally-related bacterial flagellar filament assembly (55, 155, 186). The monomer tails were buried inside the needle wall in this model with the head domain localized at the outside surface. The N-terminal helix is proposed to line the inner surface of the tunnel. The C-terminus of the monomer, which is buried within the needle wall, displays an important role in needle assembly based on this model where the C-terminus

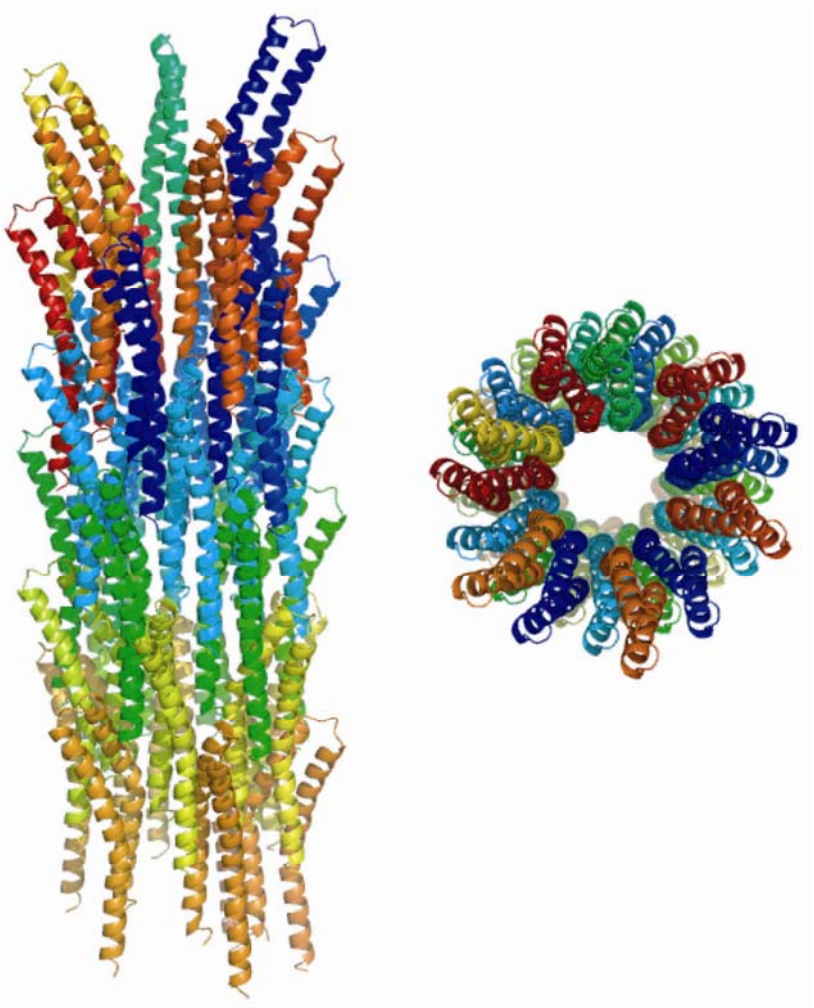

Figure 21. Molecular model of the *Shigella* TTSS needle assembly. Molecular modeling based on the crystal structure of MxiH (55) and cryo-EM pictures (38) has allowed for *in silico* reconstruction of the *Shigella* TTSA needle. A side view of the needle is shown on the left with an end-on view shown on the right (PDB file generated by Dr. W. Im, University of Kansas, based on MxiH structure (PDB ID: 2ca5)).

of MxiH has direct contact with three other molecules in the assembly. Deleting the five C-terminal residues of MxiH interferes with the self-polymerization and leads to monomeric MxiH. Published mutagenesis results agree with this model (107).

It was not until late 2005 that a tip complex formed by LcrV of *Yersinia* was reported to exist at the top of the TTSA needle when the apparatus was in a resting state (129). This was quickly corroborated with the finding that IpaD forms a "tip complex" for the TTSA of *S. flexneri* (63). It is likely that these needle tip complexes are needed to sense environment signals and subsequently control the secretion and insertion of translocators into host membranes as the first step in translocon pore formation. Some of the known tip complex proteins have been sorted into specific classes based on sharing sequence similarity, especially within their C-terminal sequences. The X-ray structure of LcrV was the first reported in the LcrV/PcrV family (Figure 20F). LcrV has a dumbbell shape with a novel intramolecular coiled-coil motif formed by a long central helix and a C-terminal helix. This coiled-coil stabilizes the overall structure of the protein. Smaller α helices and β strands form the distal domain which, together with the N-terminal domain, flank the coiled-coil handle as the globular portions of the dumbbell. This coiled-coil motif was found to be a hallmark of TTSA tip proteins when the X-ray structures of BipD and IpaD revealed similar overall dumbbell shapes (Figure 20G and 20H). These proteins, however, possessed larger N-terminal globular domains. It is perhaps not surprising that the N-terminal domains of BipD and IpaD resemble the structure of the LcrV chaperone

LcrG since homologs of this chaperone are absent in *Shigella* and *Burkholderia* and it has been suggested that IpaD and BipD may possess a self-chaperoning ability.

The presumed positioning of TTSA needle tip proteins suggests that they directly interact with the needle and the translocon pore. Precisely how tip complex proteins interact with the underlying needle monomers is currently unknown, however, different approaches have been made to try to address this question. The N-terminal helix-turn-helix domain of the *Shigella* tip protein IpaD looks remarkably like the two-helix bundle of the needle protein MxiH, suggesting a possible model for of needle monomer-tip protein interaction (190). We proposed that when IpaD is secreted and localized to the tip of the needle, its N-terminal domain swings away, leaving the binding interface of the coiled-coil motif accessible to MxiH. MxiH thus mimics the IpaD N-terminus and binds to the lower part of the coiled-coil motif in the same fashion as the N-terminus itself was previously bound to the coiled-coil motif (see Figure 11). NMR spectroscopy chemical shift mapping results and the findings from subsequent mutagenesis studies support the suggested binding interface. It has been shown that the N-terminal domain of IpaD is not buried inside needle and is exposed to outside environment where anti-IpaD antibodies can neutralize some IpaD functions (146), which is consistent with this model of needle tip complex assembly. Furthermore, only a small number of residues deleted from the C-terminus of IpaD are capable of leading to a dramatic decrease in of pathogen's ability to infect cultured cells or to maintain IpaD at the needle tip (146). From the proposed model of IpaD retention at the MxiH needle tip, it

appears that the C-termini of needle tip complex proteins play an important role in stabilizing their interaction with the tip of the TTSA needle. It remains to be determined if this is also the case for other needle tip complex proteins and their respective needle partners. Because BipD is able to stably associate with the MxiH needle of *S. flexneri* and the C-terminal sequences of IpaD and BipD are quite conserved, this model seems plausible (100). Likewise, the divergence of C-terminal sequences for the LcrV/PcrV family and their inability to be retained at the *Shigella* MxiH needle tip are also consistent with this model.

In general, the three translocators from different TTSSs share a common feature that two of them are hydrophobic (e.g. IpaB and IpaC in *Shigella*) and the third is hydrophilic (e.g. IpaD in *Shigella*) (16, 85). All three of them are encoded in a single operon, with a smaller chaperone protein serving for the hydrophobic translocators. The two hydrophobic translocators form a translocon pore in the host membrane where they create a path for later bacterial effectors to be delivered directly into the host cytoplasm (85, 97, 183). The tip complex serves as a platform that connects the bacterial and host cell cytoplasms. The position of the tip complex suggests an interaction between tip proteins and translocators. Despite the high resolution structures of tip proteins, however, detailed structural information on the translocators is absent due to their overall hydrophobic nature. How the tip and translocon proteins interact with each other has not yet been worked out (137, 179). The bile salt DOC interacts with IpaD to recruit IpaB to the TTSA needle tip where it remains stably bound without further induction of TTS. NMR

chemical shift perturbation shows that there are specific residues in IpaD that either interact with DOC directly or are involved in conformational changes following DOC binding. Our hypothesis is that DOC induces a conformational change in IpaD, which allows IpaB's secretion and its co-localization with IpaD at the TTSA needle tip to form a MxiH-IpaD-IpaB ternary complex.

Bibliography

1. 2002. Pertussis--United States, 1997-2000. MMWR Morb Mortal Wkly Rep **51:**73-6.
2. 1999. Pertussis vaccines. Wkly Epidemiol Rec **74:**137-43.
3. **Adam, T., M. Arpin, M. C. Prevost, P. Gounon, and P. J. Sansonetti.** 1995. Cytoskeletal rearrangements and the functional role of T-plastin during entry of *Shigella flexneri* into HeLa cells. J Cell Biol **129:**367-81.
4. **Adam, T., M. Giry, P. Boquet, and P. Sansonetti.** 1996. Rho-dependent membrane folding causes *Shigella* entry into epithelial cells. Embo J **15:**3315-21.
5. **Akeda, Y., and J. E. Galan.** 2005. Chaperone release and unfolding of substrates in type III secretion. Nature **437:**911-5.
6. **Allaoui, A., P. J. Sansonetti, R. Menard, S. Barzu, J. Mounier, A. Phalipon, and C. Parsot.** 1995. MxiG, a membrane protein required for secretion of *Shigella* spp. Ipa invasins: involvement in entry into epithelial cells and in intercellular dissemination. Mol Microbiol **17:**461-70.
7. **Allaoui, A., P. J. Sansonetti, and C. Parsot.** 1992. MxiJ, a lipoprotein involved in secretion of *Shigella* Ipa invasins, is homologous to YscJ, a secretion factor of the *Yersinia* Yop proteins. J Bacteriol **174:**7661-9.
8. **Andrews, G. P., A. E. Hromockyj, C. Coker, and A. T. Maurelli.** 1991. Two novel virulence loci, mxiA and mxiB, in *Shigella flexneri* 2a facilitate excretion of invasion plasmid antigens. Infect Immun **59:**1997-2005.
9. **Bacon, G. A., and T. W. Burrows.** 1956. The basis of virulence in *Pasteurella pestis*: an antigen determining virulence. Br J Exp Pathol **37:**481-93.
10. **Bahrani, F. K., P. J. Sansonetti, and C. Parsot.** 1997. Secretion of Ipa proteins by *Shigella flexneri*: inducer molecules and kinetics of activation. Infect Immun **65:**4005-10.
11. **Barzu, S., Z. Benjelloun-Touimi, A. Phalipon, P. Sansonetti, and C. Parsot.** 1997. Functional analysis of the *Shigella flexneri* IpaC invasin by insertional mutagenesis. Infect. Immun. **65:**1599-1605.
12. **Baudry, B., M. Kaczorek, and P. J. Sansonetti.** 1988. Nucleotide sequence of the invasion plasmid antigen B and C genes (ipaB and ipaC) of *Shigella flexneri*. Microb Pathog **4:**345-57.
13. **Baudry, B., A. T. Maurelli, P. Clerc, J. C. Sadoff, and P. J. Sansonetti.** 1987. Localization of plasmid loci necessary for the entry of *Shigella flexneri* into HeLa cells, and characterization of one locus encoding four immunogenic polypeptides. J Gen Microbiol **133:**3403-13.
14. **Bax, S. G. a. A.** 1993. The importance of not saturating H2O in protein NMR. Application to sensitivity enhancement and NOE measurements. J. Am. Chem. Soc **115 (1993), pp. 12593–12594**.

15. **Bennish, M. L., J. R. Harris, B. J. Wojtyniak, and M. Struelens.** 1990. Death in shigellosis: incidence and risk factors in hospitalized patients. J Infect Dis **161:**500-6.
16. **Blocker, A., P. Gounon, E. Larquet, K. Niebuhr, V. Cabiaux, C. Parsot, and P. Sansonetti.** 1999. The tripartite type III secreton of *Shigella flexneri* inserts IpaB and IpaC into host membranes. J Cell Biol **147:**683-93.
17. **Blocker, A., N. Jouihri, E. Larquet, P. Gounon, F. Ebel, C. Parsot, P. Sansonetti, and A. Allaoui.** 2001. Structure and composition of the *Shigella flexneri* "needle complex", a part of its type III secreton. Mol Microbiol **39:**652-63.
18. **Blocker, A., K. Komoriya, and S. Aizawa.** 2003. Type III secretion systems and bacterial flagella: insights into their function from structural similarities. Proc Natl Acad Sci U S A **100:**3027-30.
19. **Bodey, G. P., R. Bolivar, V. Fainstein, and L. Jadeja.** 1983. Infections caused by *Pseudomonas aeruginosa*. Rev Infect Dis **5:**279-313.
20. **Broz, P., C. A. Mueller, S. A. Muller, A. Philippsen, I. Sorg, A. Engel, and G. R. Cornelis.** 2007. Function and molecular architecture of the *Yersinia* injectisome tip complex. Mol Microbiol **65:**1311-20.
21. **Brubaker, R. R.** 2003. Interleukin-10 and inhibition of innate immunity to *Yersiniae*: roles of Yops and LcrV (V antigen). Infect Immun **71:**3673-81.
22. **Burr, S. E., K. Stuber, and J. Frey.** 2003. The ADP-ribosylating toxin, AexT, from *Aeromonas salmonicida* subsp. salmonicida is translocated via a type III secretion pathway. J Bacteriol **185:**6583-91.
23. **Burrows, T. W., and G. A. Bacon.** 1956. The basis of virulence in *Pasteurella pestis*: the development of resistance to phagocytosis in vitro. Br J Exp Pathol **37:**286-99.
24. **Buttner, D., and U. Bonas.** 2002. Port of entry--the type III secretion translocon. Trends Microbiol **10:**186-92.
25. **Buysse, J. M., C. K. Stover, E. V. Oaks, M. Venkatesan, and D. J. Kopecko.** 1987. Molecular cloning of invasion plasmid antigen (ipa) genes from *Shigella flexneri*: analysis of ipa gene products and genetic mapping. J Bacteriol **169:**2561-9.
26. **Carniel, E.** 2003. Evolution of pathogenic *Yersinia*, some lights in the dark. Adv Exp Med Biol **529:**3-12.
27. **CDC.** http://www.cdc.gov/ncidod/dbmd/diseaseinfo/melioidosis_g.htm.
28. **CDC.** Melioidosis http://www.cdc.gov/ncidod/dbmd/diseaseinfo/melioidosis_g.htm.
29. **CDC.** Salmonellosis: http://www.cdc.gov/ncidod/dbmd/diseaseinfo/salmonellosis_g.htm.
30. **CDC.** Shigellosis http://www.cdc.gov/ncidod/dbmd/diseaseinfo/shigellosis_t.htm.

31. **Chaowagul, W., Y. Suputtamongkol, D. A. Dance, A. Rajchanuvong, J. Pattara-arechachai, and N. J. White.** 1993. Relapse in melioidosis: incidence and risk factors. J Infect Dis **168:**1181-5.
32. **Chen, Y., M. R. Smith, K. Thirumalai, and A. Zychlinsky.** 1996. A bacterial invasin induces macrophage apoptosis by binding directly to ICE. EMBO J. **15:**3853-3860.
33. **Clark, M. A., M. A. Jepson, N. L. Simmons, and B. H. Hirst.** 1994. Preferential interaction of *Salmonella typhimurium* with mouse Peyer's patch M cells. Res Microbiol **145:**543-52.
34. **Cleary, J., L. C. Lai, R. K. Shaw, A. Straatman-Iwanowska, M. S. Donnenberg, G. Frankel, and S. Knutton.** 2004. Enteropathogenic *Escherichia coli* (EPEC) adhesion to intestinal epithelial cells: role of bundle-forming pili (BFP), EspA filaments and intimin. Microbiology **150:**527-38.
35. **Collmer, A., and D. W. Bauer.** 1994. *Erwinia chrysanthemi* and *Pseudomonas syringae*: plant pathogens trafficking in extracellular virulence proteins. Curr Top Microbiol Immunol **192:**43-78.
36. **Collmer, A., M. Lindeberg, T. Petnicki-Ocwieja, D. J. Schneider, and J. R. Alfano.** 2002. Genomic mining type III secretion system effectors in *Pseudomonas syringae* yields new picks for all TTSS prospectors. Trends Microbiol **10:**462-9.
37. **Cordes, F. S., S. Daniell, R. Kenjale, S. Saurya, W. L. Picking, W. D. Picking, F. Booy, S. M. Lea, and A. Blocker.** 2005. Helical packing of needles from functionally altered *Shigella* type III secretion systems. J Mol Biol **354:**206-11.
38. **Cordes, F. S., K. Komoriya, E. Larquet, S. Yang, E. H. Egelman, A. Blocker, and S. M. Lea.** 2003. Helical structure of the needle of the type III secretion system of *Shigella flexneri*. J Biol Chem **278:**17103-7.
39. **Cornelis, G., Y. Laroche, G. Balligand, M. P. Sory, and G. Wauters.** 1987. *Yersinia enterocolitica*, a primary model for bacterial invasiveness. Rev Infect Dis **9:**64-87.
40. **Cornelis, G. R.** 2003. How Yops find their way out of *Yersinia.* Mol Microbiol **50:**1091-4.
41. **Cornelis, G. R.** 2006. The type III secretion injectisome. Nat Rev Microbiol **4:**811-25.
42. **Cornelis, G. R.** 2002. Yersinia type III secretion: send in the effectors. J Cell Biol **158:**401-8.
43. **Cornelis, G. R.** 2002. The *Yersinia* Ysc-Yop 'type III' weaponry. Nat Rev Mol Cell Biol **3:**742-52.
44. **Cornelis, G. R., and H. Wolf-Watz.** 1997. The *Yersinia* Yop virulon: a bacterial system for subverting eukaryotic cells. Mol Microbiol **23:**861-7.
45. **Cossart, P., and P. J. Sansonetti.** 2004. Bacterial invasion: the paradigms of enteroinvasive pathogens. Science **304:**242-8.

46. **Cotter, P. A., and J. F. Miller.** 1994. BvgAS-mediated signal transduction: analysis of phase-locked regulatory mutants of *Bordetella bronchiseptica* in a rabbit model. Infect Immun **62:**3381-90.
47. **Cotter, P. A., and J. F. Miller.** 2000. Genetic analysis of the *Bordetella* infectious cycle. Immunopharmacology **48:**253-5.
48. **Cullinane, L. C., M. R. Alley, R. B. Marshall, and B. W. Manktelow.** 1987. *Bordetella parapertussis* from lambs. N Z Vet J **35:**175.
49. **Currie, B. J., D. A. Fisher, D. M. Howard, and J. N. Burrow.** 2000. Neurological melioidosis. Acta Trop **74:**145-51.
50. **Dames, S. A., M. Martinez-Yamout, R. N. De Guzman, H. J. Dyson, and P. E. Wright.** 2002. Structural basis for Hif-1 alpha /CBP recognition in the cellular hypoxic response. Proc Natl Acad Sci U S A **99:**5271-6.
51. **Dance, D. A.** 2000. Melioidosis as an emerging global problem. Acta Trop **74:**115-9.
52. **Dance, D. A.** 1991. Melioidosis: the tip of the iceberg? Clin Microbiol Rev **4:**52-60.
53. **Daniell, S. J., N. Takahashi, R. Wilson, D. Friedberg, I. Rosenshine, F. P. Booy, R. K. Shaw, S. Knutton, G. Frankel, and S. Aizawa.** 2001. The filamentous type III secretion translocon of enteropathogenic *Escherichia coli*. Cell Microbiol **3:**865-71.
54. **Darboe, N., R. Kenjale, W. L. Picking, W. D. Picking, and C. R. Middaugh.** 2006. Physical characterization of MxiH and PrgI, the needle component of the type III secretion apparatus from *Shigella* and *Salmonella*. Protein Sci **15:**543-52.
55. **Deane, J. E., P. Roversi, F. S. Cordes, S. Johnson, R. Kenjale, S. Daniell, F. Booy, W. D. Picking, W. L. Picking, A. J. Blocker, and S. M. Lea.** 2006. Molecular model of a type III secretion system needle: Implications for host-cell sensing. Proc Natl Acad Sci U S A **103:**12529-33.
56. **Delaglio, F., S. Grzesiek, G. W. Vuister, G. Zhu, J. Pfeifer, and A. Bax.** 1995. NMRPipe: a multidimensional spectral processing system based on UNIX pipes. J Biomol NMR **6:**277-93.
57. **Derewenda, U., A. Mateja, Y. Devedjiev, K. M. Routzahn, A. G. Evdokimov, Z. S. Derewenda, and D. S. Waugh.** 2004. The structure of *Yersinia pestis* V-antigen, an essential virulence factor and mediator of immunity against plague. Structure **12:**301-6.
58. **Diavatopoulos, D. A., C. A. Cummings, L. M. Schouls, M. M. Brinig, D. A. Relman, and F. R. Mooi.** 2005. *Bordetella pertussis*, the Causative Agent of Whooping Cough, Evolved from a Distinct, Human-Associated Lineage of B. bronchiseptica. PLoS Pathog **1:**e45.
59. **Donnenberg, M. S., and T. S. Whittam.** 2001. Pathogenesis and evolution of virulence in enteropathogenic and enterohemorrhagic *Escherichia coli*. J Clin Invest **107:**539-48.

60. **DuPont, H. L., M. M. Levine, R. B. Hornick, and S. B. Formal.** 1989. Inoculum size in shigellosis and implications for expected mode of transmission. J Infect Dis **159:**1126-8.
61. **Erskine, P. T., M. J. Knight, A. Ruaux, H. Mikolajek, N. Wong Fat Sang, J. Withers, R. Gill, S. P. Wood, M. Wood, G. C. Fox, and J. B. Cooper.** 2006. High resolution structure of BipD: an invasion protein associated with the type III secretion system of *Burkholderia pseudomallei*. J Mol Biol **363:**125-36.
62. **Espina, M., S. F. Ausar, C. R. Middaugh, M. A. Baxter, W. D. Picking, and W. L. Picking.** 2007. Conformational stability and differential structural analysis of LcrV, PcrV, BipD, and SipD from type III secretion systems. Protein Sci **16:**704-14.
63. **Espina, M., A. J. Olive, R. Kenjale, D. S. Moore, S. F. Ausar, R. W. Kaminski, E. V. Oaks, C. R. Middaugh, W. D. Picking, and W. L. Picking.** 2006. IpaD localizes to the tip of the type III secretion system needle of *Shigella flexneri*. Infect Immun **74:**4391-400.
64. **Fan, F., K. Ohnishi, N. R. Francis, and R. M. Macnab.** 1997. The FliP and FliR proteins of Salmonella typhimurium, putative components of the type III flagellar export apparatus, are located in the flagellar basal body. Mol Microbiol **26:**1035-46.
65. **Fields, K. A., M. L. Nilles, C. Cowan, and S. C. Straley.** 1999. Virulence role of V antigen of *Yersinia pestis* at the bacterial surface. Infect Immun **67:**5395-408.
66. **Finlay, B. B., S. Ruschkowski, and S. Dedhar.** 1991. Cytoskeletal rearrangements accompanying salmonella entry into epithelial cells. J Cell Sci **99 (Pt 2):**283-96.
67. **Francis, M. S., S. A. Lloyd, and H. Wolf-Watz.** 2001. The type III secretion chaperone LcrH co-operates with YopD to establish a negative, regulatory loop for control of Yop synthesis in *Yersinia pseudotuberculosis*. Mol Microbiol **42:**1075-93.
68. **Frank, D. W.** 1997. The exoenzyme S regulon of *Pseudomonas aeruginosa*. Mol Microbiol **26:**621-9.
69. **Frank, D. W., A. Vallis, J. P. Wiener-Kronish, A. Roy-Burman, E. G. Spack, B. P. Mullaney, M. Megdoud, J. D. Marks, R. Fritz, and T. Sawa.** 2002. Generation and characterization of a protective monoclonal antibody to *Pseudomonas aeruginosa* PcrV. J Infect Dis **186:**64-73.
70. **Galan, J. E.** 1996. Molecular genetic bases of *Salmonella* entry into host cells. Mol Microbiol **20:**263-71.
71. **Galan, J. E.** 2001. *Salmonella* interactions with host cells: type III secretion at work. Annu Rev Cell Dev Biol **17:**53-86.
72. **Galan, J. E., and A. Collmer.** 1999. Type III secretion machines: bacterial devices for protein delivery into host cells. Science **284:**1322-8.

73. **Galanis, E., A. S. King, P. Varughese, and S. A. Halperin.** 2006. Changing epidemiology and emerging risk groups for pertussis. Cmaj **174:**451-2.
74. **Goodnow, R. A.** 1980. Biology of *Bordetella bronchiseptica*. Microbiol Rev **44:**722-38.
75. **Gophna, U., E. Z. Ron, and D. Graur.** 2003. Bacterial type III secretion systems are ancient and evolved by multiple horizontal-transfer events. Gene **312:**151-63.
76. **Goure, J., P. Broz, O. Attree, G. R. Cornelis, and I. Attree.** 2005. Protective anti-V antibodies inhibit *Pseudomonas* and *Yersinia* translocon assembly within host membranes. J Infect Dis **192:**218-25.
77. **Goure, J., A. Pastor, E. Faudry, J. Chabert, A. Dessen, and I. Attree.** 2004. The V antigen of *Pseudomonas aeruginosa* is required for assembly of the functional PopB/PopD translocation pore in host cell membranes. Infect Immun **72:**4741-50.
78. **Groisman, E. A., and C. Mouslim.** 2000. Molecular mechanisms of *Salmonella* pathogenesis. Curr Opin Infect Dis **13:**519-522.
79. **Groisman, E. A., and H. Ochman.** 1997. How *Salmonella* became a pathogen. Trends Microbiol **5:**343-9.
80. **Grutzkau, A., C. Hanski, H. Hahn, and E. O. Riecken.** 1990. Involvement of M cells in the bacterial invasion of Peyer's patches: a common mechanism shared by *Yersinia enterocolitica* and other enteroinvasive bacteria. Gut **31:**1011-5.
81. **Grzesiek, S., H. Dobeli, R. Gentz, G. Garotta, A. M. Labhardt, and A. Bax.** 1992. 1H, 13C, and 15N NMR backbone assignments and secondary structure of human interferon-gamma. Biochemistry **31:**8180-90.
82. **Guan, K. L., and J. E. Dixon.** 1990. Protein tyrosine phosphatase activity of an essential virulence determinant in *Yersinia*. Science **249:**553-6.
83. **Guichon, A., D. Hersh, M. R. Smith, and A. Zychlinsky.** 2001. Structure-Function Analysis of the *Shigella* Virulence Factor IpaB. J. Bacteriol. **183:**1269-1276.
84. **Guntert, P.** 2004. Automated NMR structure calculation with CYANA. Methods Mol Biol **278:**353-78.
85. **Hakansson, S., K. Schesser, C. Persson, E. E. Galyov, R. Rosqvist, F. Homble, and H. Wolf-Watz.** 1996. The YopB protein of *Yersinia pseudotuberculosis* is essential for the translocation of Yop effector proteins across the target cell plasma membrane and displays a contact-dependent membrane disrupting activity. EMBO J **15:**5812-23.
86. **Hale, T. L., E. V. Oaks, and S. B. Formal.** 1985. Identification and antigenic characterization of virulence-associated, plasmid-coded proteins of *Shigella* spp. and enteroinvasive *Escherichia coli*. Infect Immun **50:**620-9.
87. **Hanski, C., U. Kutschka, H. P. Schmoranzer, M. Naumann, A. Stallmach, H. Hahn, H. Menge, and E. O. Riecken.** 1989. Immunohistochemical and electron

microscopic study of interaction of *Yersinia enterocolitica* serotype O8 with intestinal mucosa during experimental enteritis. Infect Immun **57:**673-8.

88. **Hanski, C., M. Naumann, A. Grutzkau, G. Pluschke, B. Friedrich, H. Hahn, and E. O. Riecken.** 1991. Humoral and cellular defense against intestinal murine infection with *Yersinia enterocolitica*. Infect Immun **59:**1106-11.
89. **Hanski, C., M. Naumann, H. Hahn, and E. O. Riecken.** 1989. Determinants of invasion and survival of *Yersinia enterocolitica* in intestinal tissue. An in vivo study. Med Microbiol Immunol (Berl) **178:**289-96.
90. **Hayward, R. D., R. J. Cain, E. J. McGhie, N. Phillips, M. J. Garner, and V. Koronakis.** 2005. Cholesterol binding by the bacterial type III translocon is essential for virulence effector delivery into mammalian cells. Mol Microbiol **56:**590-603.
91. **He, S. Y., and Q. Jin.** 2003. The Hrp pilus: learning from flagella. Curr Opin Microbiol **6:**15-9.
92. **He, S. Y., K. Nomura, and T. S. Whittam.** 2004. Type III protein secretion mechanism in mammalian and plant pathogens. Biochim Biophys Acta **1694:**181-206.
93. **Healy, C. M., F. M. Munoz, M. A. Rench, N. B. Halasa, K. M. Edwards, and C. J. Baker.** 2004. Prevalence of pertussis antibodies in maternal delivery, cord, and infant serum. J Infect Dis **190:**335-40.
94. **High, N., J. Mounier, M. C. Prevost, and P. J. Sansonetti.** 1992. IpaB of *Shigella flexneri* causes entry into epithelial cells and escape from the phagocytic vacuole. Embo J **11:**1991-9.
95. **Holm, L., and C. Sander.** 1993. Protein structure comparison by alignment of distance matrices. J Mol Biol **233:**123-38.
96. **Hueck, C. J.** 1998. Type III protein secretion systems in bacterial pathogens of animals and plants. Microbiol Mol Biol Rev **62:**379-433.
97. **Ide, T., S. Laarmann, L. Greune, H. Schillers, H. Oberleithner, and M. A. Schmidt.** 2001. Characterization of translocation pores inserted into plasma membranes by type III-secreted Esp proteins of enteropathogenic *Escherichia coli*. Cell Microbiol **3:**669-79.
98. **Inatsuka, C. S., S. M. Julio, and P. A. Cotter.** 2005. *Bordetella* filamentous hemagglutinin plays a critical role in immunomodulation, suggesting a mechanism for host specificity. Proc Natl Acad Sci U S A **102:**18578-83.
99. **Johnson, B. A.** 2004. Using NMRView to visualize and analyze the NMR spectra of macromolecules. Methods Mol Biol **278:**313-52.
100. **Johnson, S., P. Roversi, M. Espina, A. Olive, J. E. Deane, S. Birket, T. Field, W. D. Picking, A. J. Blocker, E. E. Galyov, W. L. Picking, and S. M. Lea.** 2007. Self-chaperoning of the type III secretion system needle tip proteins IpaD and BipD. J Biol Chem **282:**4035-44.
101. **Johnson, S., P. Roversi, M. Espina, A. Olive, J. E. Deane, S. Birket, T. Field, W. D. Picking, A. J. Blocker, E. E. Galyov, W. L. Picking, and S. M. Lea.**

2006. Self-chaperoning of the type III secretion system needle tip proteins IpaD and BipD. J Biol Chem.

102. **Jones, A. L., T. J. Beveridge, and D. E. Woods.** 1996. Intracellular survival of *Burkholderia pseudomallei*. Infect Immun **64:**782-90.

103. **Journet, L., C. Agrain, P. Broz, and G. R. Cornelis.** 2003. The needle length of bacterial injectisomes is determined by a molecular ruler. Science **302:**1757-60.

104. **Kaniga, K., D. Trollinger, and J. E. Galan.** 1995. Identification of two targets of the type III protein secretion system encoded by the inv and spa loci of *Salmonella typhimurium* that have homology to the *Shigella* IpaD and IpaA proteins. J Bacteriol **177:**7078-85.

105. **Kaniga, K., S. Tucker, D. Trollinger, and J. E. Galan.** 1995. Homologs of the *Shigella* IpaB and IpaC invasins are required for *Salmonella typhimurium* entry into cultured epithelial cells. J Bacteriol **177:**3965-71.

106. **Kato, J., K. Ito, A. Nakamura, and H. Watanabe.** 1989. Cloning of regions required for contact hemolysis and entry into LLC-MK2 cells from *Shigella sonnei* form I plasmid: virF is a positive regulator gene for these phenotypes. Infect Immun **57:**1391-8.

107. **Kenjale, R., J. Wilson, S. F. Zenk, S. Saurya, W. L. Picking, W. D. Picking, and A. Blocker.** 2005. The needle component of the type III secreton of *Shigella* regulates the activity of the secretion apparatus. J Biol Chem **280:**42929-37.

108. **Kenny, B.** 2002. Mechanism of action of EPEC type III effector molecules. Int J Med Microbiol **291:**469-77.

109. **Kenny, B., and B. B. Finlay.** 1997. Intimin-dependent binding of enteropathogenic *Escherichia coli* to host cells triggers novel signaling events, including tyrosine phosphorylation of phospholipase C-gamma1. Infect Immun **65:**2528-36.

110. **Kimbrough, T. G., and S. I. Miller.** 2000. Contribution of *Salmonella typhimurium* type III secretion components to needle complex formation. Proc Natl Acad Sci U S A **97:**11008-13.

111. **Koradi, R., M. Billeter, and K. Wuthrich.** 1996. MOLMOL: a program for display and analysis of macromolecular structures. J Mol Graph **14:**51-5, 29-32.

112. **Kubori, T., Y. Matsushima, D. Nakamura, J. Uralil, M. Lara-Tejero, A. Sukhan, J. E. Galan, and S. I. Aizawa.** 1998. Supramolecular structure of the *Salmonella typhimurium* type III protein secretion system. Science **280:**602-5.

113. **Kueltzo, L. A., J. Osiecki, J. Barker, W. L. Picking, B. Ersoy, W. D. Picking, and C. R. Middaugh.** 2003. Structure-function analysis of invasion plasmid antigen C (IpaC) from *Shigella flexneri*. J Biol Chem **278:**2792-8.

114. **Lafont, F., G. Tran Van Nhieu, K. Hanada, P. Sansonetti, and F. G. van der Goot.** 2002. Initial steps of *Shigella* infection depend on the cholesterol/sphingolipid raft-mediated CD44-IpaB interaction. Embo J **21:**4449-57.

115. **Laskowski, R. A., J. A. Rullmannn, M. W. MacArthur, R. Kaptein, and J. M. Thornton.** 1996. AQUA and PROCHECK-NMR: programs for checking the quality of protein structures solved by NMR. J Biomol NMR **8:**477-86.
116. **Macnab, R. M.** 2004. Type III flagellar protein export and flagellar assembly. Biochim Biophys Acta **1694:**207-17.
117. **Marenne, M. N., L. Journet, L. J. Mota, and G. R. Cornelis.** 2003. Genetic analysis of the formation of the Ysc-Yop translocation pore in macrophages by *Yersinia enterocolitica*: role of LcrV, YscF and YopN. Microb Pathog **35:**243-58.
118. **Marion, D., P. C. Driscoll, L. E. Kay, P. T. Wingfield, A. Bax, A. M. Gronenborn, and G. M. Clore.** 1989. Overcoming the overlap problem in the assignment of 1H NMR spectra of larger proteins by use of three-dimensional heteronuclear 1H-15N Hartmann-Hahn-multiple quantum coherence and nuclear Overhauser-multiple quantum coherence spectroscopy: application to interleukin 1 beta. Biochemistry **28:**6150-6.
119. **Marlovits, T. C., T. Kubori, A. Sukhan, D. R. Thomas, J. E. Galan, and V. M. Unger.** 2004. Structural insights into the assembly of the type III secretion needle complex. Science **306:**1040-2.
120. **Mattoo, S., and J. D. Cherry.** 2005. Molecular pathogenesis, epidemiology, and clinical manifestations of respiratory infections due to *Bordetella pertussis* and other *Bordetella* subspecies. Clin Microbiol Rev **18:**326-82.
121. **Maurelli, A. T., B. Baudry, H. d'Hauteville, T. L. Hale, and P. J. Sansonetti.** 1985. Cloning of plasmid DNA sequences involved in invasion of HeLa cells by *Shigella flexneri*. Infect Immun **49:**164-71.
122. **Menard, R., P. Sansonetti, and C. Parsot.** 1994. The secretion of the *Shigella flexneri* Ipa invasins is activated by epithelial cells and controlled by IpaB and IpaD. Embo J **13:**5293-302.
123. **Menard, R., P. Sansonetti, C. Parsot, and T. Vasselon.** 1994. Extracellular association and cytoplasmic partitioning of the IpaB and IpaC invasins of *S. flexneri*. Cell **79:**515-25.
124. **Menard, R., P. J. Sansonetti, and C. Parsot.** 1993. Nonpolar mutagenesis of the ipa genes defines IpaB, IpaC, and IpaD as effectors of *Shigella flexneri* entry into epithelial cells. J Bacteriol **175:**5899-906.
125. **Mohle-Boetani, J. C., M. Stapleton, R. Finger, N. H. Bean, J. Poundstone, P. A. Blake, and P. M. Griffin.** 1995. Communitywide shigellosis: control of an outbreak and risk factors in child day-care centers. Am J Public Health **85:**812-6.
126. **Morgan, D. G., C. Owen, L. A. Melanson, and D. J. DeRosier.** 1995. Structure of bacterial flagellar filaments at 11 A resolution: packing of the alpha-helices. J Mol Biol **249:**88-110.
127. **Morita-Ishihara, T., M. Ogawa, H. Sagara, M. Yoshida, E. Katayama, and C. Sasakawa.** 2005. *Shigella* Spa33 is an essential C-ring component of type III secretion machinery. J Biol Chem.

128. **Morita-Ishihara, T., M. Ogawa, H. Sagara, M. Yoshida, E. Katayama, and C. Sasakawa.** 2006. *Shigella* Spa33 is an essential C-ring component of type III secretion machinery. J Biol Chem **281:**599-607.
129. **Mueller, C. A., P. Broz, S. A. Muller, P. Ringler, F. Erne-Brand, I. Sorg, M. Kuhn, A. Engel, and G. R. Cornelis.** 2005. The V-antigen of *Yersinia* forms a distinct structure at the tip of injectisome needles. Science **310:**674-6.
130. **Nilles, M. L., K. A. Fields, and S. C. Straley.** 1998. The V antigen of *Yersinia pestis* regulates Yop vectorial targeting as well as Yop secretion through effects on YopB and LcrG. J Bacteriol **180:**3410-20.
131. **Nouwen, N., N. Ranson, H. Saibil, B. Wolpensinger, A. Engel, A. Ghazi, and A. P. Pugsley.** 1999. Secretin PulD: association with pilot PulS, structure, and ion-conducting channel formation. Proc Natl Acad Sci U S A **96:**8173-7.
132. **Nouwen, N., H. Stahlberg, A. P. Pugsley, and A. Engel.** 2000. Domain structure of secretin PulD revealed by limited proteolysis and electron microscopy. Embo J **19:**2229-36.
133. **Oaks, E. V., T. L. Hale, and S. B. Formal.** 1986. Serum immune response to *Shigella* protein antigens in rhesus monkeys and humans infected with *Shigella* spp. Infect Immun **53:**57-63.
134. **Ogino, T., R. Ohno, K. Sekiya, A. Kuwae, T. Matsuzawa, T. Nonaka, H. Fukuda, S. Imajoh-Ohmi, and A. Abe.** 2006. Assembly of the type III secretion apparatus of enteropathogenic *Escherichia coli*. J Bacteriol **188:**2801-11.
135. **Ohnishi, K., F. Fan, G. J. Schoenhals, M. Kihara, and R. M. Macnab.** 1997. The FliO, FliP, FliQ, and FliR proteins of *Salmonella typhimurium*: putative components for flagellar assembly. J Bacteriol **179:**6092-9.
136. **Ohnishi, K., Y. Ohto, S. Aizawa, R. M. Macnab, and T. Iino.** 1994. FlgD is a scaffolding protein needed for flagellar hook assembly in *Salmonella typhimurium*. J Bacteriol **176:**2272-81.
137. **Olive, A. J., R. Kenjale, M. Espina, D. S. Moore, W. L. Picking, and W. D. Picking.** 2007. Bile salts stimulate recruitment of IpaB to the *Shigella flexneri* surface, where it colocalizes with IpaD at the tip of the type III secretion needle. Infect Immun **75:**2626-9.
138. **Page, A. L., H. Ohayon, P. J. Sansonetti, and C. Parsot.** 1999. The secreted IpaB and IpaC invasins and their cytoplasmic chaperone IpgC are required for intercellular dissemination of *Shigella flexneri*. Cell Microbiol **1:**183-93.
139. **Pallen, M. J., S. A. Beatson, and C. M. Bailey.** 2005. Bioinformatics, genomics and evolution of non-flagellar type-III secretion systems: a Darwinian perspective. FEMS Microbiol Rev **29:**201-29.
140. **Pang, T., Z. A. Bhutta, B. B. Finlay, and M. Altwegg.** 1995. Typhoid fever and other salmonellosis: a continuing challenge. Trends Microbiol **3:**253-5.
141. **Parsot, C., and P. J. Sansonetti.** 1996. Invasion and the pathogenesis of *Shigella* infections. Curr Top Microbiol Immunol **209:**25-42.

142. **Pastor, A., J. Chabert, M. Louwagie, J. Garin, and I. Attree.** 2005. PscF is a major component of the *Pseudomonas aeruginosa* type III secretion needle. FEMS Microbiol Lett **253:**95-101.

143. **Pervushin, K., R. Riek, G. Wider, and K. Wuthrich.** 1997. Attenuated T2 relaxation by mutual cancellation of dipole-dipole coupling and chemical shift anisotropy indicates an avenue to NMR structures of very large biological macromolecules in solution. Proc Natl Acad Sci U S A **94:**12366-71.

144. **Phan, J., B. P. Austin, and D. S. Waugh.** 2005. Crystal structure of the *Yersinia* type III secretion protein YscE. Protein Sci **14:**2759-63.

145. **Picking, W. L., L. Coye, J. C. Osiecki, A. Barnoski Serfis, E. Schaper, and W. D. Picking.** 2001. Identification of functional regions within invasion plasmid antigen C (IpaC) of *Shigella flexneri*. Mol Microbiol **39:**100-11.

146. **Picking, W. L., H. Nishioka, P. D. Hearn, M. A. Baxter, A. T. Harrington, A. Blocker, and W. D. Picking.** 2005. IpaD of *Shigella flexneri* is independently required for regulation of Ipa protein secretion and efficient insertion of IpaB and IpaC into host membranes. Infect Immun **73:**1432-40.

147. **Polissi, A., and M. R. Soria.** 2005. Functional genomics of bacterial pathogens: from post-genomics to therapeutic targets. Mol Microbiol **57:**307-12.

148. **Pope, L. M., K. E. Reed, and S. M. Payne.** 1995. Increased protein secretion and adherence to HeLa cells by *Shigella* spp. following growth in the presence of bile salts. Infect Immun **63:**3642-8.

149. **Porter, J. F., K. Connor, and W. Donachie.** 1994. Isolation and characterization of *Bordetella parapertussis*-like bacteria from ovine lungs. Microbiology **140 (Pt 2):**255-61.

150. **Quinaud, M., J. Chabert, E. Faudry, E. Neumann, D. Lemaire, A. Pastor, S. Elsen, A. Dessen, and I. Attree.** 2005. The PscE-PscF-PscG complex controls type III secretion needle biogenesis in *Pseudomonas aeruginosa*. J Biol Chem **280:**36293-300.

151. **Quinaud, M., S. Ple, V. Job, C. Contreras-Martel, J. P. Simorre, I. Attree, and A. Dessen.** 2007. Structure of the heterotrimeric complex that regulates type III secretion needle formation. Proc Natl Acad Sci U S A **104:**7803-8.

152. **Rainbow, L., C. A. Hart, and C. Winstanley.** 2002. Distribution of type III secretion gene clusters in *Burkholderia pseudomallei*, *B. thailandensis* and *B. mallei*. J Med Microbiol **51:**374-84.

153. **Reckseidler, S. L., D. DeShazer, P. A. Sokol, and D. E. Woods.** 2001. Detection of bacterial virulence genes by subtractive hybridization: identification of capsular polysaccharide of *Burkholderia pseudomallei* as a major virulence determinant. Infect Immun **69:**34-44.

154. **Rosenshine, I., S. Ruschkowski, M. Stein, D. J. Reinscheid, S. D. Mills, and B. B. Finlay.** 1996. A pathogenic bacterium triggers epithelial signals to form a functional bacterial receptor that mediates actin pseudopod formation. Embo J **15:**2613-24.

155. **Samatey, F. A., H. Matsunami, K. Imada, S. Nagashima, T. R. Shaikh, D. R. Thomas, J. Z. Chen, D. J. Derosier, A. Kitao, and K. Namba.** 2004. Structure of the bacterial flagellar hook and implication for the molecular universal joint mechanism. Nature **431:**1062-8.
156. **Sansonetti, P. J.** 2001. Rupture, invasion and inflammatory destruction of the intestinal barrier by *Shigella*, making sense of prokaryote-eukaryote cross-talks. FEMS Microbiol Rev **25:**3-14.
157. **Sansonetti, P. J., D. J. Kopecko, and S. B. Formal.** 1982. Involvement of a plasmid in the invasive ability of *Shigella flexneri*. Infect Immun **35:**852-60.
158. **Sasakawa, C., B. Adler, T. Tobe, N. Okada, S. Nagai, K. Komatsu, and M. Yoshikawa.** 1989. Functional organization and nucleotide sequence of virulence Region-2 on the large virulence plasmid in *Shigella flexneri* 2a. Mol Microbiol **3:**1191-201.
159. **Sasakawa, C., S. Makino, K. Kamata, and M. Yoshikawa.** 1986. Isolation, characterization, and mapping of Tn5 insertions into the 140-megadalton invasion plasmid defective in the mouse Sereny test in *Shigella flexneri* 2a. Infect Immun **54:**32-6.
160. **Schroeder, G. N., and H. Hilbi.** 2008. Molecular pathogenesis of *Shigella* spp.: controlling host cell signaling, invasion, and death by type III secretion. Clin Microbiol Rev **21:**134-56.
161. **Schuch, R., and A. T. Maurelli.** 1999. The Mxi-Spa Type III Secretory Pathway of *Shigella flexneri* Requires an Outer Membrane Lipoprotein, MxiM, for Invasin Translocation. Infect. Immun. **67:**1982-1991.
162. **Sekiya, K., M. Ohishi, T. Ogino, K. Tamano, C. Sasakawa, and A. Abe.** 2001. Supermolecular structure of the enteropathogenic *Escherichia coli* type III secretion system and its direct interaction with the EspA-sheath-like structure. Proc Natl Acad Sci U S A **98:**11638-43.
163. **Shan X, G. K., Muhandiram DR, Rao NS, Arrowsmith CH and Kay LE.** 1996. Assignment of 15N, 13C(z, 13C~ and HN resonances in an 15N, 13C, 2H labeled 64 kDa trp repressor-operator complex using triple resonance NMR spectroscopy and 2H, -decoupling. J Am Chem Soc **118:6570-6579**.
164. **Skoudy, A., J. Mounier, A. Aruffo, H. Ohayon, P. Gounon, P. Sansonetti, and G. Tran Van Nhieu.** 2000. CD44 binds to the *Shigella* IpaB protein and participates in bacterial invasion of epithelial cells. Cell Microbiol **2:**19-33.
165. **Stensrud, K. F., P. R. Adam, C. D. La Mar, A. J. Olive, G. H. Lushington, R. Sudharsan, N. L. Shelton, R. S. Givens, W. L. Picking, and W. D. Picking.** 2008. Deoxycholate interacts with IpaD of *Shigella flexneri* in inducing the recruitment of IpaB to the type III secretion apparatus needle tip. J Biol Chem **283:**18646-54.
166. **Stevens, M. P., A. Haque, T. Atkins, J. Hill, M. W. Wood, A. Easton, M. Nelson, C. Underwood-Fowler, R. W. Titball, G. J. Bancroft, and E. E. Galyov.** 2004. Attenuated virulence and protective efficacy of a *Burkholderia*

pseudomallei bsa type III secretion mutant in murine models of melioidosis. Microbiology **150:**2669-76.

167. **Stevens, M. P., M. W. Wood, L. A. Taylor, P. Monaghan, P. Hawes, P. W. Jones, T. S. Wallis, and E. E. Galyov.** 2002. An Inv/Mxi-Spa-like type III protein secretion system in *Burkholderia pseudomallei* modulates intracellular behaviour of the pathogen. Mol Microbiol **46:**649-59.
168. **Suarez, M., and H. Russmann.** 1998. Molecular mechanisms of *Salmonella* invasion: the type III secretion system of the pathogenicity island 1. Int Microbiol **1:**197-204.
169. **Sun, P., J. E. Tropea, B. P. Austin, S. Cherry, and D. S. Waugh.** 2008. Structural Characterization of the *Yersinia* pestis Type III Secretion System Needle Protein YscF in Complex with Its Heterodimeric Chaperone YscE/YscG. J Mol Biol.
170. **Takeuchi, A.** 1967. Electron microscope studies of experimental Salmonella infection. I. Penetration into the intestinal epithelium by *Salmonella typhimurium*. Am J Pathol **50:**109-36.
171. **Tamano, K., S. Aizawa, E. Katayama, T. Nonaka, S. Imajoh-Ohmi, A. Kuwae, S. Nagai, and C. Sasakawa.** 2000. Supramolecular structure of the *Shigella* type III secretion machinery: the needle part is changeable in length and essential for delivery of effectors. Embo J **19:**3876-87.
172. **Tamano, K., E. Katayama, T. Toyotome, and C. Sasakawa.** 2002. *Shigella* Spa32 is an essential secretory protein for functional type III secretion machinery and uniformity of its needle length. J Bacteriol **184:**1244-52.
173. **Terry, C. M., W. L. Picking, S. E. Birket, K. Flentie, B. M. Hoffman, J. R. Barker, and W. D. Picking.** 2008. The C-terminus of IpaC is required for effector activities related to *Shigella* invasion of host cells. Microb Pathog **45:**282-9.
174. **Torruellas, J., M. W. Jackson, J. W. Pennock, and G. V. Plano.** 2005. The *Yersinia pestis* type III secretion needle plays a role in the regulation of Yop secretion. Mol Microbiol **57:**1719-33.
175. **Tran Van Nhieu, G., A. Ben-Ze'ev, and P. J. Sansonetti.** 1997. Modulation of bacterial entry into epithelial cells by association between vinculin and the *Shigella* IpaA invasin. Embo J **16:**2717-29.
176. **Tran Van Nhieu, G., R. Bourdet-Sicard, G. Dumenil, A. Blocker, and P. J. Sansonetti.** 2000. Bacterial signals and cell responses during *Shigella* entry into epithelial cells. Cell Microbiol **2:**187-93.
177. **Troisfontaines, P., and G. R. Cornelis.** 2005. Type III secretion: more systems than you think. Physiology (Bethesda) **20:**326-39.
178. **van den Akker, W. M.** 1997. *Bordetella bronchiseptica* has a BvgAS-controlled cytotoxic effect upon interaction with epithelial cells. FEMS Microbiol Lett **156:**239-44.

179. **Veenendaal, A. K., J. L. Hodgkinson, L. Schwarzer, D. Stabat, S. F. Zenk, and A. J. Blocker.** 2007. The type III secretion system needle tip complex mediates host cell sensing and translocon insertion. Mol Microbiol **63:**1719-30.
180. **Venkatesan, M. M., J. M. Buysse, and E. V. Oaks.** 1992. Surface presentation of *Shigella flexneri* invasion plasmid antigens requires the products of the spa locus. J Bacteriol **174:**1990-2001.
181. **Viboud, G. I., and J. B. Bliska.** 2005. *Yersinia* outer proteins: role in modulation of host cell signaling responses and pathogenesis. Annu Rev Microbiol **59:**69-89.
182. **Wang, Y., A. N. Ouellette, C. W. Egan, T. Rathinavelan, W. Im, and R. N. De Guzman.** 2007. Differences in the electrostatic surfaces of the type III secretion needle proteins PrgI, BsaL, and MxiH. J Mol Biol **371:**1304-14.
183. **Warawa, J., B. B. Finlay, and B. Kenny.** 1999. Type III secretion-dependent hemolytic activity of enteropathogenic *Escherichia coli*. Infect Immun **67:**5538-40.
184. **WHO.** http://www.who.int/vaccine_research/diseases/diarrhoeal/en/index6.html.
185. **Wishart, D. S., and A. M. Nip.** 1998. Protein chemical shift analysis: a practical guide. Biochem Cell Biol **76:**153-63.
186. **Yonekura, K., S. Maki-Yonekura, and K. Namba.** 2003. Complete atomic model of the bacterial flagellar filament by electron cryomicroscopy. Nature **424:**643-50.
187. **Yonekura, K., S. Maki, D. G. Morgan, D. J. DeRosier, F. Vonderviszt, K. Imada, and K. Namba.** 2000. The bacterial flagellar cap as the rotary promoter of flagellin self-assembly. Science **290:**2148-52.
188. **Yuk, M. H., E. T. Harvill, P. A. Cotter, and J. F. Miller.** 2000. Modulation of host immune responses, induction of apoptosis and inhibition of NF-kappaB activation by the *Bordetella* type III secretion system. Mol Microbiol **35:**991-1004.
189. **Yuk, M. H., E. T. Harvill, and J. F. Miller.** 1998. The BvgAS virulence control system regulates type III secretion in *Bordetella bronchiseptica*. Mol Microbiol **28:**945-59.
190. **Zhang, L., Y. Wang, A. J. Olive, N. D. Smith, W. D. Picking, R. N. De Guzman, and W. L. Picking.** 2007. Identification of the MxiH needle protein residues responsible for anchoring invasion plasmid antigen D to the type III secretion needle tip. J Biol Chem **282:**32144-51.
191. **Zhang, L., Y. Wang, W. L. Picking, W. D. Picking, and R. N. De Guzman.** 2006. Solution structure of monomeric BsaL, the type III secretion needle protein of *Burkholderia pseudomallei.* J Mol Biol **359:**322-30.
192. **Zierler, M. K., and J. E. Galan.** 1995. Contact with cultured epithelial cells stimulates secretion of *Salmonella typhimurium* invasion protein InvJ. Infect Immun **63:**4024-8.

193. **Zychlinsky, A., C. Fitting, J. M. Cavaillon, and P. J. Sansonetti.** 1994. Interleukin 1 is released by murine macrophages during apoptosis induced by *Shigella flexneri*. J Clin Invest **94:**1328-32.

APPENDIX A: Buffers and Reagents

Agarose gel for DNA electrophoresis:

25ml 1X TAE
13ul 6mM Ethidium bromide
0.3g high melting DNA grade agarose

Running buffer for agarose DNA gel (TAE):

4.84g Tris
1.142ml Acetic acid
2ml 0.5M EDTA
Dilute to 1000 ml

HISBIND binding buffer:

5 mM imidazole
0.5M NaCl
20mM Tris-HCl pH 7.9
Adjust to pH 7.9

HISBIND charge buffer:

50mM $NiSO_4$

HISBIND elute buffer:

1M imidazole
0.5M NaCl
20mM Tris-HCl pH 7.9
Adjust to pH 7.9

HISBIND strip buffer:

100mM EDTA
0.5M NaCl
20mM Tris-HCl pH 7.9
Adjust to pH 7.9

HISBIND wash buffer:

60mM imidazole
0.5M NaCl
20mM Tris-HCl pH 7.9
Adjust to pH 7.9

Luria-Burtani Broth:

10g Tryptone
5g Yeast extract
10g NaCl
Dilute to 1000ml

Luria-Burtani Agar:

10g Tryptone
5g Yeast extract
10g NaCl
15g agar
Dilute to 1000ml

M9 Minimal Media:

6.7g Na_2HPO_4
3.0g KH_2PO_4
1.5g NaCl
2ml 0.1M $CaCl_2$
1ml 1M $MgSO_4$
1g NH_4Cl
10ml 40% glucose
10ml vitamin solution
1ml 1000× trace metal solution
Dilute to 1000ml

Minimum Essential Medium Eagle (Modified) (MEME):

9.53g MEME
2.2g $NaHCO_3$
Dilute to 1000ml and filter sterilize

Minimum Essential Eagle (Modified) MEME + Calf Serum (CS):

9.53g MEME
2.2g $NaHCO_3$
100ml calf serum
Dilute to 1000ml and filter sterilize

Minimum Essential Eagle MEME + Gentamycin (GENT):

9.53g MEME
2.2g $NaHCO_3$
50ml calf serum
50mg gentamycin
Dilute to 1000ml and filter sterilize

Minimum Essential Eagle MEME + Glucose (GLUC):

9.53g MEME
2.2g $NaHCO_3$
4.5g glucose
Dilute to 1000ml and filter sterilize

Phosphate-Buffered Saline (150mM PBS):

10mM Na_2HPO_4
1.5mM K_2HPO_4
130mM NaCl
3mM KCl

Sodium Dodecyl Sulfate-Polyacrylamide Gel Electrophoresis (SDS-PAGE) destain:

5% (v/v) methanol
7.5% (v/v) glacial acetic acid

SDS-PAGE running buffer:

2.42g Tris
14.41g glycine
1.0g SDS
bring to 1 liter with H_20

10% SDS-PAGE resolving gel:

3.33ml 29:1% (w/v) acrylamide:bisacrylamide
2.5ml 1.5 M Tris-HCl pH 8.8
0.1ml 10% (w/v) SDS
0.15ml 10% (w/v) ammonium persulfate (APS)
13µl N,N,N',N'-tetra-methylethylenediamine (TEMED)

5% SDS-PAGE stacking gel:

2ml 29:1% (w/v) acrylamide:bisacrylamide
2.5ml 0.5 M Tris-HCl pH 6.8
0.1ml 10% (w/v) SDS
88µl 10% (w/v) APS

10μl TEMED

SDS-PAGE stain:

0.1% (w/v) Coomassie Brilliant Blue R-250
5% (v/v) methanol
7.5% (v/v) glacial acetic acid

SOC Medium:

2.0% tryptone
0.5% yeast extract
10mM NaCl
2.5mM KCl
10mM $MgCl_2$-$6H_2O$
20mM glucose

Solution A:

0.8% (w/v) NaCl
0.04% (w/v) KCl
0.035% (w/v) $NaHCO_3$
0.1% (w/v) glucose

Trace Metal Solution 1000×:

5000mg $FeSO_4$
10mg $CuSO_4$
5mg $MnSO_4$
5mg $ZnSO_4$
1300mg $CaCl_2$
1.0mg $CoCl_2$
0.7mg H_3BO_4
1.0mg $NaMoO_4$
Dilute to 100ml

Tryptic Soy Agar:

15g Tryptone
5g Soytone
5g NaCl
15g Agar
Dilute to 1000ml

Tryptic Soy Broth:

15g Tryptone
5g Soytone

5g NaCl
Dilute to 1000ml

Tris-Buffered Saline (TBS):

2.42g tris base (20mM)
8g NaCl (137mM)
3.8ml 1M HCl
Dilute to 1000 ml and pH to 7.0

Tris-Buffered Saline + 0.1% Tween 20 (TBST):

2.42g tris base (20mM)
8g NaCl (137mM)
3.8ml 1M HCl
4ml 25% Tween 20
Dilute to 1000 ml and pH to 7.0

Uranyl acetate 2%

Diluted in distilled water at 2% w/v and filtered.
pH not adjusted
Store at 4^{o}C in foil.

APPENDIX B: Table of Primers

Plasmid PWPsf4	Primers	Sequence 5' to 3'
MxiHL34A	MxiH216F	GAGAGAGAGAACGTTGGCAGCAGATAAATTAGCTAAAAATCCT
	MxiH217R	GAGAGAGAGAACGTTAGTTCACCTTGTAATGT
MxiHN40A	MxiH218R	GAGAGAGAGTTCGAAGGAGCTTTAGCTAATTTATCTAGTGC
	MxiH219F	GAGAGAGAGTTCGAATCCACAGTTGCTGGCTG
MxiHN43A	MxiH220R	GAGAGAGAGCAATTGTGGTGCCGAAGGATTTTTAGCTAATTT
	MxiH21F	GAGAGAGAGCAATTGCTGGCTGAATACCAAA
MxiHN43K	MxiH221R	GAGAGAGAGCAATTGTGGTTTCGAAGGATTTTTAGCTAATTT
	MxiH21F	GAGAGAGAGCAATTGCTGGCTGAATACCAAA
MxiHL47A	MxiH214F	GAGAGAGAGCAATTGGCTGCTGAATACCAAAGTAAATTA
	MxiH211R	GAGAGAGAGCAATTGTGGATTCGAAGGATTTT
MxiHL47D	MxiH215F	GAGAGAGAGCAATTGGATGCTGAATACCAAAGTAAATTA
	MxiH211R	GAGAGAGAGCAATTGTGGATTCGAAGGATTTT
MxiHY50F	MxiH212F	GAGAGAGAGCAATTGCTGGCTGAATTTCAAAGTAAATTATCTGAATAT
	MxiH211R	GAGAGAGAGCAATTGTGGATTCGAAGGATTTT
MxiHY50L	MxiH213F	GAGAGAGAGCAATTGCTGGCTGAACTGCAAAGTAAATTATCTGAATAT
	MxiH211R	GAGAGAGAGCAATTGTGGATTCGAAGGATTTT
IpaDN146Q	D206F	GAGAGAGAGCTTAAGGTATATGAACATGCCGTTAG
	D207R	GAGAGAGAGCTTAAGATACTGTTCTTGAATATCATTGATGGAGTTTG
IpaDN149F	D206F	GAGAGAGAGCTTAAGGTATATGAACATGCCGTTAG
	D208R	GAGAGAGAGCTTAAGAAACTGTTCATTAATA

		TCATTGATGGAGTTTG
IpaDN146Q/Y149F	D206F	GAGAGAGAGCTTAAGGTATATGAACATGCCG TTAG
	D209R	GAGAGAGAGCTTAAGAAACTGTTCTTGAATA TCATTGATGGAGTTTG
IpaDS158L	D210F	CTATATCCACTAAATAATACTGTTAGTCAGGA ACAA
	D211R	CGGTTTATCTTTATATTTTTCC
IpaDA214L	D195F	GAGAGAGAGCTTAAGGAAAAATATAAAGATA AACCGCTATATCCACTAAATAATACTGTTAGT CAG
	D196R	GAGAGAGAGCTTAAGTTCTTCCAATGCCTTTT T

APPENDIX C: List of abbreviations

CR – Congo red

HSQC - Heteronuclear single quantum coherence

Ipa – Invasion plasmid antigen

Ipg – Invasion plasmid gene

IPTG – isopropyl thio-β-D-galactoside

kb – kilobase

kDa – kilodaltons

LB – Luria Bertani broth

min – minute

MW – molecular weigth

Mxi – membrane expression of invasion plasmid antigen

nm – nanometers

NMR – nuclear magnetic resonance

PBS – phosphate-buffered saline

PCR – polymerase chain reaction

SDS-PAGE – sodium dodecyl sulfate-polyacrylamide gel electrophoresis

Spa – surface presentation of invasion plasmid antigen

spp. – species

TTSS – type III secretion system

TTSA – type III secretion appratus

TTS – type III secretion

TBS – tris-buffered saline

TSA – tryptic soy agar

TSB – tryptic soy broth

TROSY - Transverse relaxation optimized spectroscopy